



HAL
open science

Low molecular weight hydrogels as a strategy to coat enzymatic biofuel cells to enhance functionality and biocompatibility

Kotagudda Ranganath Sindhu

► **To cite this version:**

Kotagudda Ranganath Sindhu. Low molecular weight hydrogels as a strategy to coat enzymatic biofuel cells to enhance functionality and biocompatibility. Human health and pathology. Université de Bordeaux, 2019. English. NNT : 2019BORD0058 . tel-02528818v1

HAL Id: tel-02528818

<https://theses.hal.science/tel-02528818v1>

Submitted on 2 Apr 2020 (v1), last revised 15 May 2020 (v2)

HAL is a multi-disciplinary open access archive for the deposit and dissemination of scientific research documents, whether they are published or not. The documents may come from teaching and research institutions in France or abroad, or from public or private research centers.

L'archive ouverte pluridisciplinaire **HAL**, est destinée au dépôt et à la diffusion de documents scientifiques de niveau recherche, publiés ou non, émanant des établissements d'enseignement et de recherche français ou étrangers, des laboratoires publics ou privés.

THÈSE PRÉSENTÉE

POUR OBTENIR LE GRADE DE

DOCTEUR DE

L'UNIVERSITÉ DE BORDEAUX

ÉCOLE DOCTORALE SCIENCES DE LA VIE ET DE LA SANTÉ
BIOLOGIE CELLULAIRE ET PHYSIOPATHOLOGIE

Par Sindhu KOTAGUDDA RANGANATH

**Low molecular weight hydrogels'' : une stratégie de revêtement de biopiles
enzymatiques pour augmenter la fonctionnalité et la biocompatibilité**

Sous la direction de : Claudine BOIZIAU
Olivier Chassande

Soutenue le 19 Avril 2019

Membres du jury :

Mme. Catherine Le Visage	Directrice de recherche Inserm, Université de Nantes	Rapporteur
M. Nihal Engin Vrana	Chercheur affilié, Université de Strasbourg	Rapporteur
Mme. Marie-Christine Durrieu	Directrice de recherche Inserm, Université de Bordeaux	Examineur
M. Olivier Chassande	Chargé de recherche CNRS, Université de Bordeaux	Invité
M. Alexander Kuhn	Professeur, Université de Bordeaux	Invité
Mme. Claudine Boiziau	Chargée de recherche Inserm, Université de Bordeaux	Directrice de thèse

Abstract/Resume

Low molecular weight hydrogels : une stratégie de revêtement de biopiles enzymatiques pour augmenter la fonctionnalité et la biocompatibilité

Les biopiles enzymatiques miniatures représentent un potentiel important pour la future génération de dispositifs médicaux implantables, utilisés pour le diagnostic, le pronostic et le traitement. Ces derniers fonctionnent actuellement avec des sources d'énergie externes. Ces biopiles utilisant les molécules présentes dans les fluides biologiques sont des dispositifs médicaux prometteurs. Le glucose, qui est abondamment disponible dans le corps, est à l'étude comme biocarburant permettant de produire de l'énergie. Les enzymes utilisées pour produire l'énergie à partir des produits biochimiques sont immobilisées sur des électrodes en or par des médiateurs redox. Cependant, la faible puissance actuellement disponible et la sensibilité des enzymes à l'environnement limitent leur application *in vivo*. Malgré des recherches intensives, de nombreux problèmes restent à résoudre, notamment l'amélioration de la puissance, de la stabilité et de la biocompatibilité des biopiles.

La réaction à corps étranger et l'isolement du dispositif médical par la formation d'une capsule fibreuse peuvent d'une part dénaturer les enzymes et, d'autre part, entraver la diffusion des analytes et de l'oxygène. Le travail décrit dans cette thèse vise à protéger les biopiles fonctionnant à base de glucose. Afin de résoudre les problèmes mentionnés ci-dessus, les hydrogels, actuellement développés pour diverses applications telles que l'administration de médicaments, l'ingénierie tissulaire et les dispositifs médicaux, offrent des propriétés prometteuses en tant que matériaux de revêtement.

La première partie de la thèse est centrée sur l'évaluation de différents hydrogels injectables de faible poids moléculaire, en analysant à la fois la gélification *in vitro* et *in vivo*, la cinétique de dégradation, la réaction à corps étranger et l'angiogenèse. Les hydrogels étudiés présentent une dégradation lente et une intégration tissulaire optimale. Une angiogenèse accrue a été observée en raison de la libération d'une molécule pro-angiogénique pendant la dégradation de l'hydrogel.

Dans la seconde partie de la thèse, l'un des hydrogels étudiés a été utilisé pour recouvrir l'électrode en or : le choix de l'enzyme a été basé sur des études de stabilité *in vitro*. En parallèle, le processus de revêtement a été optimisé, à la fois pour son uniformité et son épaisseur. Même si un revêtement plus épais présente l'avantage de protéger l'électrode contre la réaction à corps étranger, il est nécessaire de limiter l'épaisseur afin de maintenir une diffusion efficace des analytes et de l'oxygène.

Les expériences en cours décrites dans la dernière partie de la thèse sont axées sur l'optimisation de l'implantation chez le rat et la mesure de l'activité des biopiles. De plus, les électrodes ont été connectées à une antenne pour établir une communication sans fil ; en effet, cela permettrait une mesure non invasive de l'activité enzymatique.

En conclusion, ces travaux ont permis d'identifier un hydrogel pouvant être utilisé pour revêtir les électrodes de biopiles. Le sous-produit libéré lors de la biodégradation favorise l'angiogenèse au voisinage du matériau. Grâce à ce revêtement, on peut donc s'attendre à un échange accru d'analytes et d'oxygène, préalable indispensable à l'activité enzymatique.

Mots clés : hydrogels, biopiles enzymatiques, fonctionnalité, biocompatibilité, réaction à corps étranger.

Low molecular weight hydrogels as a strategy to coat enzymatic biofuel cells to enhance functionality and biocompatibility.

Miniature enzymatic biofuel cells hold great potential to power the future generation of implantable medical devices, which are currently working on external power sources used for diagnosis, prognosis and treatment. Enzymatic biofuel cells appear to be promising in harvesting the energy from biochemicals present in physiological body fluids. Glucose, which is abundantly available in the body, is being explored as a biofuel to harvest energy. The enzymes employed to harvest the energy from the biochemicals are electrically wired on gold electrodes by redox mediators. However, the limitation of insufficient power and the sensitivity of the enzymes towards host environment restrict their in vivo application. Despite several attempts, numerous challenges remain to be addressed, such as improved current density, increased stability, and biocompatibility of enzymatic biofuel cells.

Foreign body reaction and isolation of the medical device by the formation of a fibrous capsule may firstly denature the enzymes, and secondly hinder the diffusion of analytes and oxygen. The work described in this thesis aims at protecting glucose-based biofuel cells. As a strategy for combatting the bottlenecks mentioned above, hydrogels, currently developed for various applications such as drug delivery, tissue engineering, and medical device, offer promising properties as coating materials.

The first part of the thesis is focused on characterisation and evaluation different low molecular weight injectable hydrogels by analysing both in vitro and in vivo gel formation, degradation kinetics, foreign body reaction and angiogenesis. The hydrogels exhibit slow degradation and optimal tissue integration. Enhanced angiogenesis was observed due to a pro-angiogenic molecule released during hydrogel degradation.

In the second part of the thesis, one of the studied hydrogels was used to coat the gold electrode functionalised with enzyme: the selection of the enzyme (bilirubin oxidase) was based on in vitro stability studies. In parallel, the process of the coating was optimised, both for uniformity and thickness. Although a thicker coating should protect the electrode against foreign body reaction, it was necessary to limit the thickness to maintain efficient analyte and oxygen diffusion.

Ongoing experiments described in the last part of the thesis are focused on the optimisation of implantation in rat and measurement of the biofuel cell activity. Also, the electrodes were connected to an antenna for wireless communication; indeed, such a device would allow for non-invasive measurement of enzyme activity.

To conclude, this work allowed for the identification of a hydrogel that can be used to coat the electrodes of biofuel cells. The by-product released during the biodegradation favours angiogenesis in the vicinity of the material. Thanks to this coating, we can, therefore, expect an enhanced exchange of analytes and oxygen, which is a prerequisite for enzyme activity.

Keywords: hydrogels, biofuel cells, functionality, biocompatibility, foreign body reaction.

This dissertation was submitted to the *École Doctorale Sciences de la Vie et de la Santé* of the University of Bordeaux in fulfilment of the requirements for the degree of Doctor of Cell Biology and Pathophysiology.

The work presented in this dissertation was developed in *The Laboratory for the Bioengineering of Tissues - Institut national de la santé et de la recherche médicale* (INSERM U1026 – “BioTis”) under the supervision of Doctor Olivier Chassande and Doctor Claudine Boiziau and supported by funds from the LabEx *AMADEus and ANR*.

The results presented in this dissertation are submitted or in preparation for future submission to international peer-review scientific journals:

Note: the data presented in this dissertation is partially formatted according to the style of the journals of publication with minor modifications.

ACKNOWLEDGEMENTS

It is a pleasure to thank many people who made this thesis possible.

Very special gratitude goes out to all down at AMADEus Fellowship, for helping and providing the funding for the work providing support for my PhD program, international conferences and collaborations.

My deepest gratitude goes to my supervisors: Dr Claudine Boiziau, Dr Olivier Chassande, Prof. Philippe Barthelemy, Dr Nicolas Mano and Prof. Alexander Kuhn. Your patient guidance, encouragement and advice have been beyond enough to see me through this amazing but challenging journey. The great efforts you put at improving this manuscript humbles me, and I will forever be grateful.

I express my appreciation for Dr Claudine Boiziau for holding my hand during the most difficult part of my PhD and helping me to finish it.

I am also grateful to the director of the unit Pr Jean Christophe Fricain, co-director Dr Nicolas L'Heureux, and Dr Helene Boeuf for their immense support during my hard days in PhD.

I want to thank Sophie for hosting me at home during the beginning of my PhD; I do not have words to express my gratitude towards her.

My stay at BIOTIS was memorable; I would like to thank each one individually for making this happen.

I would like to thank all my PhD colleagues, with whom I have shared moments of deep anxiety but also of big excitement. Their presence was very important in a process that is often felt as tremendously solitaire. I also appreciate Nitin, Chole, Cristina, Lugi and Murielle for helping me with my experiments.

I am very thankful to Dr Nicolas Mano and the members of CRPP, specially Sabrina and Emmanuel and Magdalena for their incredible support.

During this journey, technical supports are considerably important. I thank Sylvie Chatelus and Patrick Guitton for their support.

I would like to show my greatest gratitude towards Prof. Boris Hinz and lab mates at University of Toronto (Nina, Monica and Henna). You guys made my stay at the lab a total bliss.

Some special words of gratitude go to my friends who have always been a major source of support when things would get a bit discouraging: Maruthi, Narendra, and Vijay Bhaskar Reddy. Thanks, guys, for always being there for me.

I would like to thank my Indian friends Harsha, Supriya, and Ram for the amazing trips and a lot of fun that we had together. The evening chats and the food exchange parties with them relieved my home sick.

I am grateful to my parents, sisters and family for their longstanding support from the beginning of my life till today.

Table of Contents

List of Figures

List of Tables

Abbreviations

Introduction to Thesis

1 Introduction

1.1. A brief overview of the biofuel cell

1.1.1. Energy harvesting from the fuel in the body

1.2. Enzymatic Biofuel cell (EBFC)

1.2.1. Enzymes used in electrocatalysis

1.2.2. Enzymes at anode

1.2.3. Enzymes at cathode

1.3. Electron transfer between enzymes and electrodes

1.4. Immobilization method

1.5. Electrochemical principles and analytic methods

1.5.1. Capacitive current

1.5.2. Faradaic current

1.5.3. Cyclic voltammogram

1.5.4. Chronoamperometry

1.6. The implantation sites for BFC: Physiological and Medical aspects

1.7. Physiological practicalities for implantable biomaterial/medical devices.

1.8. Host tissue response

1.8.1. Acute inflammation in FBR cascade

1.8.2. Chronic inflammation in FBR cascade

1.8.3. Macrophages

1.8.4. Fibrosis and Fibrous capsule formation

1.9. Strategies to improve biocompatibility

- 1.9.1. Modification to reduce protein adsorption
- 1.9.2. Angiogenic drugs
- 1.9.3. Steroidal and non-steroidal Anti-inflammatory drugs
- 1.9.4. Biocompatible material coatings

1.10. **Hydrogels**

- 1.10.1. Classification of hydrogels
 - 1.10.1.1. Natural and synthetic hydrogels
 - 1.10.1.2. Physical and chemical hydrogels
- 1.10.2. Properties of hydrogel
 - 1.10.2.1. Swelling properties
 - 1.10.2.2. Permeability properties
 - 1.10.2.3. Mechanical properties
 - 1.10.2.4. Theory of elasticity

- 1.11. Biocompatibility assessment

2 **Hypothesis and objective of the work**

3 **Results section**

1. **Article:** Low molecular weight hydrogels and their biocompatibility (articles)
 2. **Article:** Low molecular weight hydrogels and their biocompatibility (articles)
 3. **Electrochemical measurement of the Biofuel cell**
 - 3.1 Functionalization of electrodes
 - 3.2 Optimisation of the cathode electrode for its function using bare electrode
 - 3.3 Subcutaneous implantation of the cathode electrode in mice
 4. **Progress in the Biofuel cell functionality.**
 - 4.1 Optimisation of subcutaneous implantation of electrodes in rats
 - 4.2 Wireless detection
 - 4.3 Subcutaneous implantation of complete biofuel cell in rat and continuous wireless measurement
-

4 **Discussion**

5 **Conclusion and outlook**

List of Figures

Figure 1. 1: Examples of batteries based-implantable devices.	26
Figure 1. 2: Various form of energy in the human body	28
Figure 1. 3: Scheme of an EBFC utilising immobilised enzymes at the anode and cathode	29
Figure 1. 4: Structure of the MCO	32
Figure 1. 5: Crystal structure of Bilirubin oxidase PDB ID:2XLL	33
Figure 1. 6: Schematic representation of the electron transfer mechanism of glucose oxidase	34
Figure 1. 7: Schematic image of the electron transfer mechanism of bilirubin oxidase (BOD)	34
Figure 1. 8: Schematics of enzyme immobilisation techniques	37
Figure 1. 9: Electrode-electrolyte interface acting as a capacitor	39
Figure 1. 10: Schematic representation of electron transfer in the faradaic current	40
Figure 1. 11: A cyclic voltammogram scan	40
Figure 1. 12: A standard chrono-amperometry scan	42
Figure 1. 13: Progress in the implantation of EBFC in various organisms	44
Figure 1. 14: EBFC implanted at a different site in living animals	47
Figure 1. 15: Cascade of events during innate host immune response after biomaterial	49
Figure 1. 16: A schematic view of the Vroman effect on the surface	50
Figure 1. 17: Overview of the interactions between neutrophils and biomaterials	52
Figure 1. 18: Schematic representation of monocyte migration to biomaterial/tissue interface	53
Figure 1. 19: Summary of different macrophage phenotypes	54
Figure 1. 20: Scheme of macrophage response to biomaterials	55
Figure 1. 21: The host response to the degradable and non-biodegradable material	58
	14

Figure 1. 22: Scheme explaining the hypothesis that non-specific protein adsorption	60
Figure 1. 23: Timeline of advancements in biomaterials and hydrogels	64
Figure 1. 24: Classification of hydrogels	65
Figure 1. 25: Thermo-responsive hydrogels:	67
Figure 1.26: Brief overview of the steps involved in the translation of newly developed biomaterials from bench to bedside	78

List of Tables

Table 1. 1: The power requirement of different IMDs in comparison with the main characteristics of modern batteries	26
Table 1. 2: Summary of the most common enzymes at bianode	35
Table 1. 3: Comparison of different immobilisation techniques	37
Table 1. 4: Summary of maximum power generated/harvested	44
Table 1. 5: Summary of most commonly used materials for biomedical applications	62
Table 1. 6: Natural and synthetic monomers for hydrogel preparation	66
Table 1. 7: Summary of materials, crosslinking and their applications	69
Table 1. 8: Physical properties of hydrogels and their applications in tissue engineering	73
Table 1. 9: Cell viability tests and their advantages and disadvantages	75

Abbreviations

bFGF	:	Basic fibroblast growth factor
BOD	:	Bilirubin oxidase
CE	:	Counter electrode
CSF	:	Cerebrospinal fluid
CV	:	Cyclic voltammogram
DAMPs	:	Damage associated molecular patterns
DET	:	Direct electron transfer
EBFC	:	Enzymatic biofuel cell
FAD	:	Flavin adenine dinucleotide
FADH ₂	:	Flavin adenine dinucleotide hydrogen
FBGC	:	Foreign body giant cells
FBR	:	Foreign body response
GO _x	:	Glucose oxidase
IGF-1	:	Insulin-like growth factor-1
IMD	:	Implantable medical device
ISO	:	International standard of organization
LCST	:	Low critical solution temperature
LMWH	:	Low molecular weight hydrogel

MC	:	Methylcellulose
MCO	:	Multicopper oxidase
MET	:	Mediated electron transfer
MMP-9	:	Myeloperoxidase, matrix metalloprotease-9
MvBOD	:	Myrothecium verrucariabilirubin oxidase
NET	:	Neutrophil extracellular traps
NIPA	:	N-isopropylacrylamide
NRU	:	Neutral red uptakes
PAA	:	Polyallylamine
PCL	:	Poly caprolactone.
PEG	:	Polyethylene glycol
PEO	:	Poly(ethyleneoxide)
PHEMA	:	Poly(2-hydroxyethyl methacrylate)
PLA	:	Poly(lactic acid)
PLGA	:	Poly(lactic-co-glycolic) acid
PVA	:	Polyvinyl alcohol
PVI	:	Polyvinyl imidazole
PVP	:	Polyvinyl pyridine
RE	:	Reference electrode

ROS	:	Reactive oxygen species
ROIs	:	Reactive oxygen intermediates
SCE	:	Saturated caramel electrode
TNC	:	Trinuclear center
TNF- α	:	Tumour necrosis factor alpha
UCST	:	Upper critical solution temperature
VEGF	:	Vascular endothelial growth factor
WE	:	Working electrode

Scope of the thesis.

In the present generation, many human beings suffer chronic metabolic diseases that necessitate treatments during their whole life. Among these, diabetes is one of the most prevalent, as it affects many adults and children in developed countries. The administered dose of drugs is based on averages optimised for large populations. In the case of diabetic patients, discontinuous measures of blood glucose and an inappropriate dose of insulin treatment can cause long term deleterious effects and discomfort. To overcome the discrepancy between body needs and drug supply, researchers strive to develop new devices for measuring the real-time key physiological parameters in the patient's body which determine the amount of drug that must be administered.

Considerable progress has also been made in the field of glucose sensors and insulin pumps for the treatment of type I diabetes. Such feedback loop-based individualised, integrated medical systems, comprising an implanted sensor, battery, amplifier, processor, and actuator, are now in use. However, these devices still rely on an external energy source, and they need to replace frequently.

In this field, miniature enzymatic biofuel cells (EBFC) have been the subject of extensive research, to engineer energy-autonomous devices. EBFCs are those which convert chemical energy stored in biomolecules such as glucose, fructose and lactate into electrical energy by utilizing enzymes (Fig. 1). Although the enzymes are highly active and substrate selective, they are associated with insufficient stability. EBFCs differ vastly in terms of size, power (μW to mW) and their targeted application. The power is highly dependent on electrode morphology, including the structure and adsorbed enzymes. These features the EBFCs in specialised niche applications instead of competing with the conventional fuel cell operating with larger electrochemical power source.

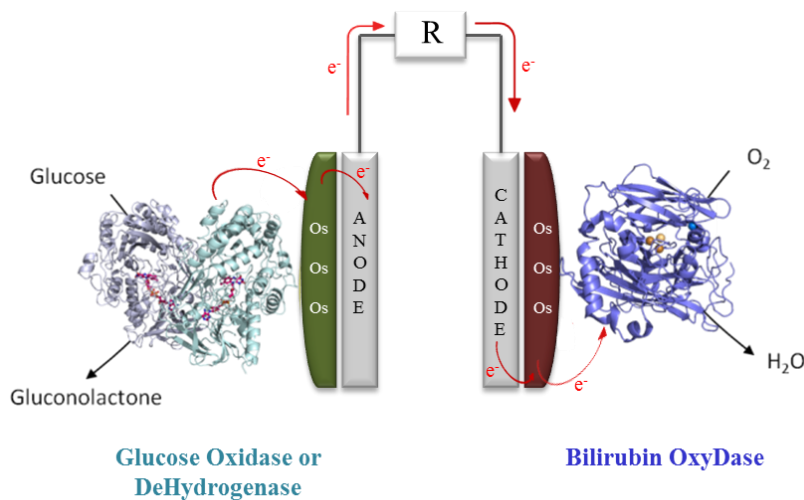


Figure 1: Feedback loop-based individualized EBFC.

The glucose oxidase immobilised at the anode oxidises glucose, the electrons flow to the cathode containing bilirubin oxidase where O₂ is reduced to water.

The need of hydrogels to coat EBFCs.

The major issues concerning the implantable EBFCs include the sensitivity of enzymes towards the hostile environment, biofouling of biological molecules at the surface of the implanted device, and biocompatibility of the device. The performance of implantable medical devices is impeded by the foreign body reaction (FBR), an inflammatory reaction resulting in the formation of a dense fibrous capsule. The thick collagenous capsule isolates the material from surrounding tissue, thereby blocking the mass transport and communication between material and the body. These issues limit the long-term *in vivo* functionality of EBFCs. To address these issues, several types of biocompatible hydrogel coatings are used to enhance their function and biocompatibility(1). Among them, most of the hydrogels are made of polymers, which are either of natural (chitosan,

alginate, silk, hyaluronic acid) or synthetic origin (poly-lactic acid, poly-lactic-co-glycolic acid, poly-ethylene-glycol, poly-vinyl-alcohol) and designed for drug delivery in regenerative medicine. However, there remain several limitations for polymer-based medical device coatings such as a multistep process for preparation (photopolymerization, electrochemically mediated, and radical polymerisation), difficulties in coating the small medical devices as they rely on crosslinker to form a hydrogel, and FBR. As an alternative to polymers, this thesis proposed the use of low molecular weight hydrogels (LMWHs) to coat EBFCs.

Low molecular weight bola amphiphile gelators take advantages over polymers due to their self-assembled, and easy coating to medical devices. These are nucleoside-based small amphiphilic molecules containing hydrophilic moieties attached to both the ends of the hydrophobic hydrocarbon chain. The molecules are generally easy to synthesize, and the formation of gels does not require cross-linking agent instead undergo self-assembly. The self-assembly of these molecules is driven by Π - Π interaction and hydrogen bonding to generate a dense network of fibers. Moreover, the sol-gel transition of these gels is often dependent on physical parameters, which can be used to control gel formation or its transition to a liquid state. It was envisaged that such self-assembled hydrogels would be ideal for biological applications such as medical device coating, drug delivery and tissue engineering due to their injectability. In this thesis, we have evaluated four different LMWHs for their, degradation, fibrosis and angiogenesis, which are crucial before using it for any biological applications. The selected desired hydrogel will be used for coating EBFCs to enhance their functionality and biocompatibility.

INTRODUCTION.1

1 General introduction

1.1 A Brief overview of the biofuel cell

Advances in miniaturised implantable medical devices (IMDs) are increasingly significant for the growth of medical devices. IMD has been utilized for various diagnosis, prognosis and treatment. An IMD can be either active or passive in function depending on whether it requires a power source or not (2). The current biomedical devices implanted in the body such as pacemakers, cochlear implants, defibrillators, insulin pumps, biosensors, etc. (**Table 1.1, Figure 1.1**) operate via an external power source (3). To provide the external power source for such devices, the existing technology is focused on lithium batteries alkaline electrolyte batteries. However, the main limitations of the current batteries include their corrosive nature, their size, and unwanted chemical reactions (4). It is, therefore, necessary to consider the addition of a protective coating to isolate the device from the surrounding environment. Apart from this, the longevity of medical devices relies on the battery shelf life and such batteries have limited lifetime from months to several years and require frequent charging/replacement for their efficient function (5). These limitations encouraged many researchers to find an attractive alternate called enzymatic biofuel cell (EBFC) (6). The EBFCs are electrochemical devices that harvest the electricity from the chemical energy stored in biomolecules *in vivo* such as glucose, sweat, and lactate. The power generated in EBFCs relies on the use of redox enzymes, utilised for charging the implantable device continuously without the need for an external power source (7).

Table 1. 1: The power requirement of different IMDs in comparison with the main characteristics of modern batteries (3).

IMD	Power	Battery lifetime
Pacemaker	10 μ W-30 W	5-7 years
Insulin pump	70 μ W	Up to 5 years
Neurological stimulator	0.03 mW-3 mW	Up to 3 years
Cochlear implant	0.02 W-1W	-
Artificial organs	30 W	Several hours

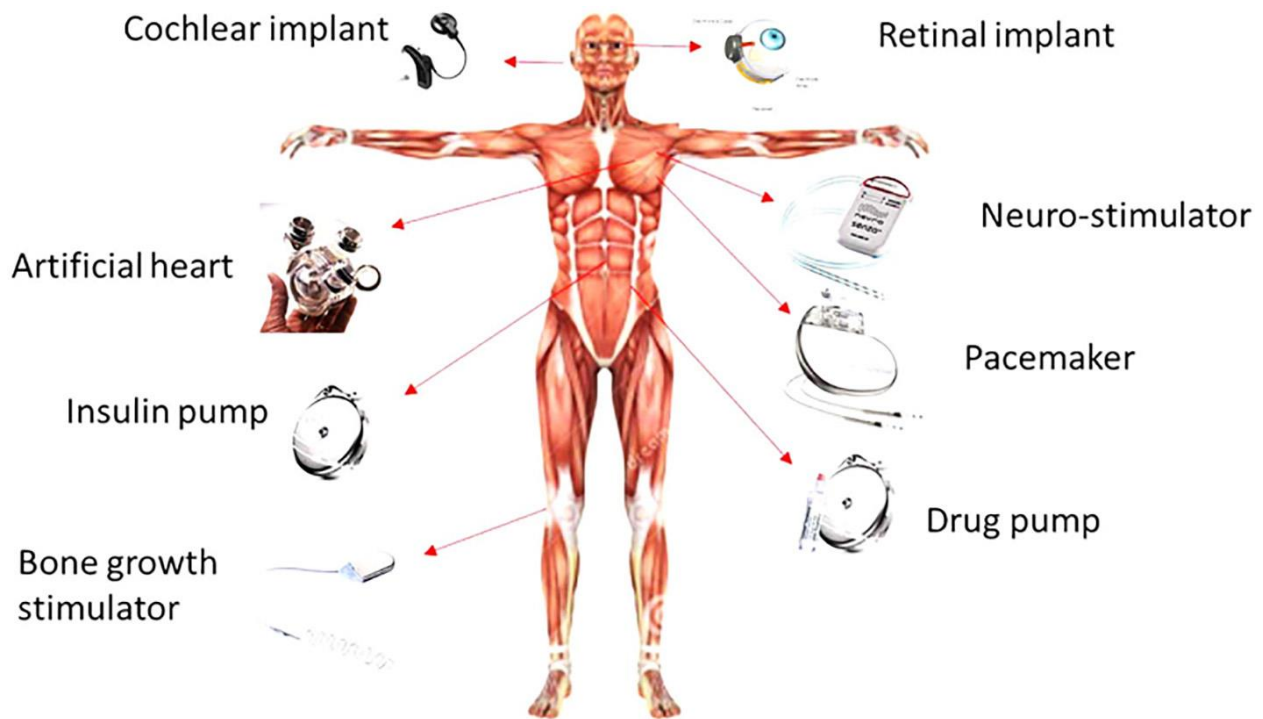


Figure 1. 1: Examples of batteries based-implantable devices (3).

1.1.1 Energy harvesting from biofuels inside the body

The human body generates various forms of energy, for example, chemical energy through glucose and the physical way such as breathing and limb motion. Energy harvesting systems are the devices that convert these forms of energy into electricity for charging the implantable devices. Approximate power generated from various forms is shown in **Figure 1.2**. Based on the amount of energy needed, biofuel cells can be used to power implantable medical devices.

Harvesting the power from biochemical fuel is promising since the electricity generated from chemical energy is >100 W. The constant availability of fuel within the body encouraged the researchers to develop EBFCs. Among various biofuels, glucose is the most commonly used fuel due to its abundance in most of the body fluids (3).

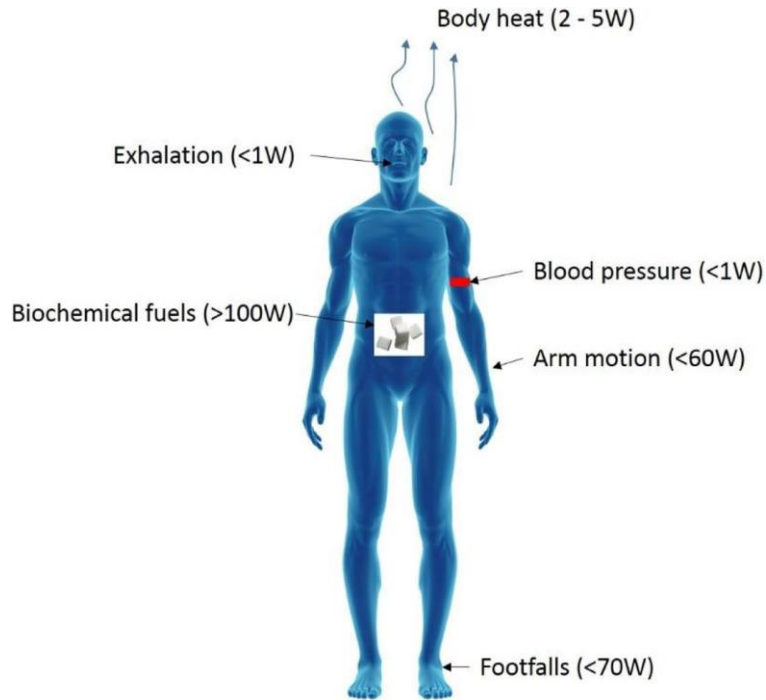


Figure 1. 2: Various forms of energy in the human body (3)

1.2 Enzymatic Biofuel cell (EBFC)

Enzymes are well known as exceptional catalysts due to their high substrate specificity, selectivity, efficiency, and sensitivity. Enzymes are proteins in nature and just like all catalysts, expedite the rate of reaction by lowering the activation energy. To utilize the enzymes for sensors, and implantable devices, immobilisation onto the electrode is primarily essential to achieve electrical connection of enzymes to the electrode surface (8)

The EBFC involves the utilisation of redox enzymes for converting the chemical energy (analytes such as glucose, lactate) into electrical energy using biochemicals present in physiological fluids (9–11). The conversion of biochemical energy is achieved by oxidation, which generates electrons and protons, coupled with reduction by using these electrons and protons at

the cathode. The generated electrons are forced through an external circuit to reach the cathode, while protons diffuse through the electrolyte solution to reach the cathode, thereby maintaining the charge balance and completing the electrical circuit (**Figure 1.3**). Biofuel cells that use biocatalysts are advantageous over chemical fuel cells, as they operate in mild conditions and do not require expensive metal catalysts such as platinum. Although EBFCs hold great potential as miniature medical devices, there are numerous persistent challenges such as improved power density, increased stability and biocompatibility of the device (12,13).

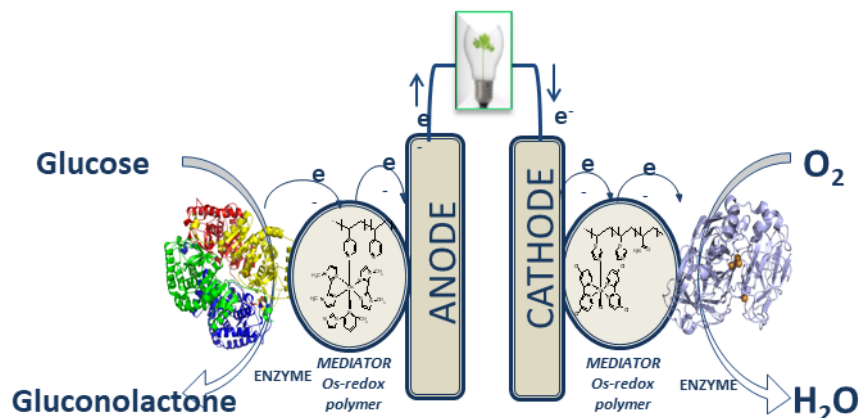


Figure 1.3: Scheme of an EBFC utilising immobilised enzymes at the anode and cathode. The glucose oxidase immobilised at the anode oxidises glucose, the electrons flow to the cathode containing bilirubin oxidase where O_2 is reduced to water.

The work of *Yahiro et al.* (14,15) in 1964 has been considered as the first report of an enzymatic biofuel cell in the literature. The system consists of glucose oxidase at the anode and non-enzymatic platinum cathode with low open circuit potential (175-350mV). However, this pioneering work demonstrated the proof of concept to advance from a simple device to prototypes implanted in living animals, which can power small electronic devices (5,16,17). The selectivity

of enzymatic reaction allows the construction of a single compartment cell containing both anode and cathode upon implantation, which could feed autonomous and implantable medical devices (18,19). Despite the potential application, insufficient power output, stability and incomplete oxidation of fuel limits their utilisation to power larger devices. This instigated many researchers to improve the design, immobilisation, and the performance of EBFCs (8,20).

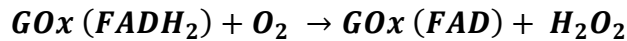
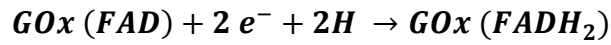
1.2.1 Enzymes as a catalyst

In an EBFC, enzymes employed as catalysts have been isolated from the biological source and wired on either anode or cathode or both electrodes. Bioanode and biocathode utilise the enzymes as biocatalysts for oxidation and reduction of fuel and oxidants, thereby, generating the power (11). The catalysis and the harvesting of energy are enzyme specific, where an oxidoreductase oxidises the fuel to transfer electrons from fuel to anode. Electrons flow to the cathode, where oxidants such as molecular oxygen (O_2), hydrogen peroxide (H_2O_2), or organic peroxides, are reduced by another oxidoreductase (21).

1.2.1.1 Enzymes employed at the anode

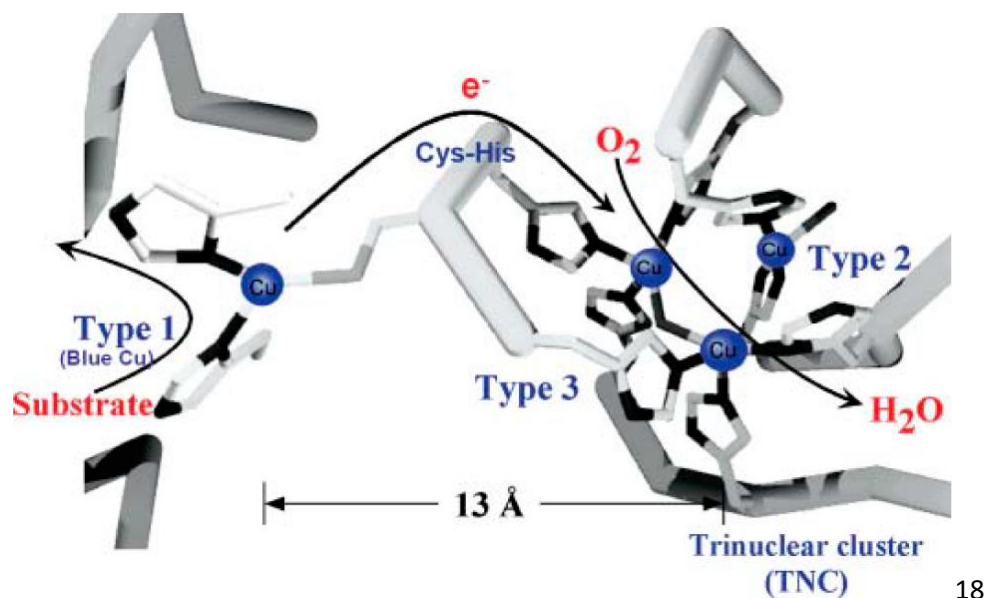
There is a wide range of fuels that can be targeted for enzyme oxidation on the anode. Most of the researchers focused on utilising glucose as a fuel since it is the most abundant fuel available in the body. The most used enzyme for catalytic oxidation of glucose is glucose oxidase (GOx) (22).

GOx is derived from the *Aspergillus niger* (23). It is a well-known oxidoreductase enzyme which catalyses the oxidation of glucose to gluconolactone. The catalytic function is due to the presence of cofactor FAD/FADH₂, as shown in **Figure 1.4** (22).



1.2.1.2 Enzymes employed at the cathode

A class of multicopper oxidase (MCO) such as laccase and bilirubin oxidase (BOD) have been received much attention as a biocatalyst at the cathode (24). MCOs can reduce four electrons of oxygen to water at the relatively high reduction potential and under mild condition. MCOs contains four copper ions, T1 is the primary site that accepts the electrons from the electrode. The electrons are further transferred to trinuclear copper T2/T3 cluster (TNC) where molecular oxygen is reduced to water (Fig. 1.5) (25).



18

Figure 1.4: Structure of the MCO active site with arrows showing the flow of substrate, electrons (e^-), and O_2 . Copyright 2012 Royal Society of Chemistry (25)

BOD catalyses the oxidation of bilirubin to biliverdin, concomitantly reducing oxygen to water in a four-electron reduction system. BOD was isolated from different sources such as *Myrothecium verrucaria*, *Magnaporate orzae*, and *Bacillus pumillus* (26–28). The enzyme consists of 4 redox active copper atoms; T1 where the substrate oxidation occurs and tri-nuclear T2/T3 in which oxygen is reduced to water. A *Myrothecium verrucaria* bilirubin oxidase (MvBOd) is a first reported BOD based oxygen-reducing cathode (26,29,30), from then BOD has gained much interest as an ideal candidate for EBFC as it works under physiological conditions for reduction of oxygen at the cathode.

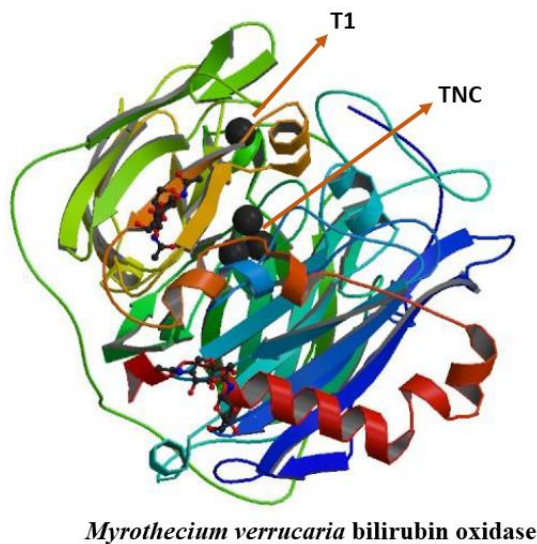


Figure 1. 5: Crystal structure of Bilirubin oxidase (PDB ID:2XLL) (26)

1.2.2 Electron transfer between enzyme and electrode

The sensitivity and the overall performance of the biofuel cell depend on the efficient electron shuttle system from the enzyme to/from the electrode surface. As we know, the enzymes are proteins in nature with high molecular weight, the active centre of the enzyme is located either on the surface or several angstroms deep from the surface in the protein. Thus, the efficient electron shuttle system relies on the distance of the redox centre of the enzyme and the electrode surface (31,32). Different strategies corresponding to the electron transport system, such as direct electron transfer (DET) and mediated electron transfer (MET) have been used, as shown in **Figure 1.6** and **1.7**. In DET, the electrons are transferred directly from enzymes to the electrode surface. Whereas in mediated electron transfer, the electrons are shuttled through the redox mediators. Polyvinyl imidazole (PVI), polyallylamine (PAA) and polyvinyl pyridine (PVP) complexes of osmium, ruthenium, iron (II) are generally used as a mediator for electron transfer (21,33–35).

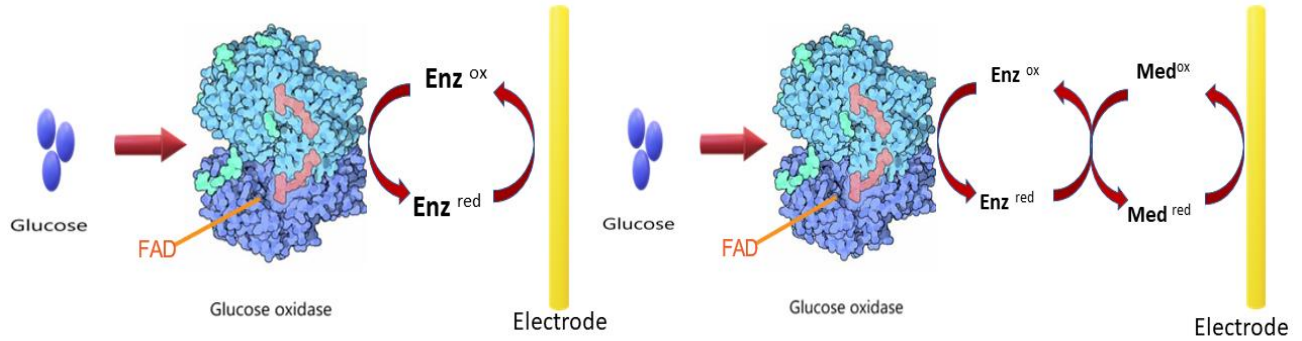


Figure 1.6: Schematic representation of the electron transfer mechanism of glucose oxidase (GOx) showing the direct and mediated electron shuttle system at the anode surface.

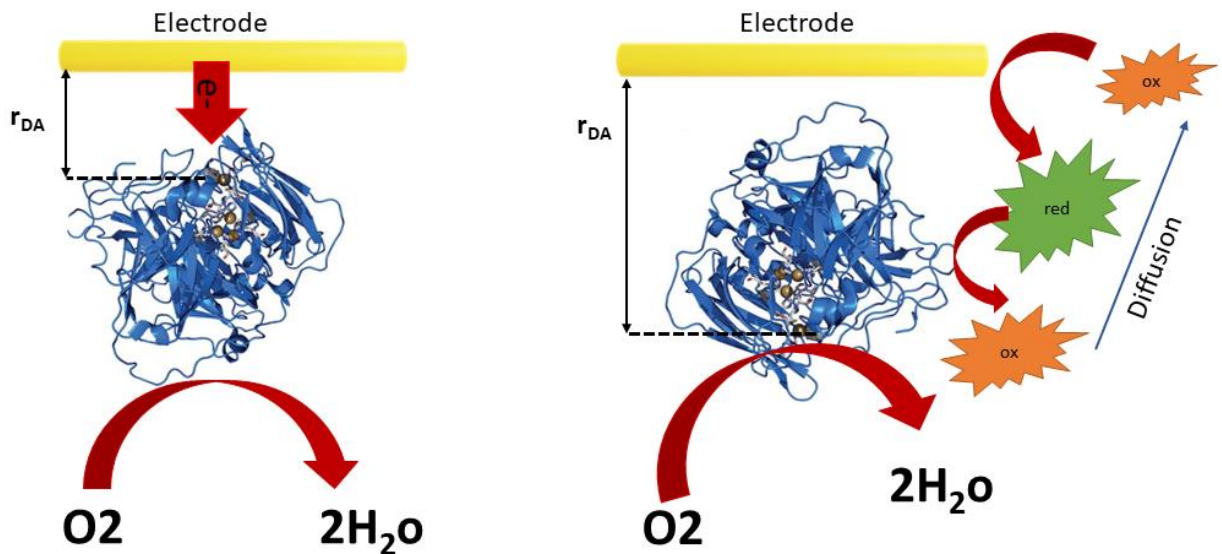


Figure 1.7: Schematic image of the electron transfer mechanism of bilirubin oxidase (BOD) showing the direct and mediated electron shuttle system at the cathode surface (25)

The selection of DET or MET method is based on the location of an active centre of the enzyme (**Figure 1.7**). For a few enzymes such as glucose oxidase (**Figure 1.6**) at the anode, the redox centre FAD/FADH₂ is deeply buried inside the enzyme. To overcome the distance of electron

transfer, MET is employed when the distance between the active centre of enzyme to the electrode surface is greater than 15 angstroms (**Table 1.2**). The mediator assists in the rapid transfer of electrons continuously between enzyme and the electrode by undergoing oxidation and reduction. The efficiency of mediator depends on its redox potential; it should be as close as the potential of the redox enzymes. The literature indicates that for optimal performance of EBFC, the potential difference between the mediator and the redox centre of the enzyme lays around 50mV (12). Also, the mediator should have an approximate potential to show oxidation and reduction without interfering with the analyte and oxidant electrochemical reaction, and the chemical stability is vital in both oxidation and reduction state of a mediator.

Table 1. 2: Summary of the most common enzymes at bianode. (36)

Enzyme	Cofactor	Electron Transfer Mechanism	Substrate
Glucose oxidase	FAD	MET	Glucose
Glucose dehydrogenase	NAD	MET	Glucose
Glucose dehydrogenase	PQQ	ET	Glucose
Glucose dehydrogenase	FAD	DET	Glucose
Lactate oxidase (LOx)	FAD	MET	Lactate
Lactate dehydrogenase	NAD	MET	Lactate
Cellobiose dehydrogenase	-	DET	Glucose
Alcohol dehydrogenase	NAD	MET	Alcohol

1.2.3 Immobilisation methods

During the immobilisation technique, enzymes can undergo substantial changes with the surface microenvironment, conformational change and protein refolding, which can lead to the diminished activity and stability of the enzyme (37,38). Hence, the critical consideration for immobilising the enzyme onto the electrode requires proper selection of an attachment method, where the active centre of enzymes is appropriately oriented towards the support for an effective electron transfer. The principal techniques for immobilisation of enzymes onto the support includes entrapment, adsorption, and covalent coupling /crosslinking, as shown in **Figure 1.8 and Table 1.3**. Adsorption involves physical methods, in which enzymes attach to the surface through weak interactions such as hydrogen bonds, Van der Waals forces, ionic bonding, affinity bonding and hydrophobic interaction with the support material (39,40). Covalent crosslinking involves chemical methods by forming covalent bonds with thioester, amide and carbamate bonds (38,41). The ideal choice of immobilisation technique depends on the support and complex nature of the protein structure.

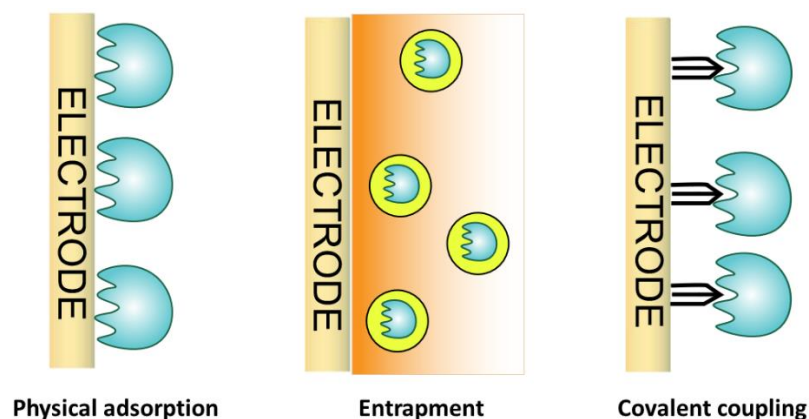


Figure 1.8: Schematics of enzyme immobilisation techniques a) physical adsorption, b) entrapment, c) covalent coupling.

Table 1.3: Comparison of different immobilisation techniques. (40,42,43)

Immobilisation method	Stability permanence	Complexity	Time	Electron transfer
Van der Waals adsorption	Very low	Low	~24h	DET/MET
Ionic bonding	low	Low	~24h	DET/MET
Affinity binding	Variable (sensitive to pH)	Variable (on surface area)	~24h	DET/MET
Electrostatic attraction	Variable (sensitive to pH and charge)	Low	< 1h	DET/MET
Covalent coupling	Irreversible	High	h to days	DET/MET
Gel encapsulation	Irreversible (mediator leaching possible)	High	72h to weeks	MET
Sandwich entrapment	Irreversible	Variable	< 1h	DET/MET
Microencapsulation	Irreversible (improved pH resistance)	High	~24h	DET/MET

1.3 Electrochemical principles and analytical methods

Electrochemistry is the study of exchange between electrical and chemical energy. The electrochemical processes utilise oxidation and reduction reactions. Oxidation is the loss of electrons from a chemical species, while a reduction is the gain of n electrons by a chemical species. When oxidation and a reduction are paired together in a redox reaction; electrons can flow from the oxidised species to the reduced species via redox agents.

The experiment is performed using a potentiostat comprising three electrodes: a working electrode (WE), reference electrode (RE) and counter electrode (CE). The working electrode is generally made of an inert carbon, graphite or inert metals such as glassy carbon, platinum and gold. The reference electrode is usually the silver/silver chloride (Ag/AgCl) (44) or a saturated calomel electrode (SCE). The platinum wire is generally used as a counter electrode, with enough surface area without limiting the flow through the working electrode (45,46). The potential difference is measured between the WE and the RE, while the current is monitored between WE and CE.

A brief description of the basic principles of electrochemistry analysis adopted in the experiments is discussed in the following sections.

1.3.1 Capacitive current

The capacitive current is also called as "non-faradaic" or "double-layer" current. Capacitive current is generated by the events occurring within small distance at an electrode surface. It does not involve the flow of electrons (Charge transfer). However, the processes such as adsorption and desorption can occur at the electrode-solution interface with changing potential or solution

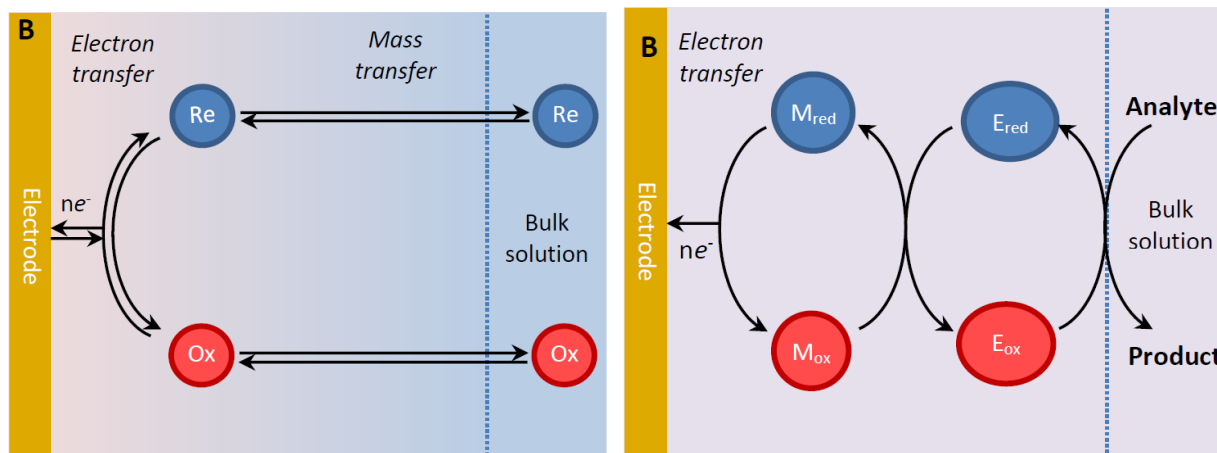


Figure 1.10: schematic representation of electron transfer in the faradaic current.

1.3.3 Cyclic voltammetry (CV)

Cyclic voltammetry is one of the widely used electrochemical technique to characterize the reduction and oxidation processes of reactions. It can also determine the capacitance of the electrode in the given electrolyte solution, as well as the potential of the electrode surface and the bulk reaction at which the reaction is taking place (45,47). An illustration of the voltammogram is provided in **Figure 1.11**.

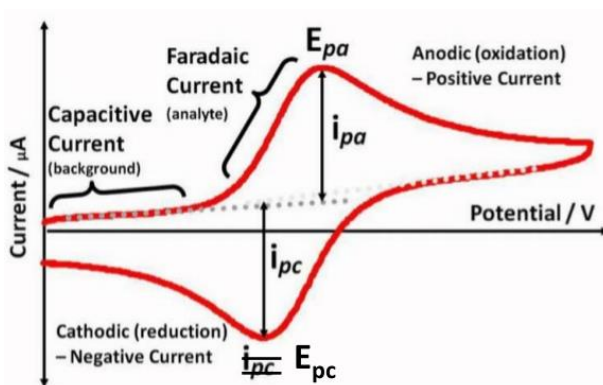


Figure 1.11: A cyclic voltammogram scan.

As observed in Figure 1.11

- A capacitive current resulting from redistribution of charged and polar species at the electrode surface, and
- Faradaic current, the increase in the voltage intensifies the current until it reaches the oxidation peak (anodic peak). When the reactants become diffusion limited, the current drops to a lower and sometimes constant value, while reversing the sweep results, the reduction of the oxidised species and a cathodic peak is recorded.

Depending on the shape of the curve and the number of scans, it is possible to determine whether the reaction is reversible or irreversible.

1.3.4 Chrono-amperometry

Chrono-amperometry works under constant potential held at the working electrode, while the current flow is monitored over time (**Figure 1.12**) (48). The method is used to check if the current remains stable at the given concentration of an analyte or decays with time.

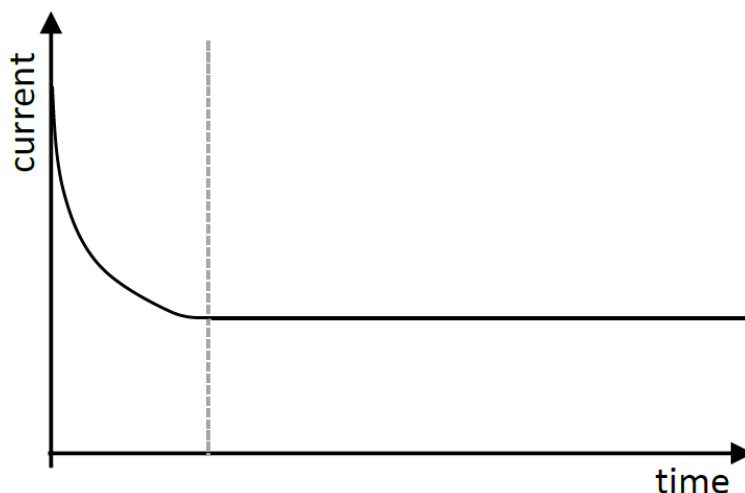


Figure 1.12: A standard chrono-amperometry scan.

From the typical scan, it is observed that at the beginning of a scan, a relatively large current is observed followed by a rapid decay and a plateau (no more decline) in the current. The decrease is due to either the system's capacitance (i.e. the flow of current from a sudden shift in potential difference) or to the formation of a diffusive layer as the supply of reactants at the surface is rapidly exhausted (49). The Plateau in the current signifies that no further reactions are taking place and thus the current was solely due to the electrode surface itself acting as a reactant (e.g. due to metal oxidation).

1.4 The implantation sites for EBFC: Physiological and medical aspects

Significant advances on enzymatic biofuel architecture, the stability of the enzymes, and wiring of enzymes on electrode have led to the development of a wide range of prototype EBFCs, which have been proven to generate power in living organisms (**Figure 1.13**) for a short period (17,50). One of the critical elements for the implantation of the biofuel cell is the selection of the desired implantation site (3). The selected implantation site should contain an adequate amount of analyte and substrate. It should replenish the formed catabolites efficiently, without accumulating at the site. Further, the vital consideration for the implantation site is the biofouling process, which should not be augmented at the site since biofouling hinders the exchange of analytes between the electrode and the surrounding tissue.

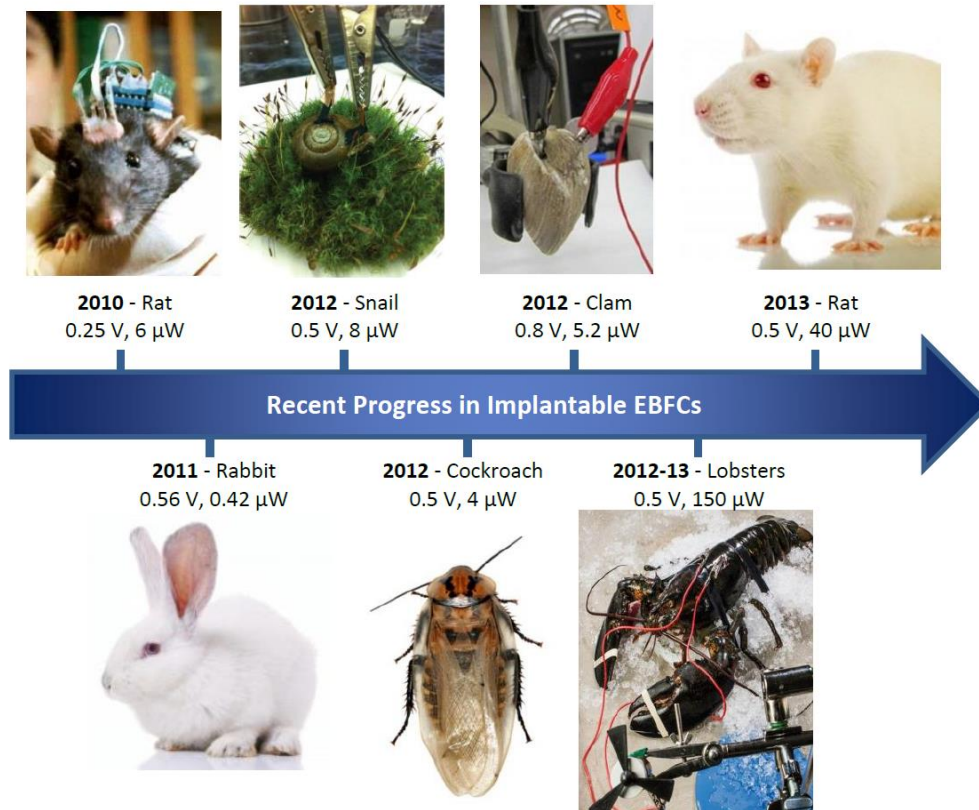


Figure 1.13: Progress in the implantation of EBFC in various organisms (51).

Based on these considerations, as mentioned earlier, the various research groups attempted multiple efforts to develop and implant EBFCs at different sites in animals (**Figure 1.14, Table 1.4**). The first biofuel cell implanted in a living system was by Mano in 2003 (52) while Cinquin and coworkers (53) were the first to harvest the power from an animal by implanting the EBFC in retroperitoneal space of Wistar rat.

Miyake and coworkers (54) implanted the electrodes in the rabbit ear for a short duration (1hr) while placing the cathode at the surface (air breathing electrode). This implantation has the advantage to circumvent the limitation of low oxygen issues in the body. Another group, from Crespilho (55), implanted modified carbon fibre microelectrodes containing glucose oxidase

on the anode and platinum nanoparticles at the cathode in a rat jugular vein using a polyethylene catheter.

Rapport and coworkers (56) implanted microelectrodes with gold nanoparticles in cerebrospinal fluid (CSF). The CSF was considered due to its limited cell content and low protein concentration (0.02 to 0.04 %), while in plasma it is 8 %. However, the limitation with this site poses difficulties in miniaturising the device. Also, the low buffering capacity of CSF might affect the function of the cathode due to an acidic environment created by gluconic acid produced during the oxidation of glucose.

Katz and group (57) have tested the multiwalled carbon nanotube electrodes in cremaster muscle of rat as an implantation site, considered as a highly vascularized region of the body with enough oxygen supply (58). Nevertheless, the implantation was only for a short duration.

In the group of Cinquin, Cosnier *et al.* (59) tested in 2014 the implantation of a prototype biofuel cell in the intraperitoneal space. In this study, the connection was tunnelled subcutaneously to the rat neck to connect to the potentiostat for electrochemical measurement. In previous studies, more than two decades ago, researchers provided proof about the abdominal cavity as an implantation site. The site contains an extracellular fluid; the movement of organs facilitates the diffusion of oxygen and the analyte.

Later, Cadet *et al.* performed in 2016 the glucose/O₂ biofuel activity in human blood (60). Design of anode and cathode was made with osmium redox polymer, a mediator to shuttle the electrons effectively. The progress opens the way for future research to test the functionality of EBFC in human blood as a step forward before *in vivo* implantation.

Despite the encouraging progress in the implantation and the performance, there exist several unmet challenges. One of the significant limitations includes the stability of enzymes. Cosnier *et al.* (61) achieved the most extended operation *in vivo* until three months in the rat. These studies opened the way by providing proof of concept to harvest the power by EBFCs. Further optimisation of the system is still required to produce enough energy for an extended period.

Table 1. 4: Summary of various implantation sites with operational lifetime (53,55,56,62,63).

Animals /Location	Operational lifetime
Rat retroperitoneal space	11 days
Rat/brain	9 days
Clam/dorso-posterior part	< 1 week
Snail/ between the body wall and internal organs	2 weeks
Rat/jugular vein	24h

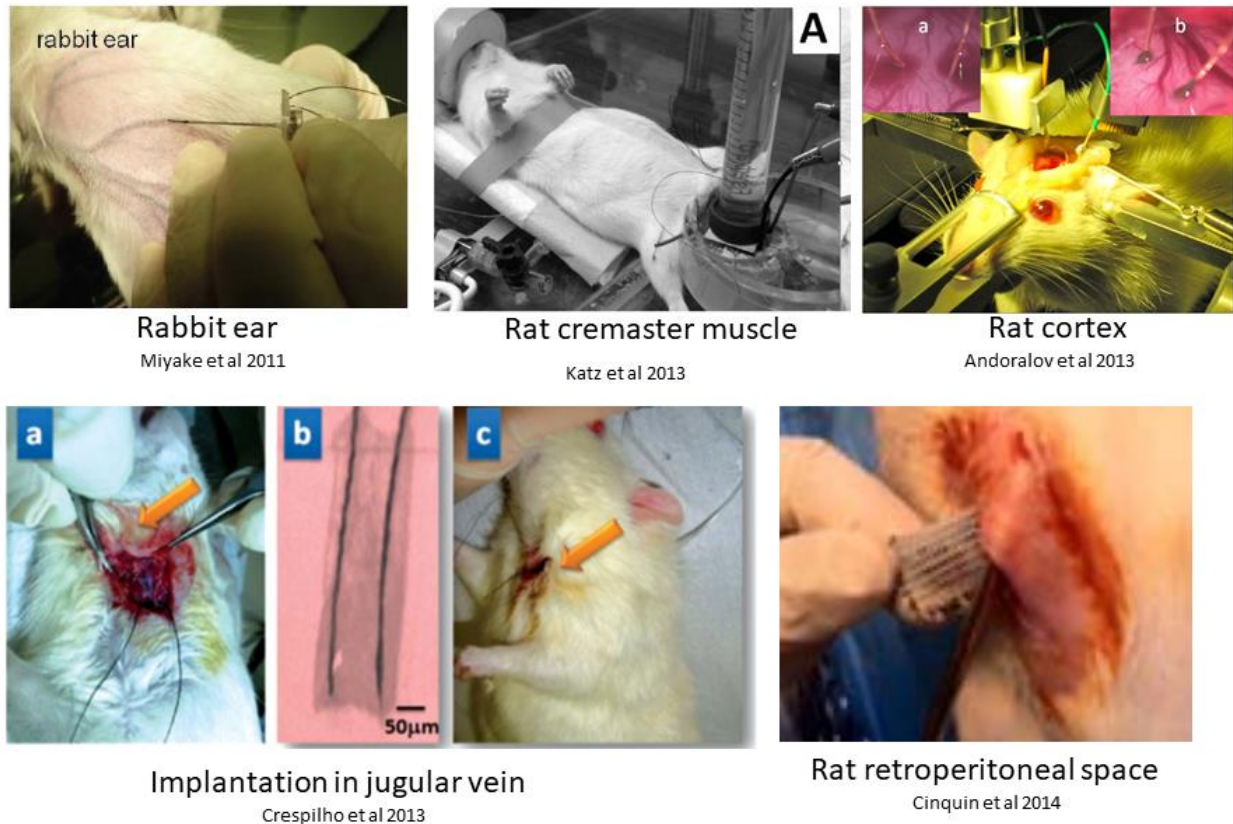


Figure 1. 14: EBFC implanted at different sites in living animals.

1.5 Bottlenecks for the implantable EBFC concerning the stability of chemical components

The main task of the EBFC is to generate enough power to charge the IMD for an extended period. This last requirement presents quite a challenge for implantable EBFCs that need to operate under physiological conditions. Enzymes are the main components and unfortunately, the labile constituent of the biofuel cells. They are sensitive to pH, ionic strength, and temperature and alteration of factor mentioned above lead to the deactivation of the enzyme resulting in the decreased power output. Apart from enzymes, various other factors influence the reduction of current density such as instability of the mediator, which affects efficient electron shuttle to the

active centre (co-factor) of the catalyst, biofouling and foreign body response. The variability of the mediator is the second most significant issue, the frequent loss of ligands after several cyclic scans reduce the active electron shuttle. Next is the sterilisation technique, as the sensitivity of enzymes hinders the use of standard sterilisation techniques (50,64).

1.6 Physiological practicalities for implantable biomaterial/medical devices

Another challenge frequently encountered is biocompatibility of the implanted EBFC. The limited *in vivo* functionality and the longevity of any medical device/biomaterial over time is still a critical issue to overcome. It is prerequisite to understand the response of a host towards any implanted material to avoid failure of devices (65).

Implantation of either non-degradable or degradable material at any site of tissue inside the body inevitably triggers the immune response. Although the initial stages of host reaction for degradable and non-degradable materials remain the same such as tissue damage during implantation and protein adsorption to the surface of the material (66), later phase of the host response undergoes quick transition depending upon the type of material being implanted. The stages involve cellular and molecular events of the innate and adaptive immune system, which determine the fate of the healing process, i.e., the formation of encapsulation or scar formation or constructive remodelling.

For both degradable and non-degradable material, implantation results in the foreign body reaction, depending on surface topography, mechanical properties, and chemical composition. The different stages of foreign body reaction include protein adsorption, provisional matrix formation, acute inflammation, chronic inflammation, granulation tissue formation, and fibrosis. Each event involves the complex interplay of inflammatory cells, cytokines, chemoattractants, and

biomaterial. The overall scheme of the innate immune response towards biomaterial is depicted in **Figure 1.15** and will now be explained in detail.

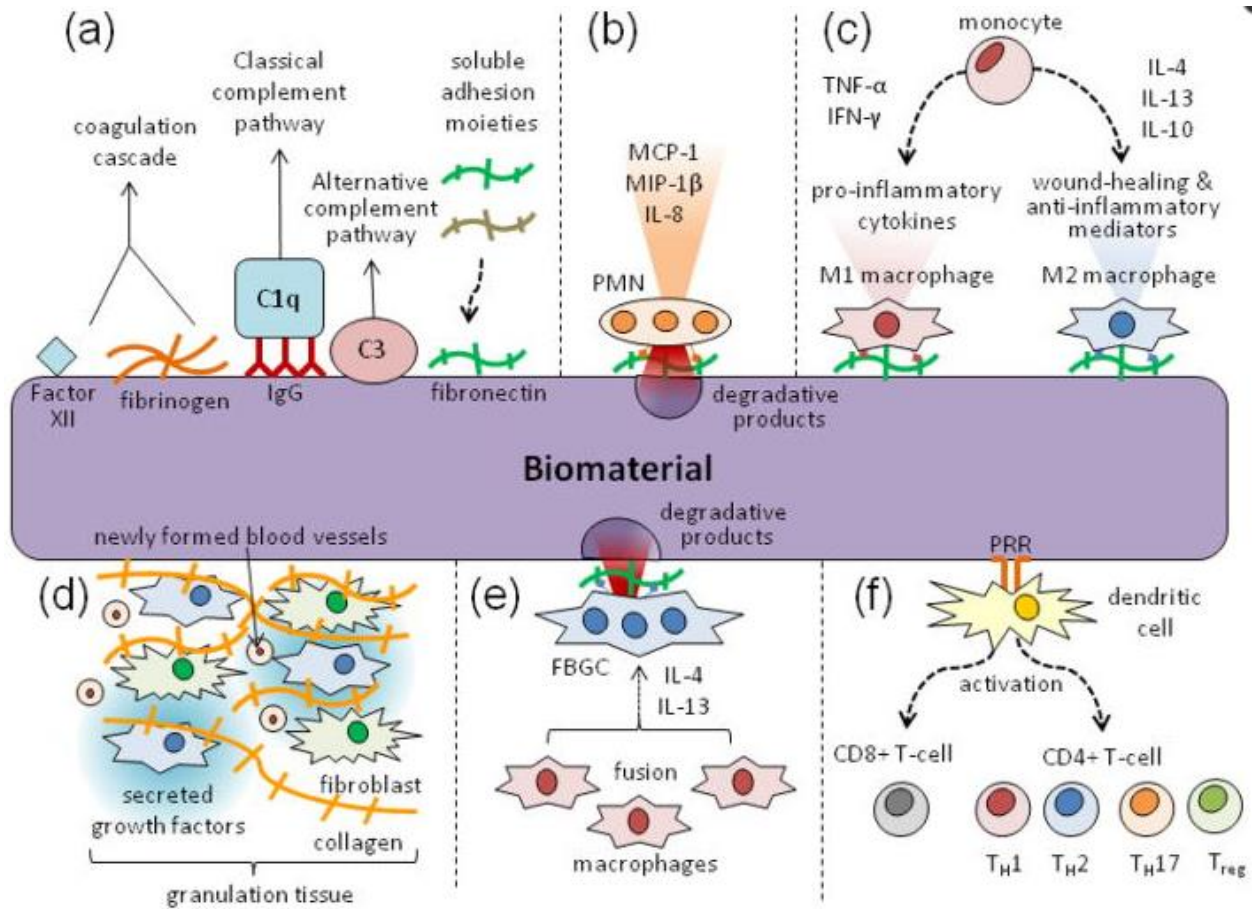


Figure 1.15: Cascade of events that occur during innate host immune response after biomaterial implantation. (a) Protein adsorption onto the material and activation of complement system (b) neutrophil recruitment and its release of cytokines and chemoattractants, which degrades the material (c) migration and infiltration of macrophages depending on the type of material, M1 to M2 macrophage polarisation to tissue remodelling and vascularization (d) formation of granulation tissue (e) fusion of macrophages to form giant cells and activation of adaptive immune system (67). Host cellular responses to implanted materials

1.6.1 Adsorption of plasma proteins

Implantation of biomaterials or medical devices in any vascularised connective tissue leads to the adsorption of proteins (66). The Vroman effect (**Figure 1.16**) explains the adsorption of protein on to the surface of the material. When the material is exposed to human serum consisting of many proteins, small, mobile and highly concentrated proteins tend to adsorb first on the surface, and then are displaced by larger and high-affinity proteins.

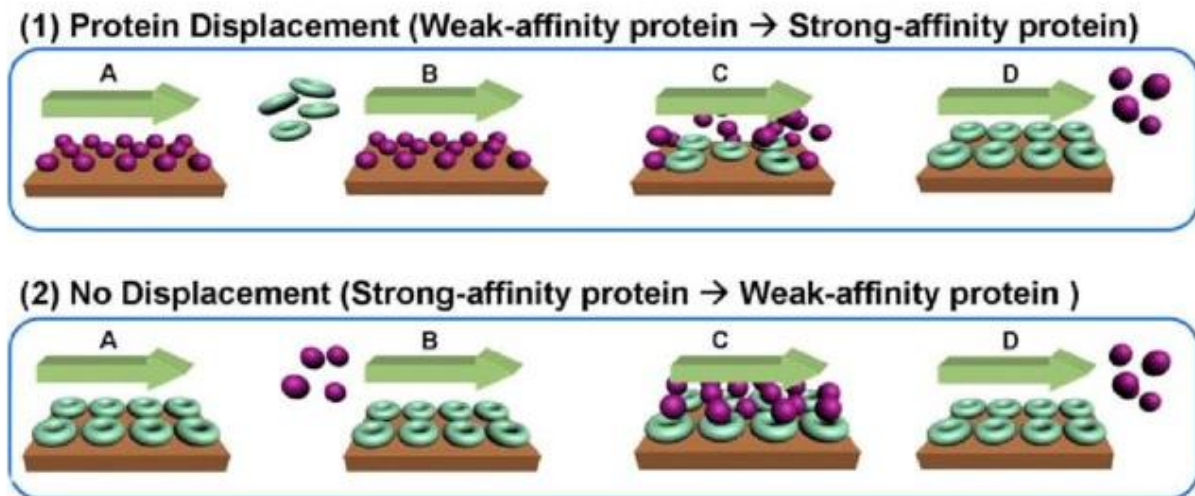


Figure 1.16: A schematic view of the Vroman effect on the surface: when a weak- affinity protein adsorbs first, and then a strong-affinity protein arrives at the surface later, protein displacement occurs. The reverse sequence does not occur (68).

Protein affinity varies with different implanted surfaces. For example, hydrophobic surfaces tend to bind more proteins as well as attaching them more tenaciously. Later, adsorbed proteins undergo time-dependent molecular spreading by unfolding/conformational change to expose internal functional groups for interaction with additional binding sites (69).

As a result of protein adsorption, direct interaction of host cells to the material does not occur, but instead, cells interact with an adsorbed protein layer. The adsorbed serum proteins in conjunction with clot formation in homeostatic mechanism results in thrombus formation defined as the provisional matrix around the biomaterial (66). The provisional matrix serves as a ligand site for cell adhesion and mediates the interplay between host cells and the implanted material. In certain types of materials, it also serves as a bridge that facilitates the cellular access and infiltration of host cells into the materials (65,70). The accumulation of certain proteins on the biomaterial surface plays a crucial role in determining the fate of the tissue-implant interface.

1.6.2 Neutrophils

Deposition of the protein layer on the material surface and their unfolding influences the neutrophil activity (71). The implantation or injection of any biomaterial causes the tissue damage resulting in the release of damage-associated molecular patterns (DAMPs) (72). Apart from DAMPs, the damaged endothelial cells and activated platelets secrete various cytokines and potent neutrophil chemoattractants IL-8 and CXCL-4, resulting in the recruitment of neutrophils to the material surface (**Figure 1.17**).

The recruited neutrophils release reactive oxygen species (ROS), granular proteins (myeloperoxidase, matrix metalloproteinase-9 (MMP-9)), various cytokines, CCL2, and CXCL1, CXCL2, which are responsible for degradation, phagocytosis, activation, and recruitment of other inflammatory cells to the material surface (73). The intensity of activation and secretion of neutrophil factors vary with the type of biomaterial implanted.

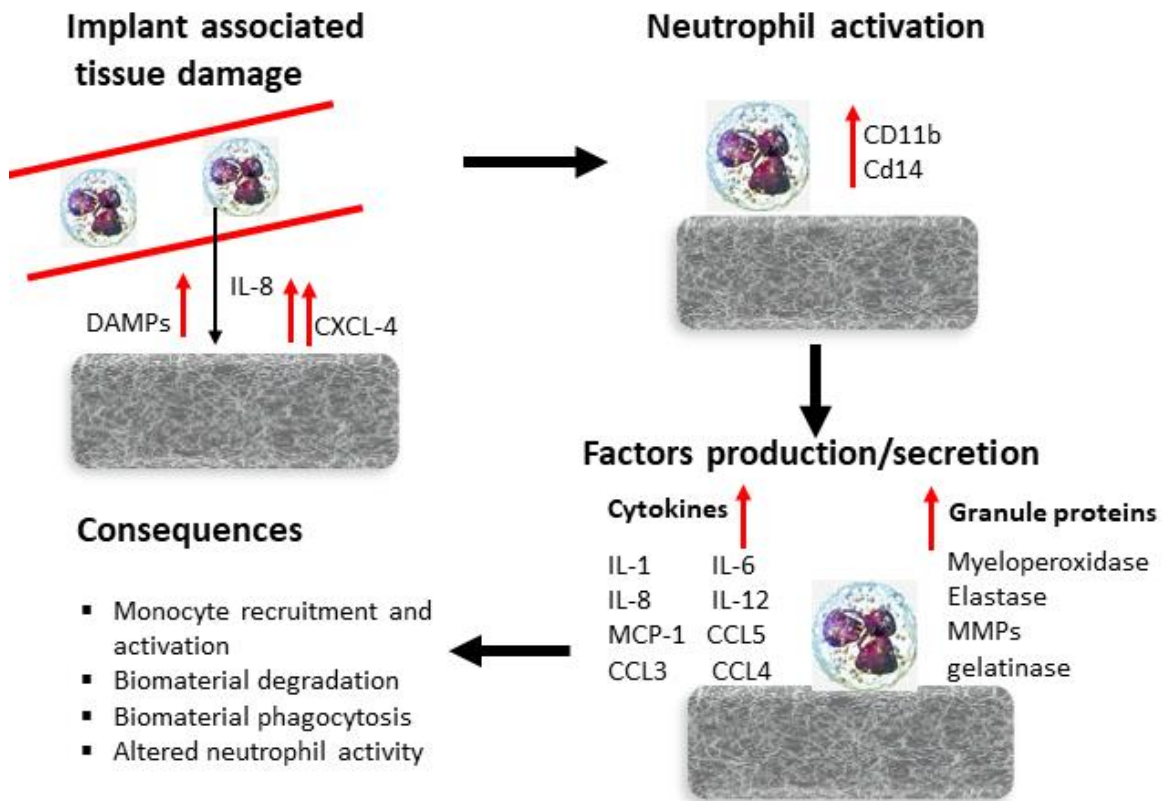


Figure 1. 17: Overview of the interactions between neutrophils and biomaterials and their consequences. Furthermore, neutrophils have also been shown to possess anti-microbial property due to their ability to release chromatin to extracellular space. The released chromatin forms a dense network that can entrap microbes to neutralise them, thereby preventing the spread of infection potentially. The release and formation of chromatin fibres are called neutrophil extracellular traps (NET) (74).

1.6.3 Macrophages

The progression of inflammation and foreign body response results in the migration of monocytes from blood capillaries to the implanted site. The chemokines and chemoattractants guide the migration of monocytes, as depicted in **Figure 1.18**.

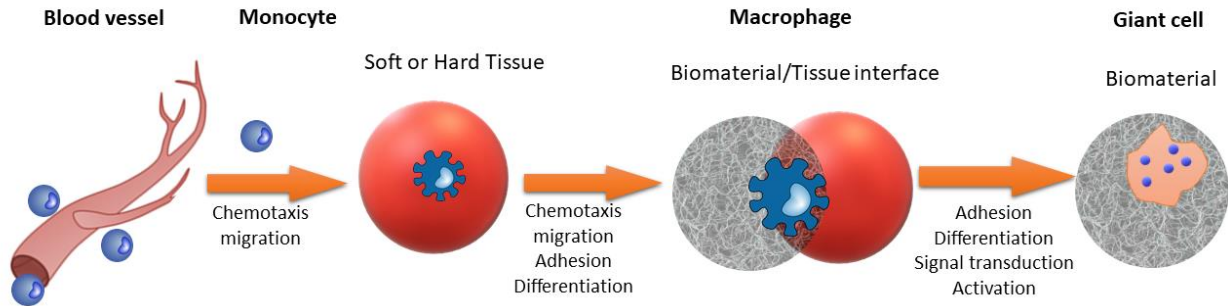


Figure 1.18: Schematic representation of monocyte migration to biomaterial/tissue interface- a fusion of macrophages to foreign body giant cell.

Macrophages are good examples for their plasticity, as they can acquire different phenotypes after their initial activation. The phenotype switching is influenced by the type of material implanted and cytokine release in response to the material (75). Besides, macrophages release multiple factors involved in neovascularisation such as vascular endothelial growth factor (VEGF), basic fibroblast growth factor (bFGF), insulin-like growth factor-1(IGF-1), tumour necrosis factor (TNF- α), and IL-8 (76). Both tissue-resident macrophages and monocytes derived macrophages are known to be involved in resolving inflammation and in promoting vessel growth. In terms of macrophage phenotypes, M1 macrophages, designed as “pro-inflammatory macrophages”, are typically meant to clear the debris by phagocytosis and releases pro-angiogenic factors, while M2 phenotype (“immuno-modulatory”) promotes tissue remodelling and blood vessel growth (67,77) as shown in **Figure 1.19**. During skin, lung and liver repair, a shift from M1 to M2 phenotypes was described as a wound healing progress from inflammation to restoration.

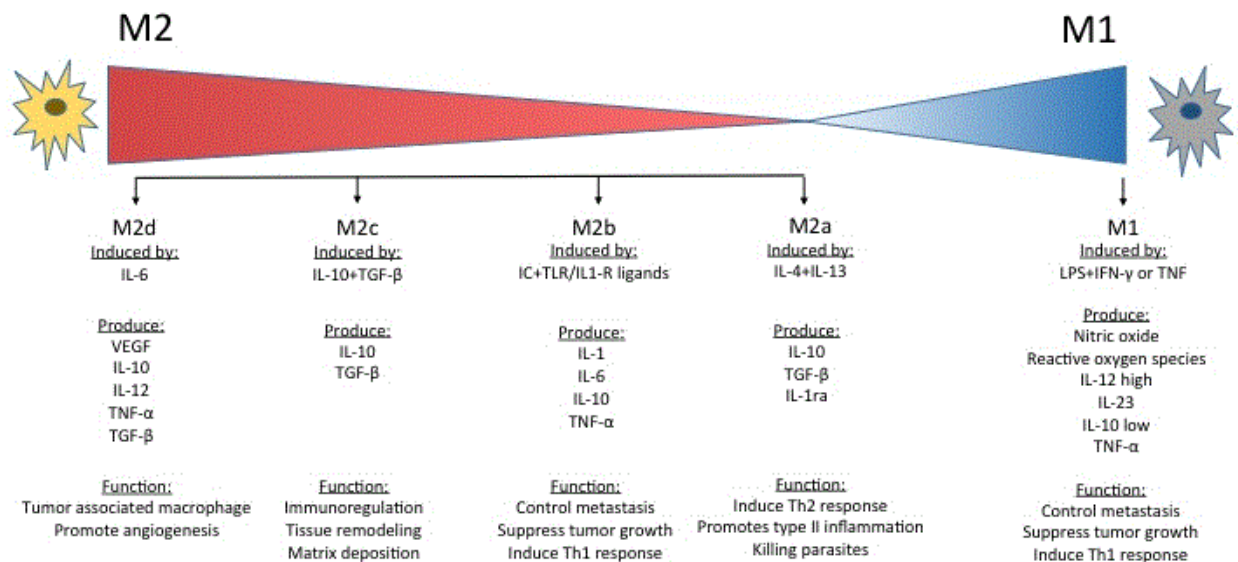


Figure 1.19: Summary of different macrophage phenotypes showing various release factors with their specific functions (78).

1.6.3.1 Macrophage-mediated phagocytosis of biomaterial

The process of phagocytosis involves the interaction of specific plasma membrane receptors to surface particle. During phagocytosis, macrophages undergo membrane reorganisation to entrap the particles into the cytoplasm, where hydrolytic enzymes are fused to form phagosomes to kill and degrade engulfed particles. When the size of the particle is between 10-100 μm , which is beyond the capacity of single macrophage to undergo phagocytosis, the fusion of macrophages takes place to form giant cells (79).

1.6.3.2 Foreign body giant cells and fibrosis

The phagocytic failure of foreign material by macrophages results in the fusion of macrophages to form foreign body giant cells (FBGC). The formation of multinucleated cells of monocytic origin occurs in three steps: first, cells acquire their ability to fuse, then the cells migrate and attach their

membranes by sharing their cellular components to become a single entity (**Figure 1.20**). Fusion involves the sharing of cytoskeletal elements that enable spreading and motility.

Apart from the function of phagocytosis, macrophages and FBGCs are also involved in the degradation of biomaterial scaffold by the release of enzymes, reactive oxygen intermediates (ROIs), and acidic products (79). For example, macrophages and FBGCs adhering to polyurethanes are known to degrade these materials by stress cracking, which leads to device failure. Further, the polymers such as polyethylene, polypropylene used for prosthesis and suture, undergo surface oxidation by ROIs generated by macrophages.

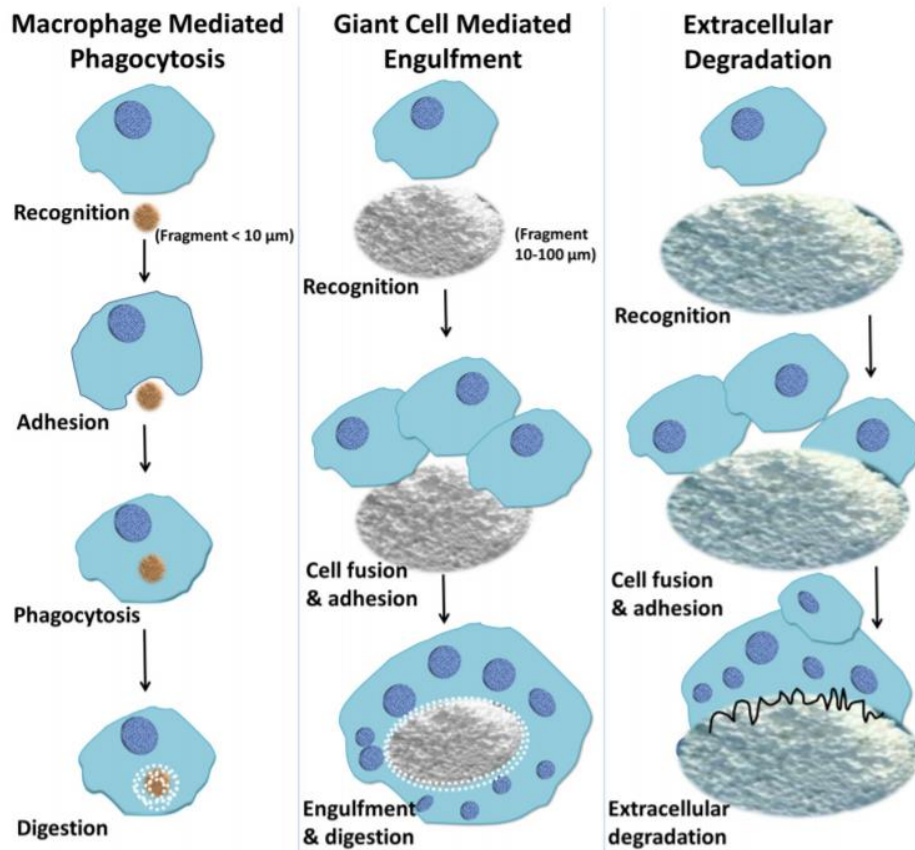


Figure 1.20: Scheme of macrophage response to biomaterials depending on the size of the implanted materials. Macrophages engulf small particles via phagocytosis (<math>< 10 \mu\text{m}</math> in diameter). For the particle size

10 -100 μm , the macrophages fuse to form giant cells which in turn engulf the particles and digest them. If the particles are larger than 100 μm , the bulk digestion is carried out via extracellular degradation by macrophages and macrophage-fused giant cells through the release of enzymes and pH lowering mechanisms (79).

Furthermore, growth factors released by macrophages attract cells such as fibroblasts, pericytes, endothelial, and smooth muscle cells that together form granulation tissue. The development of granulation tissue around the implants is also a part of chronic inflammation, where fibroblasts begin to replace the provisional matrix with fibrillar and collagen-rich extracellular matrix (ECM) having high mechanical strength. The deposition and organisation of collagen are essential to restore and maintain normal organ integrity after injury. However, in mature granulation tissue, fibroblastic cells and other cells begin to activate into contractile myofibroblasts that add further mechanical strength by remodelling the ECM, which results in the formation of fibrosis (80,81). Fibrosis is described as the degeneration of connective tissue, where the excessive accumulation of collagen-rich ECM replaces functional tissue. Depending on the material, macrophages can be beneficial in normal tissue repair or result in detrimental fibrosis (82).

1.7 Effect of degradable and non-degradable material on the foreign body response

The surface chemistry, size, and topography of biomaterial determine the foreign body reaction (**Figure 1.21**). Materials with high surface areas such as macro and nanopores device show a high ratio of macrophages and foreign body giant cells compared to smooth surface implants. As explained previously, protein adsorption instigates foreign body response, and hydrophobic

material shows a high affinity for various proteins. The adhered proteins undergo a conformational change to expose multiple binding sites and to orchestrate the inflammatory response.

The non-degradable materials such as sensors, drug delivery pumps, hip prostheses, brain implants, stents, pacemakers, orthopaedic implants, etc., (83) are usually implanted to exert certain mechanical functions in tissues for the long term. The intended host reaction against these implants includes integration and fixation to the host tissue without undergoing degradation from macrophages and foreign body giant cells (FBGC) (84). Formation of fibrosis impedes the exchange of analytes from the host to the implants, which creates discontinuity and weakens the interface and results in the failure of devices.

Therefore, the surface coating is necessary to protect from the host environment to enhance its biocompatibility and its functionality. The functional failure explains the importance of biocompatible surface coatings to protect the materials from foreign body reaction.

In contrast, biodegradable materials are considered as good candidates for developing therapeutic devices such as tissue engineering scaffolds, medical device coatings and as controlled drug release vehicles (83). The materials are expected to be degraded by different mechanisms, biological or chemical ones over a predetermined time to achieve a function.

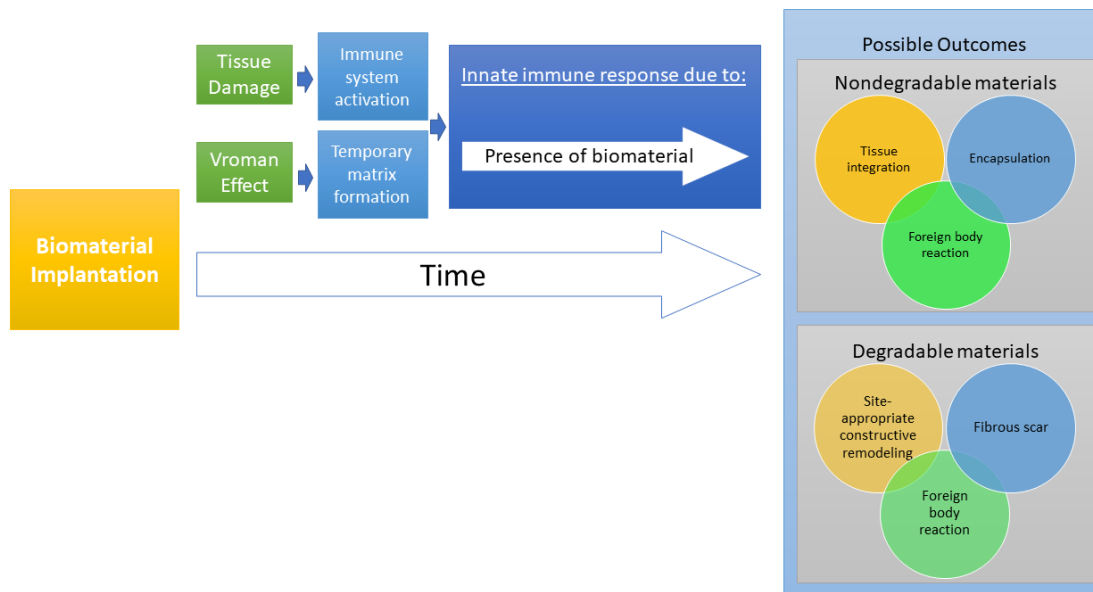


Figure 1.21: The host response to the degradable and non-biodegradable material (85).

1.8 Strategies to improve biocompatibility

As discussed previously, the major challenge is to control the inflammation and fibrosis to enhance the functionality and biocompatibility of implantable devices. Numerous approaches have been made, such as biomaterial coating and composite coating with drugs around implantable devices to overcome the limitation mentioned above.

1.8.1 Reduction of protein adsorption by biocompatible material coatings

The biomaterial selected alone should not trigger any inflammation and hinder the functionality of the implanted device. The primary purpose of coating with a biomaterial is to protect implantable device surface by minimising the tissue reaction. The addition of a biocompatible layer around implantable devices improves the device-host interaction, thereby increasing the functionality and longevity of the device. Various natural and synthetic materials are exploited as a coating material such as alginate, collagen, dextran, and cellulose (82) poly(lactic-acid)(PLA), poly(lactic-co-

glycolic acid) (PLGA), polyvinyl alcohol, polyethylene glycol (PEG), or 2-hydroxyethyl methacrylate (65) **Table 1.5.** Knowledge on physical, chemical and biological properties of the polymeric material is necessary to understand the foreign body response.

The protein adsorption is controlled by material characteristics such as surface groups (hydrophobic or hydrophilic), charge density, topography, and extent of hydration. One “simple” strategy to improve the function and biocompatibility of implantable medical devices is to reduce the protein adsorption by surface modification (**Figure 1. 22**).

Surface coating using Poly(ethylene oxide) (PEO), poly(ethylene glycol) (PEG), and PHEMA based materials (PEGylation materials) (86,87) have been extensively used since the 1980s to reduce non-specific protein adsorption. However, PEG derivatives are susceptible to enzymatic oxidation of the hydroxyl groups to aldehydes and acids; the oxidised surface increases protein adsorption and cell attachment. Hence, the susceptibility to the oxidation limits the long term application of PEG derivatives (88).

The next class of materials which have been extensively used for coating is zwitterionic materials. Zwitterions and mixed charge materials are well known for their ultra-low fouling property, as the protein adsorption is below $5\text{ng}/\text{cm}^2$. Recently, Zhang and coworkers (88) have mentioned the zwitterionic materials such as poly(sulfobetaine) and poly (carboxybetaine) and poly (carboxy betaine ester) for efficiently reducing the protein adsorption (82). The main disadvantage involves the cross-linking reaction containing acrylates. These linkages are not cleavable hydrolytically and enzymatically, indicating that these are not well suited for tissue engineering and drug delivery approach, where biodegradable implants are preferred.

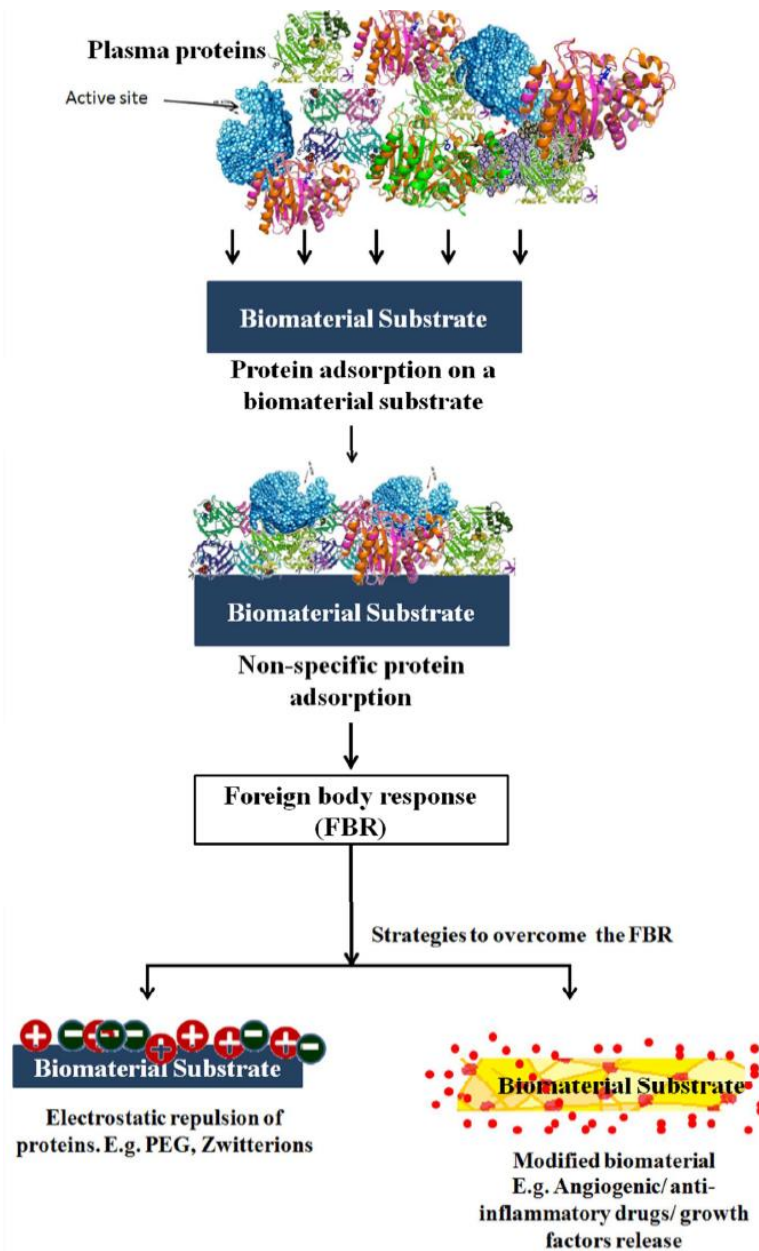


Figure 1. 22: Scheme explaining the hypothesis that non-specific protein adsorption causes a foreign body response. The conformation changes and orientation of proteins during non-specific protein adsorption. The foreign body response may be overcome by preventing protein adsorption or by modifying the biomaterial to release bioactive agents such as anti-inflammatory/ angiogenic drugs/ Vascular Endothelial Growth Factor (VEGF) (82).

1.8.2 Implant modification by the release of drugs from surface coating

1.8.2.1 Use of Angiogenic drugs

The formation of the fibrous capsule because of the device implantation limits its functionality by hindering the transportation of analyte from the tissue to the device and the diffusion of the product from the device to the tissue. The utilisation of composite coatings by releasing an angiogenic drug can promote angiogenesis, which enables the diffusion process. New blood vessels can be induced in the vicinity of the devices by slow release of growth factors like VEGF (vascular endothelial factor) (89,90). The formed blood vessels enhance the diffusion of analytes, thereby improving the functionality of the device.

1.8.2.2 Use of Steroidal and non-steroidal Anti-inflammatory drugs

Foreign body reaction can be minimized by using glucocorticoids. Such compounds have been used due to their ability to modulate the immune response. They inhibit the formation and release of inflammatory mediators, such as prostaglandins and leukotrienes (90). Besides, they also decrease capillary permeability and fibroblast proliferation, which thereby reduces inflammation at the site of injury. Many researchers employed polymer coatings (PLLA and PCL) containing dexamethasone to reduce fibrosis formation around a glucose sensor (91).

Table 1. 5: summary of most commonly used materials for biomedical applications (65).

Component	Properties	Some applications
Phospholipid-based biomimicry		
Phospholipid, Phospholipid-containing or Phospholipid-like materials	Device surface mimics cell's membrane; fragile and difficult to deposit	Coating
Phospholipid-modified polymers (proteins + PHEMA)	High water content	Coating
Natural derivates		
Albumin	Immobilisation of glucose oxidase (in combination with glutaraldehyde)	Glucose biosensor functionality
Cellulose	After hydroxylation can decrease complement activation, not long-term stability	Coating
Collagen	Extracellular matrix component	Porous sponge scaffolds
Synthetic polymers		
PE	Strength, lubricity	Orthopaedic implants and catheters
PP	Chemicals inertness and rigidity	Drug delivery, meshes, and sutures
Pluronic's surfactants (PEO-PPO-PEO)	Decrease biofouling and sensor passivation	Coating
Perfluorosulfonic acid (Nafion®)	Decrease biofouling, uncured Nafion® (not treated with FeCl ₃) leads to the high inflammatory response, not long-term stability	Coating
Hydrogels: PHEMA, PEO, PEG, PVA	Negligible Protein adsorption Surfactant and gel-forming properties	Coating The emulsifier in the drug encapsulation process and matrix for sustained drug delivery
PLA and PLGA	Negligible Protein adsorption	Coating

PE poly(ethylene), PP poly(propylene), PEO poly (ethylene oxide), PPO polypropylene oxide, PHEMA poly (hydroxyethyl methacrylate), PLA poly (lactic acid), PLGA poly (lactic co-glycolic acid), PVA poly(vinyl-alcohol)

1.9 Hydrogels

Coating with hydrogels has received considerable attention in the past 30 years due to their utilization in a wide range of applications. These include polymeric, soft and zwitterionic hydrogels. The hydrogel is defined as a three-dimensional, water-swollen network formed by monomers by cross-linking, hydrogen bonding or van der Waals interaction. The hydrogels have been employed in a wide range of fields such as pharmaceuticals, tissue engineering, regenerative medicine, clinical applications, and agriculture (92,93).

Poly (2-hydroxyethyl methacrylate) (P-HEMA) is the first synthetic hydrogel synthesised by DuPont in 1936(94). Later Wichterle and Lim in 1960 explored the importance of P-HEMA as a potential candidate for contact lens application (95). This innovation fostered the researcher to eventually develop smart hydrogels, where the properties change with the stimuli such as temperature, pH, ionic strength, electric field or light. Yannas et al. employed natural polymer collagen as a hydrogel for the artificial wound dressing ((96).

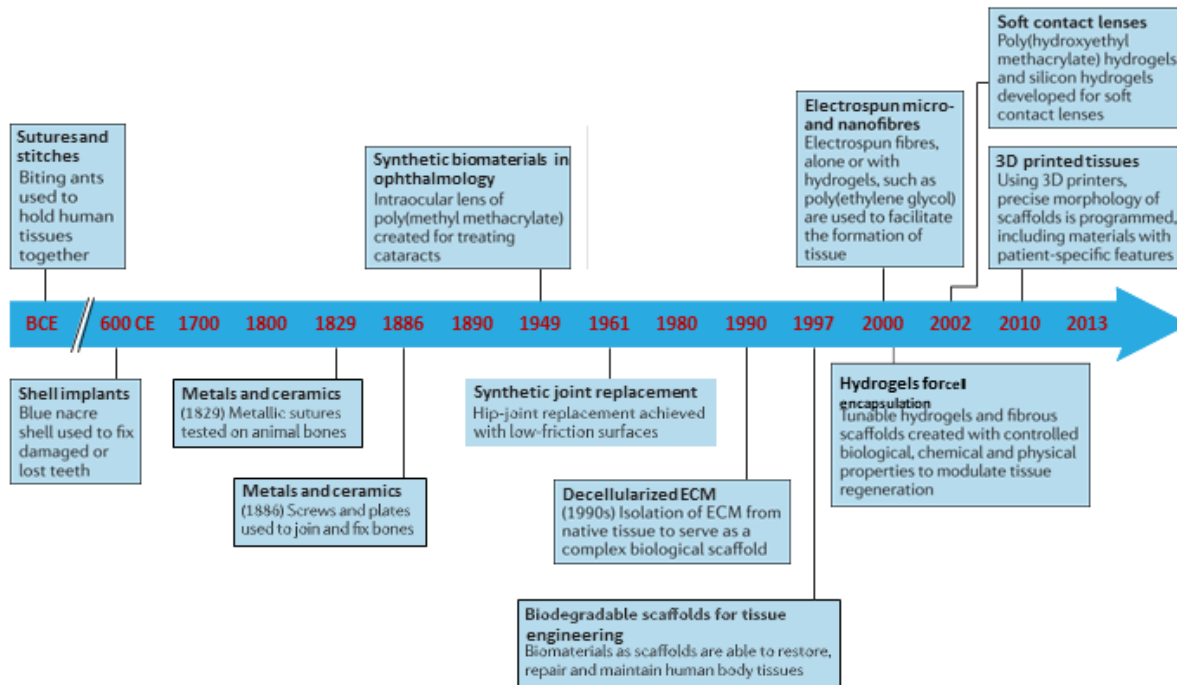


Figure 1.23: Timeline of advancements in biomaterials and hydrogels (Sadtler *et al.*, 2016) (97)

1.9.1 Classification of hydrogels

The literature reports many ways to classify the hydrogels. According to the source, hydrogels are divided into those formed from natural, or synthetic products, and the combination of both. Depending on the ionic charges present in the polymer network, hydrogels divide into anionic, cationic and neutral structures (98) (Figure 1.24).

In terms of preparation or synthetic route, hydrogels classified as homopolymers prepared by single hydrophilic monomers, copolymers made of two monomers and multipolymers consisting of two or more monomers. Further, based on size, hydrogels are divided into macrogels, microgels and nanogels. Micro and nanogels have advantages over macrogels for their less invasive delivery. Microgels having 5 μM or less in size are applied in oral and pulmonary delivery but are not

suitable candidates for intravascular injections. Whereas nanogels with 10-100 nm size are used mainly for systemic drug injections (99).

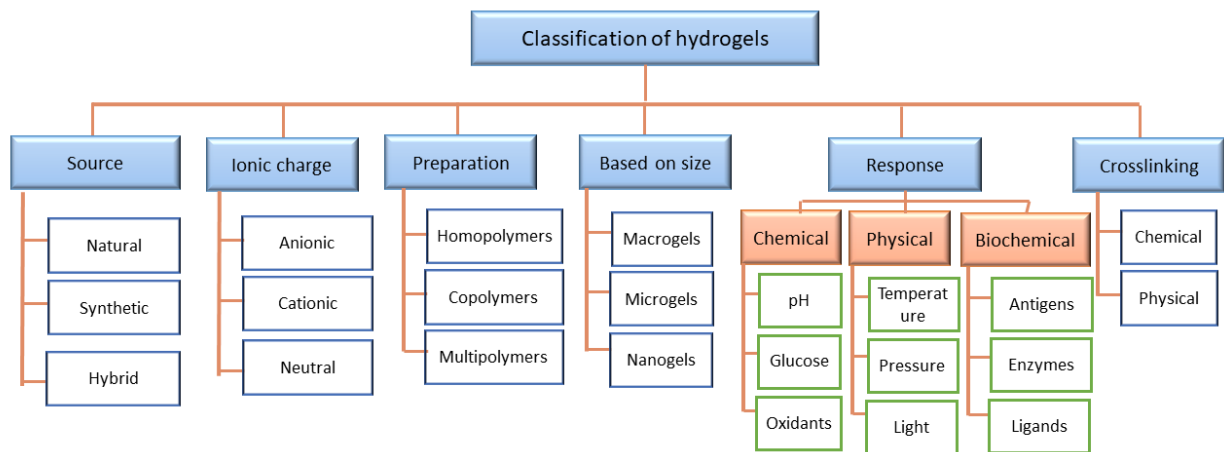


Figure 1. 24: Classification of hydrogels (Mahinroosta *et al.*, 2018)(100)

1.9.1.1 Natural and synthetic hydrogels

The two most widely used natural polymers over the years include alginate and chitosan, which have been utilized for various biomedical applications. Later collagen, gelatin, and hyaluronic acid have gained attention in the field of tissue engineering for stem cell differentiation. Also, the natural polymers show higher potential risks of immunological reaction (101).

Table 1. 6: Natural and synthetic monomers for hydrogel preparation (100)

Natural Polymers	Synthetic Monomers
Alginate	Hydroxyethyl methacrylate (HEMA)
Fibrin	N-(2-Hydroxy propyl) methacrylate (HPMA)
Collagen	Poly-Vinyl-2-pyrrolidone (PVP)
Gelatin	N-isopropylacrylamide (NIPAMM)
Hyaluronic acid	Acrylic acid (AA)
Dextran	Methacrylic acid (MAA)
	Polyethylene glycolacrylate/methacrylate (IPEGA/PEGMA)
	Polyethylene glycol diacrylate/dimethacrylate (PEGDA/PEGDMA)

1.9.1.2 Physical and chemical hydrogels

The hydrogels can also be classified based on their crosslinking network, either physical or chemical. Chemical gels are those formed by covalently– crosslinked networks. For example, poly (2-hydroxyethyl methacrylate) (pHEMA) obtained by the polymerisation reaction, crosslinking of polyvinyl alcohol with glutaraldehyde, photopolymerization of PEG derivates and hydrogels formed by gamma irradiation (101,102). Despite the formation of strong hydrogels, the crosslinking agent used to create a network is usually toxic, which often requires to remove it before the biological application. The *in-situ* photo polymerisation generates free radicals, which might cause injury to the tissues. (103).

Physical hydrogels are formed by the ionic reaction, protein interaction, hydrogen bonds, van der Waals interaction, and crystallisation. The crystallisation is indeed another way to form physical hydrogels. For example, the homopolymers such as PLLA, PVA and Dextran 6000 crosslinks by the crystallites to form a hydrogel (104).

1.9.1.3 Thermosensitive, thermoresponsive and phase transition hydrogels

Temperature sensitive hydrogels are those that contain both hydrophilic and hydrophobic molecules in their network. They undergo phase transition (hydrogel to sol or sol to hydrogel) either at low critical solution temperature (LCST) or upper critical solution temperature (UCST). The phenomenon of transition from solution to gel is commonly referred to as sol-gel transitions, where hydrogels separate from solution and solidify above a certain temperature called LCST. Below LCST, the polymers are soluble, whereas, above LCST, they become hydrophobic and insoluble, resulting in the formation of a gel. This phenomenon is used in Matrigel®, methylcellulose (MC), Chitosan- β -glycerophosphate, Poly (N-isopropylacrylamide) (poly (NIPA Am)). In contrast, the hydrogels that are formed upon cooling of polymer solution have a UCST. Gelatin, collagen and agarose are natural polymers that exhibit UCST phase transition (105,106).

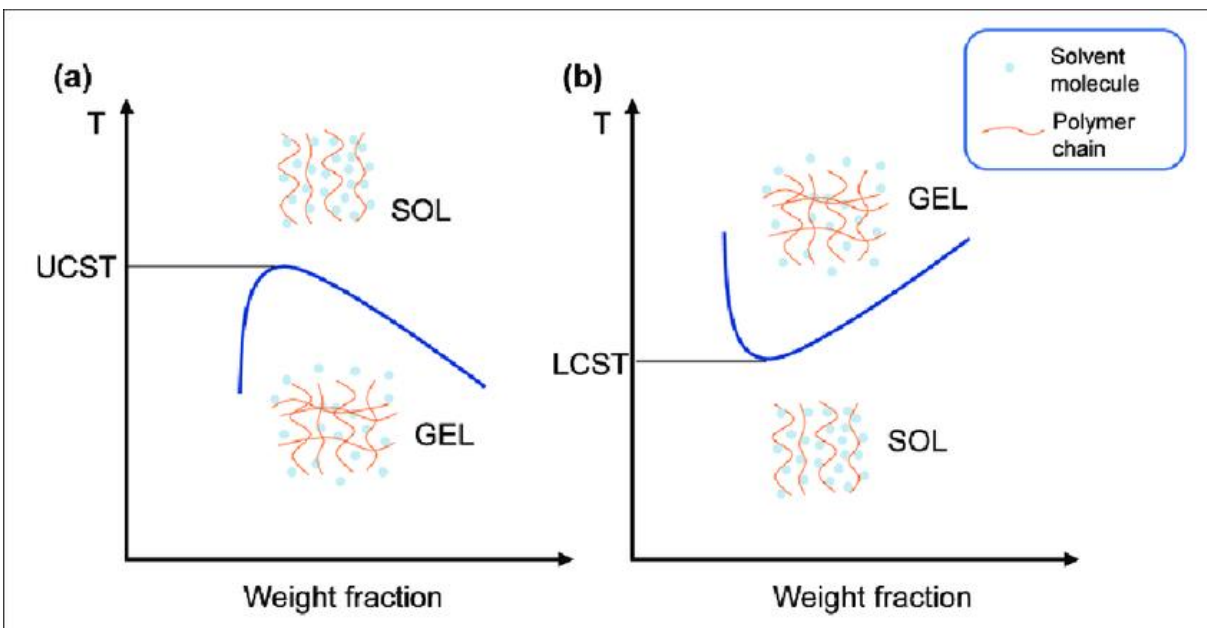


Figure 1.25: Thermo-responsive hydrogels: (a) UCST hydrogels undergo a sol-gel transition as the temperature decreases and (b) LCST hydrogels undergo a sol-gel transition as the temperature rises (106).

Recently, supramolecular gels have been developed, which provide attractive features for various biomedical applications due to their injectable property. Among which, low molecular weight gels (LMWGs) or self-assembled supramolecular gels are another interesting class of materials that form hydrogels by self-assembly through hydrogen bonds and van der Waals interactions (molecular stacking). These are soft hydrogels which possess sol-gel-sol transition (107–109).

Photo-responsive hydrogels are those which change their properties when irradiated with light of appropriate wavelength. Further, these are classified into UV sensitive and visible sensitive hydrogels. The light-sensitive hydrogels contain a chromophore, which can absorb and emit light, thereby increasing the temperature to form hydrogels like temperature sensitive hydrogels. Enzyme-responsive hydrogels are a new kind of materials that can undergo a macroscopic transition in the presence of enzymes. The ability of enzymes to undergo catalytic synthesis and hydrolysis leads to sol-gel and gel-sol phase transition. Among which, most commonly focused enzymes include protease and glycosidase responsive polymer (100).

Table 1. 7: Summary of materials, crosslinking and their applications (110,111,120–125,112–119)

Materials		Characteristics	Crosslinking methods		TE applications	
Natural Materials			Physical	Chemical		
	Gelatin		Guest-host		Cartilage TE	
		GelMA		Photo	Cartilage, tendon TE	
		Gelatin-hydroxyphenylpropionic acid (Gtn-HPA)		Enzymatic	Cartilage TE	
	Collagen			Photo	Meniscus TE	
	HA	Adamantane-functionalized HA	Guest-host		Cartilage TE	
		HA-vinyl sulfone		Michael addition	Neural engineering	
		Methacrylated HA(MeHA)		Photo	The meniscus, nucleus pulposus TE	
	Alginate			Ionic	Cartilage, retinal and Bone TE	
		Methacrylated Alginate			Photo	Bone TE
	Dextran	Dextran biofunctionalized with Methacrylate and aldehyde			Photo	Vascular TE
	Chitosan	Chitosan-g-poly(N-isopropylacrylamide)	Thermal			Cardiac, Cartilage TE
		Methacrylated glycol Chitosan			Photo	Bone TE
Synthetic and Hybrid Materials	PEG	Thiol-norbomene PEG, PEG Diacrylate (PEGDA)	Thermal	Photo	Cartilage TE Heart valve TE	

	PVA/Gelatin		Thermal		Cartilage TE
	PNIPAM/Gelatin	PNIPAAm-based copolymer, thiol-modified Gelatin	Thermal	Michael addition	Cardiac TE
	PEG/Gelatin	PEG dimethacrylate, GelMA Glycol		Photo	Bone, Cartilage TE
	PEG/Chitosan	Chitosan, benzaldehyde functioned PEG		Schiff-base	Neural engineering, vascular TE
	PEG/HA	Amino-terminated PEG, aldehyde HA		Schiff-base	Adipose TE
	Gelatin/Alginate	Oxidized Alginate, gelatin		Schiff-base	Muscle TE
		GelMA, Alginate	Ionic	Photo	Bone TE

1.9.2 Properties of hydrogels

For any material, the physical, chemical, and biological properties play an essential role in determining the desired application. Although different types of hydrogels are available, it is necessary to choose the desired hydrogel based on multiple features such as swelling behaviour, surface properties, mechanical properties, and degradation rate for the specific application.

1.9.2.1 Swelling properties

The swelling properties are crucial for the hydrogels in biomedical applications. The swelling ratio influences the degree of diffusion of analytes, permeability, and mechanical properties. When the hydrogels are exposed to solvent, they absorb water and start to swell until they reach their equilibrium in swelling state. The swelling is achieved when the polymer chains in the hydrogels interact with the solvent molecules to attain solvated state (expansion), while the crosslinked

structure retracts the chains inside until the equilibrium is reached between the expansion and retraction of the assembled molecules (126). The swelling ratio is generally described as swelling behaviour calculated by using the formula mentioned below.

$$\text{Swelling ratio } (R_s) = \frac{W_s - W_d}{W_d}$$

R_s = Swelling ratio, W_s = weight of the swollen hydrogel, W_d = weight of dried hydrogel (tap dried using Kim wipes to remove excess fluid).

1.9.2.2 Permeability properties

The permeability of hydrogels is the ability to transmit the fluids, cells and proteins. In the context of hydrogels as coating membranes, permeability is one critical parameter for adequate function of implantable medical devices.

1.9.2.3 Mechanical properties

The mechanical properties of hydrogels rely on their composition. However, it should be noted that an optimum mechanical strength is required for different applications. At the macroscopic level, mechanical properties are essential in maintaining the stability of hydrogels to withstand the tissue load. At the microscopic level, the stiffness plays a critical role in affecting cell activities and fate. For example, an increase in stiffness of hydrogels has been reported to affect cell attachment, differentiation, and spreading (127). Mechanical properties can be tuned by changing the crosslinker concentration, and molecular weight of the precursor. For example, soft hydrogels are required for neural regeneration, harder scaffolds for bone regeneration (128). The summary of hydrogels and their mechanical strengths are given in **Table 1.8**

1.9.2.4 Elasticity

Elasticity is defined as the capacity of a material to return to its original shape after the removal of the constant load. The force applied is usually referred to as stress, which is acting per unit cross-sectional area of the material, while the relative deformation of the material is called strain. The ratio between the stress and strains termed as Young modulus, often represented by E.

Viscosity is the direct measurement of the ability of a material to resist the deformation in response to the applied stress and is directly related to the ability of hydrogels to respond to changes in shear stress during the injection. Rheology is a method used to quantitatively measure the parameters of hydrogels such as viscosity, storage modulus and loss moduli, which are essential in measuring the hydrogel injectability. The storage and loss moduli provide information on the elastic modulus of the hydrogels. The extent to which a hydrogel responds to stress and absorb energy is called storage modulus, and when the hydrogel undergoes stress relaxation to dissipate energy is termed as loss modulus (129,130).

Table 1. 8: Physical properties of hydrogels and their applications in tissue engineering.
(116,119,122,124,131–133)

Physical properties	Materials	Approaches	Application
Mechanical strength	GelMA	Chitin nanofibers, Nanoparticles blending	Strain-to-failure increased 200% after chitin nanofiber assembly; stiffness of collagen-based hydrogel increased 10-fold after addition of functionalized nanoparticles
	PAMPS/PDMA Am	Double network	High strength PAMS/PDMAAm gel could induce spontaneous hyaline cartilage regeneration in an osteochondral defect
Stiffness	Four-arm maleimide-functionalized PEG	By using different PEG concentration	The proliferation, self-renewal and vascular differentiation of stem cells were enhanced in lower stiffness hydrogel
	GelMA	Using the same macromer concentration with different methacryloyl substitution	High stiffness environment was beneficial for maintaining of chondrogenic gene expression.
Degradation	GelMA	Collagenase degradable photo crosslinked gelatin hydrogel	Valvular interstitial cells had more spreading morphology in collagenase treated GelMA hydrogel than untreated hydrogel.
	HA functionalized with both maleimide and methacrylate	Thiol-ene crosslinking via MMP degradable crosslinker and Photocrosslinking	Differentiation of MSC was directed by Degradation-mediated cellular traction
	PEG-derivative	Modification of ends of PEG with oligo (lactic acid) and acryloyl, hydrolysis of the ester bonds altered the degradation	The high degradation enhanced osteogenesis of MSCs.
	PEG-derivative	Hydrogel crosslinked by PEG derivative containing nitrobenzyl ether moieties could be degradable by photo exposure	MSC spreading was enhanced after photodegradation.

1.10 Biocompatibility assessment

Biocompatibility is one of the most critical parameters that must be evaluated carefully. It is a multi-stage approach, beginning with the *in vitro* assessment, before animal testing. Various *in vitro* studies can be used for initial screening of material safety like cytotoxicity, irritation and hemocompatibility tests. *In vitro* tests are also be used to evaluate the material at early development to choose the best candidate for future *in vivo* studies, saving time and resources.

1.10.1 Cytotoxicity assessment

The choice of cell lines used for cytocompatibility must be carefully chosen according to the regulations. In most cases, continuous (immortalized) cell lines originally obtained from neoplasms or transformed by viruses or mutagens, such as HeLa, L929, WI-38, 3T3 or CHO, are used to screen the cytotoxicity (134). Whereas in some instances, cells are chosen according to the interactions investigated and prospective medical applications, which includes human or animal cells such as immune, endothelial, hepatic cells or various epithelial cell lines.

According to the US Pharmacopoeia and standards mentioned by the American society for testing and materials, the standards of British Institute, and the international for the organisation (ISO for lab comparability), primary cell culture assays used to evaluate the biocompatibility are: a) direct contact, b) extraction method. It is essential to standardise the methods on a) the number of cells, b) duration of exposure, c) the cell type, d) test sample size and e) surface area of the test sample (135,136). As per the standards, L929 mouse fibroblast cell line is extensively used to assess biomaterial testing, since they are reported to give good correlation with animal-based tests in addition to their physiological role in wound healing process around implanted materials.

Simple *in vitro* cytotoxicity is often used to check biocompatibility of the material. A combination of different assays such as inflammation, mutagenesis, immunogenicity, and proteomics can provide complementary information on the biological reaction of the biomaterial. Cytotoxicity assays provide a qualitative and quantitative estimation of possible toxicity associated with biomaterials and their components. The measurement of cytotoxicity is based on microscopic examination of cells, and viability tests based on a wide variety of cellular functions (**Table 1.9**). The most commonly used tests such as cell counting (Neubauer chamber), vital dyes (Trypan blue and Neutral red uptakes (NRU)), and biochemical based assays (MTT, MTS, XTT) for screening cell viability, proliferation and metabolic activity (1).

Table 1. 9: Cell viability tests and their advantages and disadvantages (1).

Assay	Advantages	Disadvantages
Trypan blue	A simple and rapid method able to provide approximate results.	labour intensive.
MTT 3-(4,5-dimethylthiazol-2-yl)-2,5-diphenyltetrazolium bromide	Gives precise dose-response curve on small cell numbers. Simple and high reproducibility	Cell non-specific. There is no discrimination between cytostatic and cytotoxic effects. Requires solubilization step. Disposal of organic solvent.
MTS3-(4,5-dimethylthiazol-2-yl)-5-(3-carboxymethoxyphenyl)-2-(4-sulfophenyl)-2Htetrazolium	Simple, rapid, flexible and nonradioactive. Established procedures and several publications	Chemical interference by reducing agents. Cannot collect true zero-time control values.
XTT194 (sodium 2,3-bis(2-methoxy-4-nitro-5-sulfophenyl)-5-[(phenylamino)-carbonyl]-2H tetrazolium	A single time point measurement. suitable for use with non-adherent as well as adherent cell lines	Require the presence of phenazine methosulfate (PMS) for effective reduction
WST-1 (4-[3-(4-iodophenyl)-2-(4-nitrophenyl)-2H-5-tetrazolio]-1,3-benzene disulfonate)	No volatile organic solvent is required for solubilization. More sensitive than using MTT. Short reaction time. No need to wash or harvest cells for the assay.	Measures net metabolic activity of cells. Cell-specific and media specific. which one must know how much of the enzyme can be regarded or disregarded as a usable protein
AlamarBlue®	Elimination of the washing/fixing and extraction	Not a direct cell counting technique. High cell number and

	steps. Incorporation of a fluorometric and colourimetric growth indicator.	prolonged culture times will show a reversal of the reduction process.
NRU (neutral red)	Very sensitive and readily quantifiable.	Once started it must be completed immediately

1.10.2 Protein interaction and adsorption on materials

As mentioned earlier, adsorbed proteins determine the fate of tissue-material interface, and since the amount of spontaneously adsorbed protein depends on the property of material surface chemistry, this can be used to screen the material at early stage development.

Furthermore, depending on the clinical application, a lower or higher protein adsorption on the material may be desirable. For example, it is advantageous for medical devices to have low levels of non-specific protein adsorption, while in case of bioengineering scaffolds, protein interaction with the biomaterial promotes tissue integration to enhance their regenerative capacity further. The issues mentioned above highlight the importance of studying non-specific protein adsorption to biomaterials towards evaluating biocompatibility.

Adsorbed proteins are quantified by using either simple ultraviolet-visible spectroscopy or conventional colourimetric methods such as BCA, Bradford's or Lowry based assays, and Enzyme-linked immunosorbent assay (ELISA). Other characterisation techniques involve surface plasmon resonance (SPR), Quartz Crystal Microbalance with Dissipation (QCM-D), Ellipsometry and atomic force microscopy (AFM) is used mainly to monitor the dynamics and kinetics of adsorbed proteins (134).

1.10.3 *In vivo* studies

After the biomaterial is screened through the series of *in vitro* biocompatibility test, if it is found to be non-toxic, it is recommended to evaluate its biocompatibility in animal models. The *in vivo* test allows the implanted material to be in contact with various cell types and to interact with proteins, enzymes and hormones. Although numerous animal models are available for testing the material, the selection of a suitable model is crucial depending on the type of the study.

For *in vivo* biocompatibility assessment, subcutaneous implantation tests are often used to assess the toxicity of the material components or the finished device. The *In vivo* assessment of tissue-biomaterial compatibility involves non-invasive and invasive measurements.

The non-invasive method can help to investigate the localised inflammatory response associated with neutrophils and macrophages on implanted material. Two chemiluminescent agents such as luminol (5-amino-2,3-dihydro-1,4-phthalazinedione) and lucigenin (bis-N-methyl acridinium nitrate) are widely used for non-invasive imaging of acute and late (chronic) stages of inflammation. Luminol enables to visualize the neutrophil MPO activity, while lucigenin is used to assess macrophage activity at the chronic phase of inflammation (137).

The invasive techniques to assess the biocompatibility of implanted material involve microscopic analyses such as histology. Histology consists of different staining techniques to monitor the degradation, infiltration of inflammatory cells, collagen matrix, and angiogenesis, while in immunohistochemistry, specific labelling of protein with antibodies provides quantitative information on the type of cells expressed and the extent of inflammation.

It must be noted that a biomaterial which is compatible for one application may not be compatible with another application (65,97). General steps used to evaluate the material and the devices are described in **Figure 1.26**.

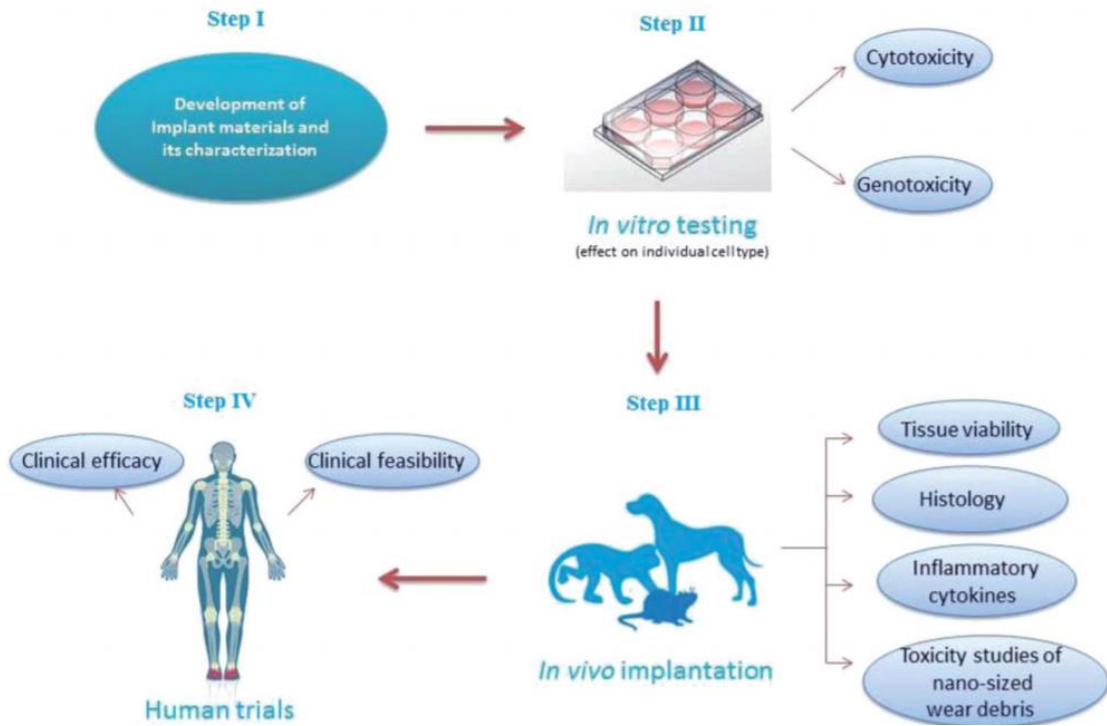


Figure 1. 26: Brief overview of the steps involved in the translation of newly developed biomaterials from bench to bedside (134).

2.HYPOTHESIS, OBJECTIVES AND EXPERIMENTAL DESIGN

2. HYPOTHESIS, OBJECTIVES AND EXPERIMENTAL DESIGN.

The thesis encompasses the aspects of extremely miniaturised glucose/O₂ EBFC as an *in vivo* continuous glucose monitoring (CGM) and power source. The current technology for monitoring glucose levels has been well established since the 1980's. The knowledge of glucose levels that are measured can allow a patient to select an appropriate dose of insulin to regulate his/her glucose levels. Several trends are emerging to monitor the glucose levels, among which, CGM can permit significantly more fine-tuned adjustments in insulin dosing. Recent advancement in implantable sensors, on the other hand, can be used to incorporate insulin pumps, which allow for instant insulin administration.

In this context, the use of enzymatic biofuel cells has spurred the interest of researchers with their dual functionality. EBFC monitors the glucose continuously and additionally, the energy generated can be used to power the integrated insulin pumps for the autonomous delivery of an appropriate dose of insulin. Although implantable glucose monitoring systems offer regular glucose level, few CGM devices have been reported to show inaccuracies of up to 21% (138). The inaccuracies are often attributed to sensor drift, caused by changes in the catalytic performance of the enzyme and inflammatory reaction. Hence these devices require periodical recalibration via the finger-pricking method. Despite the commercial glucometers, such as the Freestyle-Navigator by Abbott, and Dexcom providing real-time measurements with every 1–5 min, the longest working model without calibration is approximately two weeks(139). Consequently, there is high consumer demand for a CGM which can quantify glucose concentrations without frequent calibration. Therefore, reducing the number of calibrations is key to improving the usability of the CGM device and patient compliance.

Apart from that, other challenges must be addressed before the implantation of such devices. Operation of EBFC at high power density is challenging as it requires a large number of enzymes efficiently immobilised to the anode or the cathode. It also requires mass transport of products and reactants to/from the electrodes that are not being limited by diffusion. Last, the size of the EBFC is small enough to be eventually implanted. The most crucial aspect in this context is to ensure the biocompatibility of such a device, thus preventing foreign body reaction. Finally, it requires a device that can monitor the *in vivo* enzyme functionality non invasively.

Considering the limitations mentioned above, the thesis involves outlined strategies with interdisciplinary collaborations for the systematic development of EBFC. The strategies such as the selection of a suitable electrode architecture (macroporous gold electrode), characterisation of single electrode studies and optimisation, selection of desired hydrogels to coat EBFC for enzyme protection, testing the combination of fuel cell devices for *in vivo* functionality and biocompatibility and finally wireless antenna to measure the enzyme functionality non invasively. The power generated by EBFC will be measured by a wireless antenna consisting of a receiver outside of the body. The generated power is proportional to the glucose concentration and therefore, can be directly used as the analytical signal (sensor function). The change in transmission frequency is then related to the glucose concentration. Based on the strategies outlined, the objective of the thesis is as follows.

Obj. I. To evaluate newly synthesized different LMWHs for the foreign body response that they induce.

The hydrogels will be screened for different properties by subcutaneous implantation in mice: *in vitro* cytotoxicity, protein adsorption, *in vivo* degradation, FBR, and angiogenesis.

Obj. II. To optimise hydrogel coating on cathode electrode and *in vitro* and *in vivo* measurement of enzyme functionality.

1. The study will be focused on optimizing one electrode, the cathode, where the sluggish kinetics of O₂ reduction currently restricts its performance.
2. The selected hydrogel will be optimised for uniform coating and oxygen diffusion to protect the enzyme from a hostile environment.
3. The functionality of the enzyme wired electrode coated will be evaluated by *in vitro* and *in vivo* subcutaneous implantation in mice using electrochemical measurements.

Obj III. To optimise subcutaneous implantation of enzymatic biofuel cell and *in vitro* and *in vivo* measurement of enzyme functionality.

1. Optimization of subcutaneous implantation of biofuel cell in the rat.
2. Electrochemical measurements will evaluate EBFC functionality before and after subcutaneous implantation.
3. Also, with collaboration, wireless communication will be employed for non-invasive functionality measurement of implanted EBFC.

Thesis organization

This dissertation is divided into four parts. **Article 1** (co-author), **Article 2** (first author), and two other experimental sections on the optimization procedure. The **article 1** explores the synthesis of urea-based-bolaamphiphile hydrogels and their main physicochemical and mechanical characteristics. The studies were performed under the collaboration of Chembiopharm lab (Prof.Philippe Barthélémy). It describes the comparison of the structure of three different hydrogels which differ in one functional group for potential applications.

The **article 2** reports the biocompatibility studies of the hydrogels mentioned in **article 1**. The hydrogels were screened for the desired properties to select for coating the EBFC. The characterisation of hydrogels includes the ability to limit protein adsorption, slow degradation, minimal cell infiltration, fibrosis, and potential angiogenic properties. Part of the work described on hydrogel fibrosis has been carried out while visiting Dr Boris Hinz group, at the Department of Tissue Repair and Regenerative Medicine (University of Toronto, Canada). Based on the results, the desired hydrogel was selected for further studies to improve the EBFC functionality.

Results 3 summarize experiments done for enzyme selection and hydrogel coating onto the EBFC in collaboration with CRPP and NsysA (Dr Nicolas Mano and Prof. Alexander Kuhn). The studies were focused on performing the *in vivo* stability of the enzyme immobilised biofuel cell by subcutaneous implantation in mice. Besides, the hydrogel coatings were optimised for their thickness with the ability to allow for oxygen diffusion and their *in vitro* and *in vivo* stability.

Results 4 report the preliminary data on *in vivo* implantation of EBFC and the first assays of measurement using a wireless antenna. This work has been carried out in collaboration with IMS (Dr Simon Hemour and Pr Corinne Dejous).

Research questions

- Are the four newly synthesized hydrogels biocompatible?
- Do the selected hydrogels meet the desired properties for coating the EBFC?
- Was the hydrogel coating improving the EBFC functionality and stability?
- How was the subcutaneous implantation of EBFC optimised?
- How was the enzyme functionality measured?

Results

Article 1: Low molecular weight hydrogels derived from urea-based bola amphiphiles as new injectable biomaterials

Michael A. Ramin, Laurent Latxague, Kotagudda Ranganath Sindhu, Olivier Chassande,
Philippe Barthélémy

Accepted Date: 17 August 2017: Biomaterials

My contribution to the article: Biological characterisation of low molecular weight hydrogels by subcutaneous implantation in mice to assess their degradation and inflammation by non-invasive optical imaging and by histology.

Thanks to Philippe Barthélémy's group for the synthesis and the physical characterisation of the molecules.



Low molecular weight hydrogels derived from urea based-bolaamphiphiles as new injectable biomaterials



Michael A. Ramin^{a, b}, Laurent Latxague^{a, b}, Kotagudda Ranganath Sindhu^c, Olivier Chassande^c, Philippe Barthélémy^{a, b, *}

^a Univ. Bordeaux, ARNA Laboratory, F-33016 Bordeaux, France

^b INSERM U1212, CNRS UMR 5320, ARNA Laboratory, F-33016 Bordeaux, France

^c INSERM, U1226, Biotis Laboratory, F-33016 Bordeaux, France

ARTICLE INFO

Article history:

Received 7 April 2017

Received in revised form

18 July 2017

Accepted 17 August 2017

Available online 19 August 2017

Keywords:

Biomaterials

Low molecular weight hydrogelator

Bolaamphiphiles

Rheology

Supramolecular structures

Subcutaneous implantation

ABSTRACT

There is a critical need for soft materials in the field of regenerative medicine and tissue engineering. However, designing injectable hydrogel scaffolds encompassing both adequate mechanical and biological properties remains a key challenge for *in vivo* applications. Here we use a bottom-up approach for synthesizing supramolecular gels to generate novel biomaterial candidates. We evaluated the low molecular weight gels candidates *in vivo* and identified one urea-containing molecule, compound **16**, that avoid foreign body reactions in mice. The self-assembly of bolaamphiphiles creates a unique hydrogel supramolecular structures featuring fast gelation kinetics, high elastic moduli, thixotropic, and thermal reversibility properties. This soft material, which inhibits recognition by macrophages and fibrous deposition, exhibits long-term stability after *in vivo* injection.

© 2017 Elsevier Ltd. All rights reserved.

1. Introduction

The development of artificial materials for repairing, replacing or regenerating damaged tissues remains an important issue in the field of regenerative medicine. These materials mimic natural extracellular matrix (ECM) [1], which can be seen, as a soft matter constituted of extracellular molecules such as proteins or polysaccharides secreted by cells. These biomolecules form a macromolecular network providing a support to the surrounding cells. Likewise, engineered hydrogels that resemble to the physico-chemical characteristics of ECM have been used as scaffold in the field regenerative medicine [2]. Many different natural polymers have been used to develop hydrogels, including collagen [3], alginate [4,5] hyaluronic acid [6], chondroitin sulfate [7], and fibrin [8], for example. Also synthetic polymers and/or copolymers have been used to fabricate scaffolds. In this category, one can cite poly(lactic acid) [9,10], poly(ethylene glycol) [11] and poly(glycolic acid) [12,13]. In order to improve the biological, biophysical and

mechanical properties of these materials, chemically modified natural scaffolds [14] or hybrid hydrogels [15,16] combining natural and synthetic hydrogels have also been investigated.

Recently, a polymer free approach involving Low Molecular Weight Gels (LMWGs) has attracted great interests as novel scaffolds for biomedical applications [17–22]. These biocompatible materials, which result from the self-assemblies of small molecules possess tunable physicochemical and biological properties thanks to their supramolecular structures. Despite the first promising results reported with LMWGs [23–27], implementing injectable hydrogel scaffolds able to i) encompass the requested biophysical and mechanical properties and ii) avoid foreign body reactions remains highly desirable.

The purpose of this study was to investigate the use of novel bolaamphiphile based LMWGs possessing amide and urea functions as injectable biomaterials for *in vivo* applications. Herein, we report the synthesis of novel bolaamphiphiles featuring N-thymine glycosylated head groups linked to a lipidic moiety *via* either urea or amide functions (Fig. 1). These chemical functions impact on both mechanical and biological properties of their resulting supramolecular hydrogels. Contrary to previous bolaamphiphiles [22,28,29], the urea-containing molecules feature a fast gelation kinetic and high *in vivo* stability. The urea-based-bolaamphiphile

* Corresponding author. Univ. Bordeaux, ARNA Laboratory, F-33016 Bordeaux, France.

E-mail address: philippe.barthelemy@inserm.fr (P. Barthélémy).

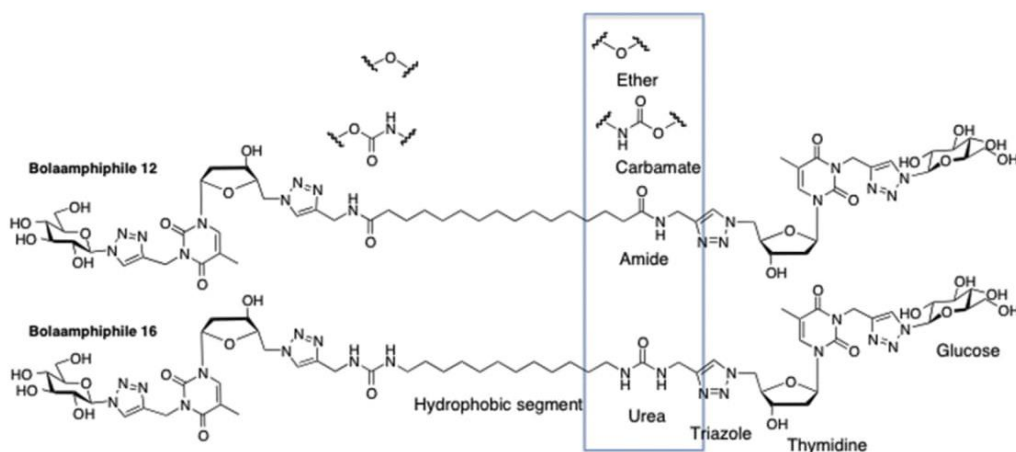


Fig. 1. Chemical structures of bolaamphiphiles. Examples of structures amide and urea based Bolaamphiphiles (**12** and **16**) reported in this study. Ether and carbamate analogues were reported previously (see ref 22 and 28, respectively).

forms a hydrogel that inhibits recognition by macrophages and fibrous deposition.

2. Experimental section

2.1. Materials and measurements

All commercially reagents and solvents (Fluka, Sigma-Aldrich, Alfa-Aesar) were used without further purification. For reactions requiring anhydrous conditions, dry solvents were used under inert atmosphere (nitrogen or argon). Analytical thin layer chromatography (TLC) was performed on pre-coated silica gel F254 plates with fluorescent indicator (Merck). The detection of compounds was accomplished with UV light (254 nm). All compounds were characterized using ^1H and ^{13}C Nuclear Magnetic Resonance (NMR) spectroscopy (Bruker Avance DPX-300 spectrometer, ^1H at 300.13 MHz and ^{13}C at 75.46 MHz). Assignments were made by ^1H - ^1H COSY (correlation spectroscopy), DEPT (distortionless enhancement by polarization transfer) and HSQC (heteronuclear single quantum correlation) experiments. Chemical shifts (δ) are given in parts per million (ppm) and all the spectra were referenced to the residual proton signals and referenced to residual solvent peaks ($\delta_{\text{H}} = 7.26$ ppm and $\delta_{\text{C}} = 77.0$ ppm for CDCl_3). Coupling constants J are given in Hertz (Hz). The multiplicity of each signal is designated using the following abbreviations: s = singlet; d = doublet; t = triplet; q = quartet; m = multiplet. High-resolution mass spectra (HRMS) were recorded with a Q-Exactive mass spectrometer (Thermo Fisher Scientific) in the electrospray ionisation (ESI) mode at the Center Régional de Mesures Physiques de l'Ouest (CRMPO, Université de Rennes).

2.2. Synthesis

The general procedure for synthesis of bolaamphiphiles is shown in [Scheme 1](#), the detailed procedures are described in Supporting Information.

2.3. Physico-chemistry and spectroscopy studies

2.3.1. Critical gelation concentration (CGC) and gelation kinetic

The gelation ability was quantitatively assessed by investigating the critical gelation concentration (CGC), which is defined as the lowest concentration (in weight percent) of hydrogelator required

to gelify 1 mL of water. For the CGC measurement, the hydrogels were successively diluted, heated until no formation of gel. The sample is considered to be a gel by the tube-inverting method.

Kinetics. All samples (1% w/w) were first heated above their sol-gel transition temperature (80 °C, 5 min) and then allowed to cool to room temperature (23 °C). The gelation kinetic corresponds to the time necessary for the gel formation.

2.3.2. Differential scanning calorimetry (DSC)

DSC was performed using a Mettler Toledo analyzer (DSC 1 STARE System, Singapore). Samples were generally sealed inside aluminium crucibles of 100 μL in volume and heated from 20 to 85 °C at a heating rate of 1 °C/min. Second heating run was selected for analysis.

2.3.3. IR spectroscopy

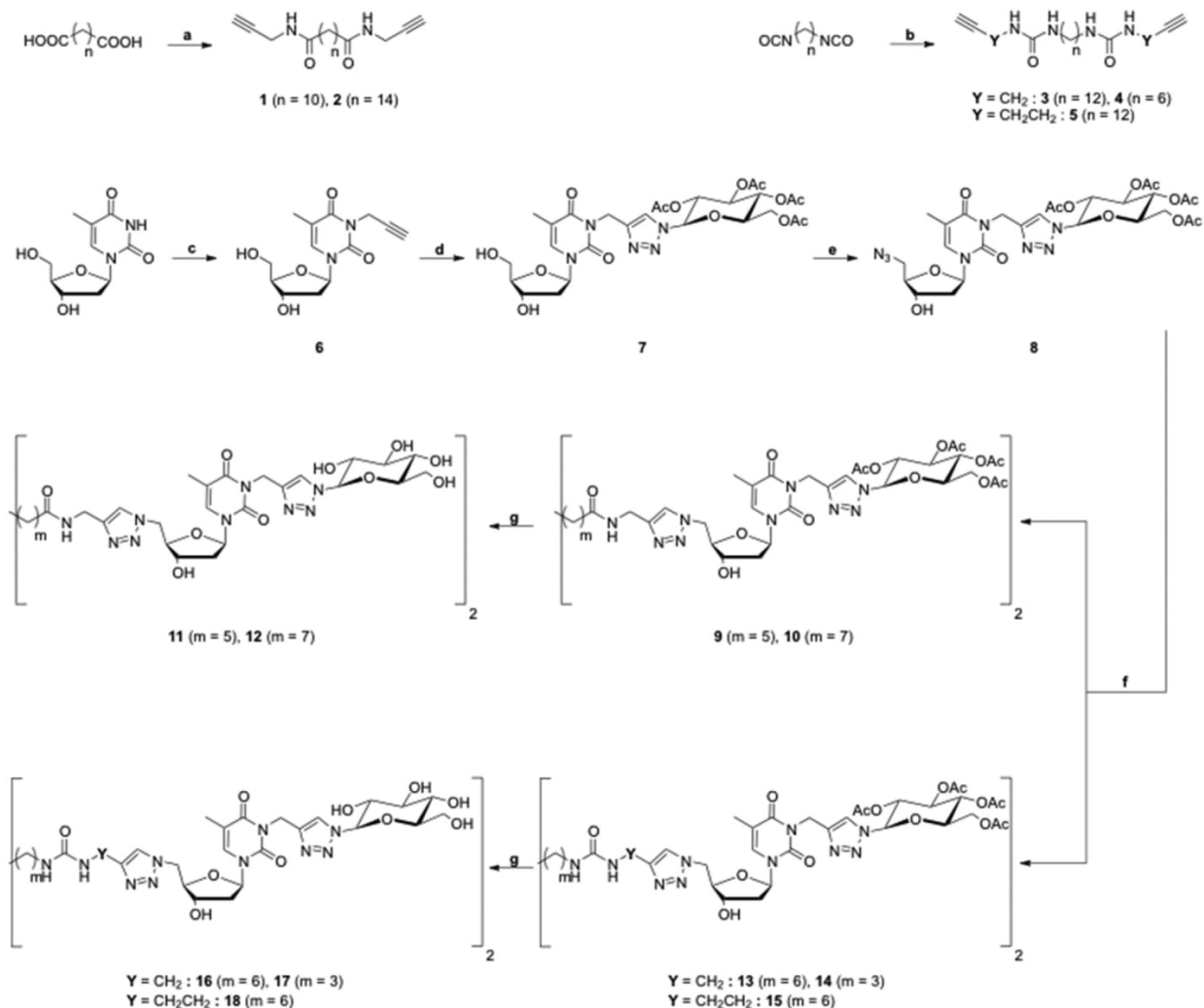
A Perkin-Elmer Spectrum Two FT-IR spectrometer with an attenuated total reflection (ATR) accessory was used to record the IR spectra. To perform infrared experiments on hydrogels, H_2O was replaced by D_2O to overcome the strong water absorption (at 1640 cm^{-1}), which can affect the analysis.

2.4. Mechanical property measurement of hydrogels

Rheological measurements were carried out on a Malvern Kinexus Pro+ rheometer with steel plate-plate geometry (diameter: 20 mm). The lower plate is equipped with a Peltier temperature control system, and all samples were studied at 25 ± 0.01 °C unless otherwise indicated. All measurements were conducted with a 0.3 mm gap distance between the plates. A solvent trap was also used to ensure homogeneous temperature and to prevent water evaporation. The hydrogels were heated at 85 °C and the resulting liquid was immediately placed into the rheometer and subjected to sinusoidal oscillations. All experiments were carried out within the linear viscoelastic regime (LVR), in which the measured shear moduli (G' , G'') are independent of the applied strain (i.e. without disruption of the gel structure). For this purpose an amplitude strain sweep (from 0.01 to 100% at an angular frequency of 6.28 rad s^{-1}) was performed for each sample.

2.5. Transmission electronic microscopy (TEM)

TEM microscopy experiments were performed with a Hitachi H



Scheme 1. The synthesis of urea and amide bolaamphiphiles. Reagents and conditions: a) propargylamine (2.2 equiv), SOCl₂ (2.1 equiv), NEt₃ (3 equiv), CH₂Cl₂, rt, 16 h; b) propargylamine (2.2 equiv), NEt₃ (3 equiv), CH₂Cl₂, rt, 16 h; c) K₂CO₃ (1.5 equiv), propargyl bromide (1.5 equiv), DMF, 50 °C; d) 1-azido-2,3,4,6-tetra-O-acetyl-β-D-glucopyranoside, CuSO₄ (10 mol %), sodium ascorbate (20 mol %), *tert*-butanol/water (50/50), 60 °C, 20 h; e) PPh₃ (1.2 equiv), CBr₄ (3equiv), NaN₃ (3 equiv), DMF; f) N,N'-dipropargylalkanediamide/urea, CuSO₄ (10 mol %), sodium ascorbate (20 mol %), *tert*-butanol/water (50/50), 60 °C, 20 h; f) sol. NaOMe 1 M, MeOH.

7650 (negative staining with Uranyle acetate 2.5% in water, Ni carbon coated grids). Before TEM imaging, the sample were dried on the grids at room temperature.

2.6. In vivo studies

2.6.1. In vivo analysis of injectability

Bilateral subcutaneous injections were performed on 10-week-old OF-1 female mice (central animal facility of the Université de Bordeaux, Bordeaux, France). Mice were gas anaesthetised (4% isofurane). Gels, previously introduced in a 1 ml syringe, were directly injected into dorsal subcutaneous sites using a 21-gauge needle. Six implantations were performed for each experimental condition. The compounds used to produce the hydrogels were mixed with cyanin 5.5 (SIGMA Aldrich, USA) at a concentration of 0.001% (w/w) just after heating and before gel formation. Six implantations were performed for each experimental condition. At

different times after surgery, fluorescence images of the cyanin-containing gels was performed using a Lumina LT device (Perkin-Elmer, USA). In order to assess inflammation in a non-invasive manner, lucigenin (2 mg per mouse) was injected subcutaneously and the luminescence was recorded 20 min after injection using the Lumina LT device. Lipopolysaccharide (SIGMA Aldrich, USA) or polystyrene beads (Polysciences, USA) were used as positive controls for inflammation. All procedures and the animal treatment complied with the Principles of Laboratory Animal Care formulated by the National Ethics committee. The studies were carried out in accredited animal facilities at the University of Bordeaux, and were approved by the Animal Research Committee of University of Bordeaux.

2.6.2. Histology

Histological characterization was performed 21 days after gel injection. Mice were sacrificed by cervical dislocation. Harvested

subcutaneous pockets were fixed in 4% PFA for 4 h at 4 °C, dehydrated and embedded in paraffin. 5 µm thick sections were cut, deparaffinized using toluene, rehydrated in decreasing concentrations of ethanol (100–50%), washed in distilled water and finally stained with Masson's trichrome.

3. Results and discussion

In order to modulate both the rheological and biological properties of LMWG-based hydrogels, we hypothesized that the insertion of hydrogen bonding functions in the bolaamphiphile architectures could impact on the supramolecular organizations. Previous experiments achieved on ether [22] and carbamate [28] linkages demonstrated that the functions linking the polar heads to the hydrophobic segments are playing an important role in the stabilization of the supramolecular assemblies. For example, the presence of carbamate in the bolaamphiphile structure increases the G' modulus compared to the ether analogue. However, despite its improved mechanical properties, the melting temperature of 36 °C measured in the case of carbamate bolaamphiphile based gels prohibited its use for *in vivo* injection applications. Hence, we designed molecular architectures in which the hydrophobic segments were attached to the nucleobase via a triazole ring and either amide or urea moieties at the 5'-position of thymidine (Fig. 1). In this contribution we selected the amide function because of structural similarity to the peptide bond and urea for its hydrogen bonding properties [30,31].

The synthetic route to the five bolaamphiphiles gelators is presented in Scheme 1. The molecules synthesized in each step were isolated and characterized by ^1H , ^{13}C NMR and mass spectrometry as shown in Figs. S1 and S2 (ESI). The synthesis of the target compounds was carried out in five steps starting from commercial thymidine (see Scheme 1). First, a propargyl group was introduced to the nitrogen at the 3 position of thymine in the presence of a potassium carbonate via a nucleophilic substitution reaction. The resulting intermediate **6** was reacted with 1-azido-2,3,4,6-tetra-O-acetyl- β -D-glucopyranoside in the presence of CuSO_4 following a 1,3-dipolar Huisgen cycloaddition yielding to compound **7**. After formation of the 5'-azido derivative **8** in the presence of sodium azide, hydrophobic segments featuring either amide (compounds **1** and **2**) or urea (**3,4** and **5**) functions were reacted with **8** to provide the peracetylated amide and urea intermediates **9, 10** and **13, 14, 15**, respectively. Finally, deprotection of acetyl groups led to the expected amide **11, 12** and urea **16, 17, 18** based bolaamphiphiles.

In order to determine the impact of structural modifications (e.g. the insertion of amide and urea), on the supramolecular behaviors of bolaamphiphiles their physicochemical properties were studied. First, the gelation properties were investigated, including i) hydrogel formation, ii) the determination of the critical gelation concentrations (CGC), infrared spectroscopy studies and the sol-gel transition temperature transitions.

Regarding gel formation assays, all bolaamphiphiles were dispersed in Milli-Q water at concentrations up to 4% (w/w). To ensure their complete solubilization, all samples were heated at 80 °C and shaken at 1000 rpm during 30 min using a Thermomixer compact (Eppendorf, USA). The samples were then allowed to cool down to room temperature. The observation was carried out 1 h later. In order to evaluate the gel formation, all samples were then turned upside-down; no flowing under its own weight corresponded to the stabilization of the gel. In these conditions the bis-amide **12** and the bis-ureas **16** and **18** form hydrogels, whereas bolaamphiphiles **11** and **17** are completely soluble (Fig. 2).

Regarding the critical gelation concentrations (CGCs), the novel bolaamphiphiles **12, 16** and **18** exhibit lower CGCs (0.14%, 0.10%,

0.21% w/w for compounds **12, 16** and **18**, respectively) than the bolaamphiphile bis ether (CGC = 0.51% w/w). The gelation kinetic is an important parameter in the design and the development of new injectable biomaterials for applications in the field of regenerative medicine. Hence, the dynamic of gel formation for the bolaamphiphiles dissolved at 1% w/w in water were investigated. In typical experiments, after heating the samples above the melting temperatures at 80 °C for 5 min, the vials were allowed to stand at room temperature (23 °C). In these conditions the gelation times determined by the vial inversion method, are 3 min 18 s, 40 s, and 43 min 58 s for compounds **12, 16** and **18**, respectively. Note that in the same conditions the bolaamphiphile bis ether precipitates and has to be sonicated at room temperature for few minutes, while compounds **12, 16** and **18** spontaneously stabilize hydrogel without any sonication.

The sol-gel transition temperature of **12, 16** and **18** were determined by differential scanning calorimetry (DSC). In the 1.5%–4% region (w/v), the bolaamphiphile based gels feature melting temperatures between 55 °C and 80 °C (at 11.55 mM, sol-gel transition temperatures are 58.5 °C, 78.8 °C and 61.8 °C for compounds **12, 16** and **18**, respectively, Fig. S4). Importantly, at the same concentration, GNBA bis ether possesses a lower gel-sol transition temperature (43 °C, Fig. S5) compared to the novel amide and urea derivatives, indicating that amide and urea functions are indeed playing a role in the stabilization of the supramolecular gels.

In order to understand the interactions involved in the supramolecular assembly (π - π stacking, hydrogen bonding etc) a series of FT-IR spectroscopy experiments was achieved. The infrared spectrum of **16** in DMSO shows a strong band at 1667 cm^{-1} , which can be assigned to the Amide I ($\nu_{\text{C=O}}$) band for a non-hydrogen bonded urea group. To perform infrared experiments on hydrogels, H_2O was replaced by D_2O to overcome the strong water absorption (at 1640 cm^{-1}), which can affect the analysis. In the 1800–1400 cm^{-1} spectral range, the assignment of vibrational modes in D_2O is consistent with the data already reported for the nucleic bases [32,33]. By a comparison of the infrared spectrum of GNBA bis ether, the bands located at 1604 and 1502 cm^{-1} were attributed to the amide I and amide II modes of the urea group, respectively (see Figs. S3 and S4). These frequencies are close to those obtained for hydrogen bonded urea groups (1610 and 1510 cm^{-1}) [34]. Moreover, the Amide I band shifts from 1667 cm^{-1} for a solution of **16** in DMSO to 1610 cm^{-1} in the gel state. These results suggest that the supramolecular assembly is also driven by the formation of hydrogen bond network. Note that the deuteration shifts the bands to lower frequencies [35]. Typically, the Amide II (δ_{NH} , $\nu_{\text{C-N}}$) band appears in the 1590–1565 cm^{-1} region but, in D_2O , this band shifts to 1510–1460 cm^{-1} with a large contribution of C-N stretching vibration [36]. For compound **12**, the infrared spectrum shows an absorption band at 1627 cm^{-1} , characteristic of the intermolecular hydrogen bonded amide groups. This band is approximately 38 cm^{-1} downshifted relative to the 1665 cm^{-1} band that is assigned to the carbonyl stretching mode of the non-hydrogen bonded amide groups (Fig. S5).

Microscopy studies using Transmission Electronic Microscopy were then undertaken to investigate gel properties with respect to the presence of a supramolecular network containing cavities. Further analysis of these images indicates different morphologies depending on bolaamphiphiles structures. Noteworthy, gel forming bolaamphiphiles **16, 18, 12** exhibit dense cross-linked networks with fibers of 6–8 nm in diameter, whereas circular fine fibers that are circularly organized are observed in the case of saturate compound **11**, which does not stabilize hydrogel (see Fig. 3).

Following the qualitative stability to inversion tests, the mechanical properties of bolaamphiphiles based gels were analyzed using oscillatory rheology to characterize the strength of the gel.

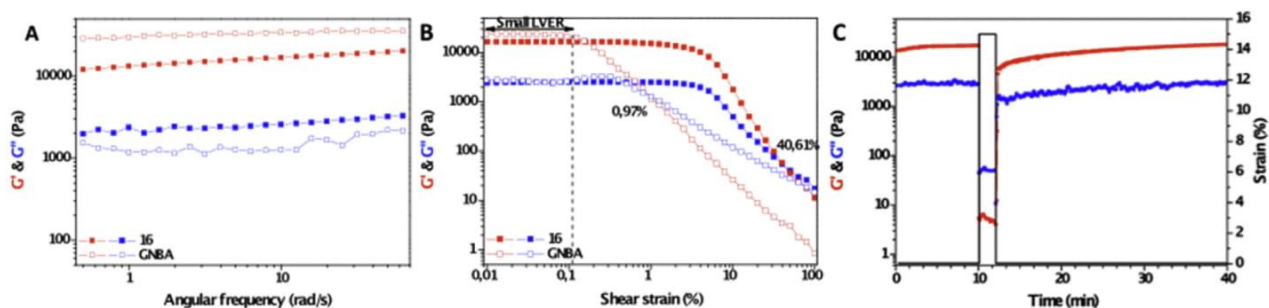


Fig. 4. Oscillatory rheological properties of hydrogels **16** and Bola-T. A) Frequency sweep results, B) Amplitude sweep results. C) Step-strain measurement of the hydrogel **16** at 2% (w/v) at a fixed angular frequency of 6.283 rad/s. The gel was successively swept from 0.03% to 15% strain, then back to 0.03% strain.

with the diether analogue, the gels exhibit a broader linear viscoelastic region (2.5% vs. 0.1%) and a higher critical strain (14–40% vs. 1%). Once the threshold of critical strain has been reached, the gel structure breaks down (see also Fig. S8).

Most of the time for *in vivo* applications the hydrogels have to be delivered *via* injection through a syringe. Hence, it is important to determine whether or not the materials can recover their initial strength quickly after injection. First, the response to mechanical stress was studied by performing a basic experiment; all hydrogels were shaken vigorously to flow and after resting those samples recover their gel behavior. The injectability of these gels was then investigated by rheology by applying successive low/high strain (Fig. 4C, Fig. S10). The gel was first subjected to a high strain (15%) in order to cause the collapse of the gel structure (the G' value was much lower at this point). Upon reducing the strain to 0.03%, both moduli increase gradually and the sample returns to the gel state. In the case of bis-urea **16** the G' recovers completely its initial value in 20 min. This experiment was repeated at least three times. In each case, the G' rapidly returns to the same initial value. Concerning hydrogels **12** and **18**, the high strain applied repeatedly leads to the weakening of the thixotropic phenomenon. The G' does not reach totally its initial value during the second and third cycles (Fig. S11).

Hydrogels have potential therapeutic applications as carriers for drug release or as scaffolds for tissue regeneration. To be eligible as therapeutic agents, hydrogels should elicit a limited chronic inflammatory reaction, and reduced fibrosis. In addition, the kinetics

of gel degradation is an important parameter. Indeed hydrogels can be potentially used for the regeneration of different damaged tissues such as skin, liver, kidney, heart, cartilage or bone, which have different kinetics of regeneration. For a maximum efficiency, their degradation should be coupled to tissue formation. In order to monitor gel degradation, we incorporated a cyanin dye within each hydrogel. We checked *in vitro* for the absence of release of the dye (data not shown). Recording of the fluorescence at different time points showed a more rapid decrease of the signal with the **15** and **18** than with the **12** (Fig. 5a, b). This difference in gel degradation was confirmed by histological examination 3 weeks after implantation. We observed striking differences between the amounts of the different hydrogels still present at the site of implantation: whereas gels made of compound **16** were observed as large compact ovoid blocks integrated in the mouse skin, gels formed with compound **18** were found as small thin elongated pieces and those formed with compound **12** were almost undetectable (Fig. 6). These observations confirm our fluorescence recording data, and suggest very different degradation rates, with compound **16** being the most stable. To analyze tissue reaction to each of the bolaamphiphile based hydrogels, we performed an *in vivo* assessment of inflammation, using lucigenin, a reagent which is known to be activated by reactive oxygen species generated by macrophages, and to produce light when activated by ROS (37). This protocol has been previously used to follow chronic inflammation processes. Whereas positive controls producing a strong (LPS) or moderate

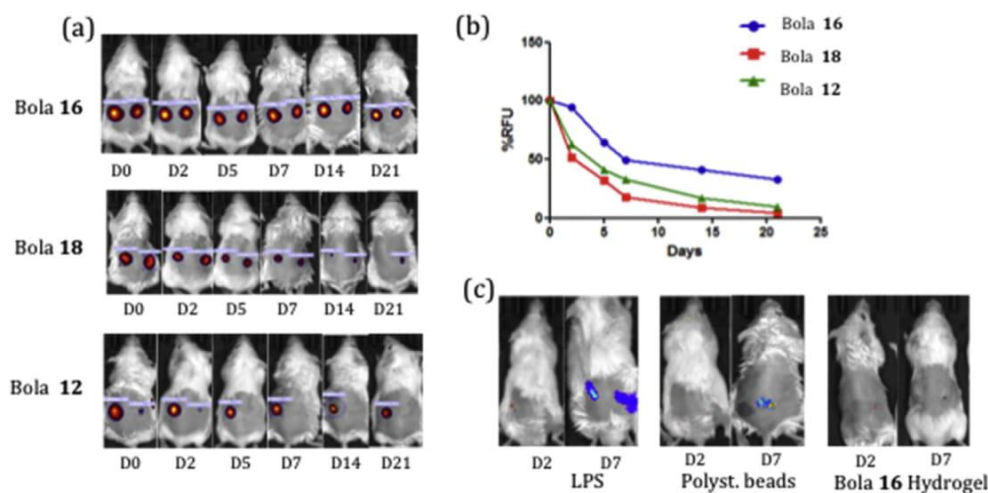


Fig. 5. (a) Imaging of the fluorescence of gel-embedded cyanin; (b) quantification of the fluorescence signal; (c) imaging of luminescence after administration of lucigenin to LPS-injected, polystyrene beads implanted or MR16 gel-implanted mice.

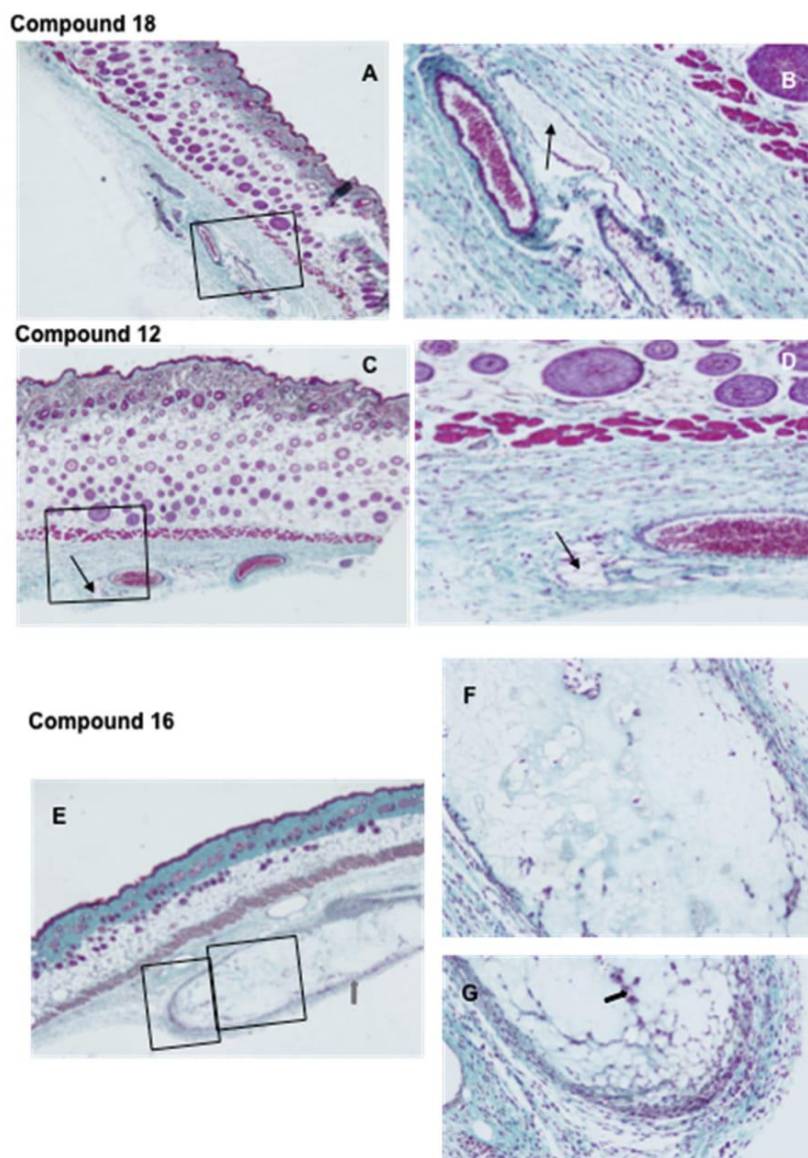


Fig. 6. The hydrogels obtained with amide derivative **12** (C and D) and urea analogue **18** (A and B) are almost completely degraded 21 days after implantation (black arrows). In contrast, gels made with urea based-bolaamphiphiles **16** is found integrated into the host tissue (E, F and G), surrounded by a fibrous capsule (grey plain arrow) and infiltrated by a few host cells (plain black arrow), more abundant in the periphery of the gel.

inflammation (polystyrene beads, as described in reference 38) showed a significant signal 7 days after injection or implantation, MR16 did not show any detectable signal (Fig. 5c). Mice, which had received the other two gels did not show any signal (data not shown), however the absence of signal may be due to the almost complete degradation of the gels at that time. To further analyze in more details tissue reactions, we examined the histological sections of biopsies harvested 21 days after implantation (Fig. 6). This time point is often considered as suitable to reveal chronic inflammation and fibrosis. We first observed striking differences between the amounts of the different hydrogels still present at the site of implantation: whereas gels made of compound **16** were observed as large compact ovoid blocks integrated in the mouse skin, gels formed with compound **18** were found as small thin elongated pieces and those formed with compound **12** were almost undetectable. These observations suggest very different degradation

rates, with compound **16** being the most stable and compound **12** the least stable. It was not possible to analyze inflammatory reaction or fibrosis with gels made of compound **12**. Gels with compound **18** were surrounded by a very thin layer of fibroblasts, with no obvious sign of inflammation. Gels formed with compound **16** were surrounded by a thicker fibrotic capsule, characterized by the presence of many cells embedded in a collagen matrix. Most of these cells were fibroblast-like cells, and macrophages were also observed at the periphery of this capsule. A few infiltrated cells, among which macrophages, were observed inside the gel. This histological feature is typical of a moderate chronic inflammation, associated with a limited fibrosis.

Altogether, these results indicate that a continuum from molecular structures, supramolecular assemblies to biological applications has to be considered when designing new injectable LMWG scaffolds. First, at the molecular level the functions selected have to

favor both intermolecular interactions and stability. The urea derivative **16**, which feature the optimum hydrophilic hydrophobic balance, induces the formation of a stable supramolecular network as demonstrated by FTIR and TEM experiments. Second, regarding the rheological properties, here again compound **16**, which shows fast gelation kinetics and optimum LVER, G' , G'' values, encompasses adequate mechanical properties allowing both injectability and stability *in vivo*. *In fine*, the combination of the optimum molecular, supramolecular and rheological properties allow the urea-derivative **16** to be: i) stable, ii) non-toxic and iii) non-immunogenic after injection *in vivo*.

4. Conclusion

In this study we have demonstrated simple and controllable synthesis of a novel type of supramolecular hydrogels, by constructing the supramolecular architecture with bolaamphiphiles as low molecular weight gelators. In order to generate novel biomaterial candidates we synthesized a series of bolaamphiphiles featuring urea and/or amide functions. Thanks to this molecular approach, we identified one urea-containing molecule, bola bis-urea **16**, which possess the optimum mechanical (injectability, fast gelation kinetics, high elastic moduli, thixotropic, etc) and biological properties (limited chronic inflammatory, reduced fibrosis, slow degradation rate *in vivo*). As compared with widely used natural polymers such as alginate, collagen hyaluronic acid, these gels obtained from small molecular weight molecules show several advantages: a perfect control of structure and purity, in contrast to batch to batch variations frequently observed with products purified from tissues; a very easy handling procedure enabling incorporation of proteins or cells in the solution just prior to gel formation, in contrast to cumbersome procedures for example to neutralize the acidic collagen solution; excellent mechanical stability, including high elastic moduli and limited shrinkage resulting from syneresis, as compared with most natural polymers.

The strategy of the supramolecular architecture and the simple synthetic procedure reported in this contribution allow fabricating various kinds of low molecular hydrogels with adapted performances for biomedical applications in the field of regenerative medicine. By using this bottom-up approach for synthesizing supramolecular gels, and the modularity of the bolaamphiphile structures (*i.e.* modulation of the sugar moieties), this approach might be a fertile area of research for many applications, including drug delivery systems, artificial scaffolds for tissue engineering etc, and may open up new fields of application for supramolecular hydrogels.

Acknowledgment

This work, realized within the framework of the Laboratory of Excellence AMADEus with the reference ANR-10-LABX-0042-AMADEUS, has benefitted from aid by the state operated "Agence Nationale de la Recherche" under the program "Initiative for Excellence IdEx Bordeaux" holding the reference ANR-10-IDEX-0003-02. The work has also been supported by the "French National Research Program for Environmental and occupational Health of ANSES" (2015/1/072). The authors thank the BIC Center for technical assistance during TEM observations.

Appendix A. Supplementary data

Supplementary data related to this article can be found at <http://dx.doi.org/10.1016/j.biomaterials.2017.08.034>.

References

- [1] M. Gurvan, T. Tonon, D. Scornet, J.M. Cock, B. Kloareg, The cell wall polysaccharide metabolism of the brown alga *Ectocarpus siliculosus*. Insights into the evolution of extracellular matrix polysaccharides in Eukaryotes, *New Phytol.* 188 (2010) 82–97.
- [2] H. Geckil, F. Xu, X. Zhang, S.J. Moon, U. Demirci, Engineering hydrogels as extracellular matrix mimics, *Nanomed. Nanomed.* 5 (2010) 469–484.
- [3] B.M. Gillette, J.A. Jensen, B. Tang, G.J. Yang, A. Bazargan-Lari, M. Zhong, S.K. Sia, In situ collagen assembly for integrating microfabricated three-dimensional cell-seeded matrices, *Nat. Mater.* 7 (2008) 636–640.
- [4] O. Smidsrød, G. Skjåk-Bræk, Alginate as immobilization matrix for cells, *Trends Biotechnol.* 8 (1990) 71–78.
- [5] S. Orr, I. Strominger, E. Eremenko, E. Vinogradov, E. Ruvinov, A. Monsonego, S. Cohen, TGF- β affinity-bound to a macroporous alginate scaffold generates local and peripheral immunotolerant responses and improves allocl transplantation, *Acta Biomater.* 45 (2016) 196–209.
- [6] S. Sahoo, C. Chung, S. Khetan, J.A. Burdick, Hydrolytically degradable hyaluronic acid hydrogels with controlled temporal structures, *Biomacromolecules* 9 (2008) 1088–1092.
- [7] Q. Li, C.G. Williams, D.D. Sun, J. Wang, K. Leong, J.H. Elisseeff, Photocrosslinkable polysaccharides based on chondroitin sulfate, *J. Biomed. Mater. Res. A* 68 (2004) 28–33.
- [8] D. Eyrich, F. Brandl, B. Appel, B.H. Wiese, G. Maier, M. Wenzel, et al., Long-term stable fibrin gels for cartilage engineering, *Biomaterials* 28 (2007) 55–65.
- [9] A.E. Ropper, D.K. Thakor, I. Han, D. Yu, X. Zeng, J.E. Anderson, et al., Defining recovery neurobiology of injured spinal cord by synthetic matrix-assisted hMSC implantation, *Proc. Natl. Acad. Sci. U. S. A.* 114 (2017) E820–E829.
- [10] C. Tu, Q. Cai, J. Yang, Y. Wan, J. Bei, S. Wang, The fabrication and characterization of poly(lactic acid) scaffolds for tissue engineering by improved solid-liquid phase separation, *Polym. Adv. Technol.* 14 (2003) 565–573.
- [11] J. Wang, F. Zhang, W.P. Tsang, C. Wan, C. Wu, Fabrication of injectable high strength hydrogel based on 4-arm star PEG for cartilage tissue engineering, *Biomaterials* 120 (2017) 11–21.
- [12] S.W. Peng, C.W. Li, I.M. Chiu, G.J. Wang, Nerve guidance conduit with a hybrid structure of a PLGA microfibrillar bundle wrapped in a micro/nanostructured membrane, *Int. J. Nanomed.* 12 (2017) 421–432.
- [13] K. Uematsu, K. Hattori, Y. Ishimoto, J. Yamauchi, T. Habata, Y. Takakura, et al., Cartilage regeneration using mesenchymal stem cells and a three-dimensional polylactideglycolic acid (PLGA) scaffold, *Biomaterials* 26 (2005) 4273–4279.
- [14] A.J. Vegas, O. Veiseh, J.C. Doloff, M. Ma, H.H. Tam, K. Bratlie, et al., Combinatorial hydrogel library enables identification of materials that mitigate the foreign body response in primates nature biotechnology, *Nat. Biotechnol.* 34 (2016) 345–352.
- [15] E.L. Smith, J.M. Kanczler, D. Gothard, C.A. Roberts, J.A. Wells, L.J. White, et al., Evaluation of skeletal tissue repair, Part 1: assessment of novel growth-factor-releasing hydrogels in an ex vivo chick femur defect model, *Acta Biomater.* 10 (2014) 4186–4196.
- [16] G.P. Chen, T. Sato, T. Ushida, N. Ochiai, T. Tateishi, Tissue engineering of cartilage using a hybrid scaffold of synthetic polymer and collagen, *Tissue Eng.* 10 (2004) 323–330.
- [17] W. Gao, Y. Liang, X. Peng, Y. Hu, L. Zhang, H. Wu, et al., In situ injection of phenylboronic acid based low molecular weight gels for efficient chemotherapy, *Biomaterials* 105 (2016) 1–11.
- [18] M.A. Ramin, K.R. Sindhu, A. Appavoo, K. Oumzil, M.W. Grinstaff, O. Chassande, P. Barthélémy, Cation tuning of supramolecular gel properties: a new paradigm for sustained drug delivery, *Adv. Mater.* 29 (2017) 1605227.
- [19] J.W. Steed, Supramolecular gel chemistry: developments over the last decade, *Chem. Commun.* 47 (2011) 1379–1383.
- [20] L. Meazza, J.A. Foster, K. Fucke, P. Metrangolo, G. Resnati, J.W. Steed, Halogen-bonding-triggered supramolecular gel formation, *Nat. Chem.* 5 (2013) 42–47.
- [21] Y. Hu, W. Gao, F. Wu, H. Wu, B. He, J. He, Low molecular weight gels induced differentiation of mesenchymal stem cells, *J. Mater. Chem. B* 4 (2016) 3504–3508.
- [22] L. Latxague, M.A. Ramin, A. Appavoo, P. Berto, M. Maisani, C. Ehret, O. Chassande, P. Barthélémy, Control of stem-cell behavior by fine tuning the supramolecular assemblies of low-molecular-weight gelators, *Angew. Chem. Int. Ed. Engl.* 15 (2015) 4517–4521.
- [23] Xuewen Du, Jie Zhou, Junfeng Shi, Bing Xu, Supramolecular hydrogelators and hydrogels: from soft matter to molecular biomaterials, *Chem. Rev.* 115 (2015) 13165–13307.
- [24] B.C. Baker, A.L. Acton, G.C. Stevens, W. Hayes, Bis amide-aromatic-ureas – highly effective hydro- and organogelator systems, *Tetrahedron* 70 (2014) 8303–8311.
- [25] M. Mathiselvam, D. Loganathan, B. Varghese, Synthesis and characterization of thiourea- and urea- linked glycolipids as low-molecular-weight hydrogelators, *RSC Adv.* 3 (2013) 14528–14542.
- [26] M. Yamanaka, Development of C₃-Symmetric tris-urea low-molecular-weight gelators, *Chem. Rec.* 16 (2016) 768–782.
- [27] M. Yamanaka, N. Haraya, S. Yamamichi, Chemical stimuli-responsive supramolecular hydrogel from amphiphilic tris-urea, *Chem. Asian J.* 6 (2011) 1022–1025.
- [28] L. Latxague, A. Gaubert, D. Maleville, J. Baillet, M.A. Ramin, P. Barthélémy,

- Carbamate-based bolaamphiphile as low-molecular-weight hydrogelators, *Gels* 2 (2016) 25–33.
- [29] M.A. Ramin, J. Baillet, S. Benizri, L. Latxague, P. Barthélémy, Uracile based glycosyl-nucleoside-lipids as low molecular weights organogelators, *New J. Chem.* 40 (2016) 9903–9906.
- [30] M. Yamanaka, Urea derivatives as low-molecular-weight gelators, *J. Incl. Phenom. Macrocycl. Chem.* 77 (2013) 33–48.
- [31] M. Obrzud, M. Rospenk, A. Koll, Self-aggregation mechanisms of N-alkyl derivatives of urea and thiourea, *Phys. Chem. Chem. Phys.* 16 (2014) 3209–3219.
- [32] M. Banyay, M. Sarkar, A. Graslund, A library of IR bands of nucleic acids in solution, *Biophys. Chem.* 104 (2003) 477–488.
- [33] C.S. Peng, K.C. Jones, A. Tokmakof, Anharmonic vibrational modes of nucleic acid bases revealed by 2D IR spectroscopy, *J. Am. Chem. Soc.* 133 (2011) 15650–15660.
- [34] M. de Loos, A. Friggeri, J. van Esch, R.M. Kellogga, B.L. Feringa, Cyclohexane bis-urea compounds for the gelation of water and aqueous solutions, *Org. Biomol. Chem.* 3 (2005) 1631–1639.
- [35] Y. Mido, An infrared study of various dialkylureas in solution, *Spectrochim. Acta* 28A (1972) 1503–1518.
- [36] M. Malferrari, G. Venturoli, F. Francia, A. Mezzetti, A new method for D2O/H2O exchange in infrared spectroscopy of proteins, *Spectrosc. Int. J.* 27 (2012) 337–342.

Results

Article 2: Proangiogenic Supramolecular Gels through Biodegradation

Sindhu, K.R.¹, Bansode, N.², Rémy, M.¹, Morel, C.¹, Bareille, R.¹, Hagedorn, M.³, Hinz, B.⁴,
Barthélémy, P.², Chassande, O.¹ & Boiziau, C.¹

Manuscript: in preparation.

Patent under review: Part of the work mentioned in the article on the proangiogenic potential of active compound released during degradation is applied for the patent application.

My contribution to the article: Biological characterisation of low molecular weight hydrogels was performed by subcutaneous implantation in mice to assess their degradation, inflammation and their angiogenesis.

Thanks to Philippe Barthélémy's group for the synthesis and the characterisation of the molecules by MALDI mass spectroscopy and NMR analysis, to Martin Hagedorn for his help with the CAM (chorioallantoic membrane) experiments and to Boris Hinz and his group for his welcome in his lab.

Proangiogenic Supramolecular Gels through Biodegradation

Sindhu, K.R.¹, Bansode, N.², Rémy, M.¹, Morel, C.¹, Bareille, R.¹, Hagedorn, M.³, Hinz, B.⁴,
Barthélémy, P.², Chassande, O.¹ & Boiziau, C.^{1,*}

1: INSERM, Univ. Bordeaux, Laboratory for the Bioengineering of Tissues, F-33000 Bordeaux, France.

2: INSERM, Univ. Bordeaux, ARNA Laboratory, F-33000 Bordeaux, France.

3: INSERM, Univ. Bordeaux, Biotherapy of Genetic Diseases, Inflammatory Disorders and Cancers, F-33000 Bordeaux, France.

4: Laboratory of Tissue Repair and Regeneration, Faculty of Dentistry, University of Toronto, Toronto, Ontario, Canada

*** To whom correspondence should be addressed: claudine.boiziau@inserm.fr.**

Key words: hydrogel, biodegradation product, bio integration, fibrosis, angiogenesis, tissue regeneration

Running title: Supramolecular hydrogels.

ACKNOWLEDGMENTS

This work was supported by a grant from ANR (Bio3, ANR-16-CE19-0001-01). SKR and NB received doctoral and postdoctoral fellowships from LabEx AMADEus, respectively (ANR-10-LABX-0042-AMADEUS). The research of BH is supported by the Canadian Institutes of Health Research (CIHR), Foundation Grant #375597. We would like to thank facilities for animal experimentation: Vivoptic, and the Animal house A1 (University of Bordeaux).

COMPLIANCE WITH ETHICAL STANDARDS

Conflict of Interest. The authors declare that they have no conflict of interest.

Ethical Approval. All applicable international, national, and institutional guidelines for the care and use of animals were followed. All procedures performed in studies involving animals were in accordance with the ethical standards of the institution or practice at which the studies were conducted (animal experimentation permission APAFIS#4375-2016030408537165).

ABSTRACT

Hydrogels for regenerative medicine are often designed to allow cellular infiltration, degradation, and neovascularization. Low molecular weight hydrogels (LMWHs), formed by self-assembly *via* non-covalent interactions, are gaining significant interest in this context due to their soft nature, ease of use and injectability. To investigate the suitability of LMWHs as body implant materials that could stimulate tissue regeneration, four new LMWHs based on molecules containing biomolecules like nucleic acid and lipid were analyzed *in vivo*: we investigated the foreign body response upon subcutaneous implantation into mice. Despite being infiltrated with

macrophages, none of the hydrogels triggered a detrimental inflammatory response, and most macrophages present in the surrounding tissue acquired an immuno-modulatory rather than inflammatory phenotype. Concomitantly, no fibrotic capsule was formed after three weeks. The tested LMWHs exhibited different degradation kinetics *in vivo* and *in vitro*. LMWH that had high angiogenic properties *in vivo* were found to release a common by-product upon degradation *in vitro*. When chemically synthesized, this glyconucleoside – a thymidine associated with deoxyribose and glucose – exerted angiogenic properties *in vitro* in scratch assays with monolayers of human endothelial cells and *in vivo* in chick chorioallantoic membrane assays. Collectively, by displaying good biointegration without causing fibrosis, and by promoting angiogenesis through the release of a pro-angiogenic degradation product, these LMWHs hold promise for various regenerative applications.

1. INTRODUCTION

Our ageing population and the worldwide development of unhealthy lifestyles increase the need for therapeutics and medical devices with improved properties. Various biomaterials are used in different applications such as scaffolds for regeneration of defective tissues, for drug delivery, or to coat implantable medical devices. For regenerative medicine applications, biomaterials are developed to be used either alone or in combination with cells and/or biomolecules to increase the success of regenerative processes or alternative to organ transplantation. First, desired biomaterial properties should resemble those of the organ to replace, such as collagen, fibrin or gelatin scaffolds mimicking extracellular matrix (ECM) of soft tissues or hydroxyapatite for bone regeneration, and reproduce complex 3D structures of native tissues [1–3]. Second, biomaterials with tunable properties can be developed into drug delivery systems for improved local and controlled release of drugs. Such biomaterials can overcome drug delivery limitations caused by hydrophobicity or enzymatic degradation before reaching the target tissue. Sustained local release from such materials is further improving drug pharmacokinetics and allows to reduce drug concentrations. Finally, the coating of implantable medical devices such as intracortical microelectrodes for micro-electrocorticography [4], deep brain stimulation [5] or enzymatic biofuel cells [6] is needed to minimize the fibrous capsule formation that inhibits the electrode functionality. In addition to these requirements, any material that is injected or implanted in the body is facing the same fundamental challenges: it must be biocompatible, and the initial structure, as well as the degradation products, must exhibit low if any cytotoxicity. Most importantly, the inflammatory reaction that is elicited by the biomaterial must be controlled, firstly to prevent a too fast elimination/degradation of the biomaterial before successful tissue regeneration is reached, and secondly to avoid a strong and/or chronic local inflammatory environment.

The body has an innate self-defence mechanism to fight any implanted biomaterial perceived as ‘foreign’ - called the foreign body reaction (FBR). The different steps of the FBR are well known [7,8] adsorption of proteins from the blood, and extracellular medium is usually the first step in FBR and occurs instantaneously to reduce the surface energy by a thermodynamically driven process. Within a few hours, neutrophils are recruited, and the degranulation process releases proteolytic enzymes and reactive oxygen species. Chemoattractant cytokines are also released, that attract blood circulating monocytes. As a first step, monocytes differentiate to macrophages with a pro-inflammatory phenotype, designed as “M1-phenotype” [9,10]. Then, depending on the material, and on microenvironment cues, the phenotype of macrophages can evolve toward an immuno-modulatory and remodelling phenotype, that is part of the large spectrum of “M2 phenotypes” [9,11]. Therefore, after 7 to 10 days, biomaterials with good biocompatibility properties can be surrounded by macrophages displaying immuno-modulatory phenotypes. Fibroblasts recruited from the adjacent tissue are involved in the formation of new ECM. In case of a sustained inflammation around the biomaterial, macrophages will fuse to form multinucleated foreign body giant cells, and an extended activation of fibroblasts will drive the formation of a fibrous capsule that aims at isolating the foreign body. This fibrotic capsule impedes the diffusion of nutrients and metabolites, leading to the failure of the medical devices. To date, several attempts have been made to develop potential biomaterials that reduce the capsule formation, albeit with limited success.

Hydrogels are attractive for clinical applications and respond to most of the demands on successful biomaterials. By definition, hydrogels are hydrophilic, which facilitates the diffusion of

oxygen and nutrients throughout their structure and, in some cases, allows cell colonization. Hydrogels are easy to use, can be mostly injected, have tunable mechanical properties, and their local swelling and gelling allow for adaptation to the 3D structure of the local host environment. Low molecular weight hydrogels (LMWHs) are one class of self-assembled physical gels, formed through reversible non-covalent interactions such as hydrogen bonding, π - π stacking, hydrophobic effect and ion pairing. Recently, synthetic hybrid molecules combining biomolecules such as nucleic acid and lipids have been investigated as hydrogelators [12]. For example, non-toxic nucleolipids (NLs, nucleoside and nucleotide lipids) and glyconucleolipids (GNLs) [13] are promising polymer-free materials for applications in health science and technology applications. The supramolecular properties of NLs and GNLs allow sustained drug release [14], use in tissue engineering [15], and use as bioinspired materials [16]. In GNLs, amide, urethanes, and urea functions play a major role in both mechanical and biological properties of supramolecular hydrogels [17,18]. The urea linkage forms more stabilized self-assembly due to the involvement in two hydrogen bonds. This self-association of urea with two hydrogen bonds is much stronger than that of amides or urethanes, usually one hydrogen bond donors. Also, the urea motif presents an attractive isosteric replacement of the amide linkage with increased resistance to protease degradation. Incorporation of aromatic moieties in conjugation with hydrogen bond donor and hydrophobic group is highly effective to improve the hydrogen bonding and the hydrophobic interactions by taking part in π - π stacking in water essentially to form stable self-assembly. Therefore, such GNLs are promising scaffolds for tissue engineering or medical device coating.

In both cases, the *in vivo* stability, cytotoxicity and body responses are major parameters that allow determining potential applications. We selected three glyconucleoside bolaamphiphile

(GNBA) featuring the hydrophobic moiety functionalized with urea or amide and N-thymine glycosylated head groups conjugated via aromatic triazoline ring (**Fig. 1**). The applications of GNF first synthesized in 2010 [19] have been published in several articles [20–23]. We compared one GNF with three GNBA bearing similar structures (single chain amphiphile versus bolaamphiphiles) with different functional groups (urea, amide). Fibrosis and cell infiltration were analysed. The kinetics of *in vitro* degradation was studied; three hydrogels produced the same degradation product, as observed by mass spectrometry analysis. After chemical synthesis of this product, its angiogenic properties were analysed both *in vitro* with HUVECs and *in vivo* with the chick chorioallantoic membrane.

2. MATERIALS AND METHODS

2.1. Hydrogel preparation

The following molecules were used to prepare the hydrogels at a concentration of 1.5 % (w/v) in sterile phosphate buffered saline (PBS) at pH 7.4: GNF [19] and three GNBA (GNBA-1, GNBA-2, and GNBA-3), corresponding to products 16, 18, and 12 in Ramin *et al.* [18]. Suspensions were heated at 65°C for GNF and 80°C for the three GNBA. The GNF solution was incubated at 37°C for 30 min to form a gel, whereas the other molecules formed the gel within 5 min at room temperature.

2.2. *In vitro* degradation of hydrogels and analysis of degradation products

To assess *in vitro* degradation/disassembly over time, hydrogel disks (100 μ l) were incubated in 7 ml of PBS at 37°C for 21 days and weighted at different time points. All hydrogel samples were pre-weighed after gelation (initial weight). At different time points (1, 2, 3, 5, 7, 15, and 21 days), the samples were removed from PBS, weighed immediately after removing the excess of PBS by gently touching the surface of Kim wipes, and returned to the same solution of PBS. Degradation/disassembly quantification was performed by comparing the hydrogel weight loss over time (done in triplicates). The degradation products generated during the 21-day incubation of the samples was determined by analyzing the PBS solution in which they were incubated (see section 2.2). At day 21, the PBS was collected and analyzed for the degradation products of individual hydrogels by using mass spectroscopy.

2.4. *In vitro* protein adsorption on hydrogels

To investigate non-specific protein adsorption, the adsorption of bovine serum albumin (BSA, GE-healthcare ref K45-001) was evaluated. Hydrogels were cut into pieces with a diameter of 4.7 mm and height of 5.7 mm (volume of 100 μ l, the surface of 119 mm²) followed by incubation in PBS overnight at 37°C to reach the swelling equilibrium. On the following day, the PBS was replaced by 400 μ l PBS containing BSA (2 mg/ml, freshly prepared), followed by incubation in a 24 well plate at 37°C for 2 h. Samples were then rinsed thoroughly several times with PBS to remove unbound BSA proteins, followed by addition of 400 μ l of sodium dodecyl sulfate solution

1 % (w/v) per well for 30 min at room temperature to strip proteins adsorbed on the hydrogel surface. The striped BSA protein was quantified using a standard bicinchoninic acid protein assay (BCA, Pierce™ BCA Protein Assay Kit) as recommended by the manufacturer. The negative control was done in a similar way, excluding the incubation with BSA. Experiments were performed in triplicates.

2.5. Cytotoxicity assessment

Cytotoxicity of hydrogels was assessed according to the international standard ISO10993-5 (Biological evaluation of medical devices -- Part 5: Tests for in vitro cytotoxicity) with some modifications. The L929 cell line (recommended by the standard) and a primary cell culture of adipose tissue-derived mesenchymal stromal cells (MSCs) were grown in alpha-MEM (Gibco, Ref A10490-01, France) without ascorbic acid, and containing 10 % (v/v) fetal calf serum (FCS, Lonza, France). Cells were then seeded at 10,000 cells/cm² in 24-well microtiter plates (Nunc, Denmark) and cultured for 72 h. At subconfluency (3 day culture), hydrogel pieces (diameter 4.7 mm, height 5.7 mm) were immersed in the culture medium using Falcon inserts (Ref: 353096, 24 well formats). The ratio of the sample surface area to the volume of the vehicle was 5 cm²/ml. Wells containing only alpha-MEM + 10% FCS were used as negative controls, wells with cytotoxic agent 0.1% Triton X100 were used as a positive control. Culture plates were then kept in the incubator at 37°C for 24 h giving the “24(1)” cell culture; then, the inserts were transferred on other sub-confluent L929 and MSC cultures for a second and then a third incubation of 24 h, giving “24(2)” and “24(3)” cell cultures. At the end of each 24 h incubation, cell viability was assessed by the Neutral Red assay and cell metabolic activity by using an MTT assay. MTT (3-(4,

5-dimethylthiazolyl-2)-2, 5-diphenyltetrazolium bromide, Sigma-Aldrich, ref M2128) (1 mg/ml stock in alpha-MEM without FCS without phenol red) was added in 125 µl per well. After 3 h of incubation at 37°C in 5% CO₂, the supernatant was removed and formed formazan crystals were dissolved by adding 100 µl of dimethyl sulfoxide (DMSO, Ref D5879-1L, Sigma-Aldrich, France). To assess cell viability, neutral red (Ref N4638, Sigma-Aldrich, France) was resuspended at 1.25% (w/v) in alpha-MEM without FCS, and 100 µl of the prepared solution was added per well. After 3 h of incubation at 37°C, the supernatant was replaced by adding 100 µl of the mixture (50:50) containing 50% ethanol/ 1% acetic acid in water to lyse the cells. In both cases, the intensity of colour was quantified by measuring the absorbance at 540 nm using a spectrophotometer (Perkin Elmer ®, 2030 Multilabel Reader VictorTMX3). The mean values of absorbance measurements obtained from colourimetric tests and their corresponding standard deviation (\pm s.d.) were calculated from n=6. The results are expressed as a percentage of the control (alpha-MEM + 10% FCS).

2.6. Migration and proliferation of human umbilical vein endothelial cells (HUVEC).

The human umbilical cord was obtained from healthy new born with the consent form from the parents under the Etablissement Francais du Sang to isolate HUVECs as previously described [24]. HUVECs were used between passages 3 and 8 in Iscove`s modified Dulbecco`s medium (IMDM; Gibco, Thermo Fisher Scientific), containing 20 % fetal bovine serum (FBS; Lonza, Verviers, Belgium), 12 µg/ml endothelial cell growth factor supplement, and 90 µg/ml heparin (ECGS/H 0.4% (v/v); PromoCell, Heidelberg, Germany).

Scratch migration assays were performed in 6 well plates, coated with 0.2 % gelatin (Sigma-Aldrich, Saint Quentin Fallavier, France). Cells were seeded at 50,000 cells/cm² (subconfluency) in 6 wells with the EBM2 media (Lonza, 00190860, medium allowing endothelial cells to proliferate only with a low efficient) containing 10 % FBS without growth factors for 24 h. Wells containing a confluent monolayer of HUVECs were then washed with Hanks balanced salt solution (HBSS), and a straight-line scratch was made using a 100 µl pipette tip. The wells were gently washed with HBSS to remove detached cells and debris. 2 ml of positive control, test and negative control media were added to the wells (complete EGM-2MV medium as a positive control (Lonza, CC-3202, optimized for efficient endothelial cell proliferation), test sample containing the tested compound GN-1 at a concentration of 1 mM in EBM2-10% FBS and EBM2 medium containing 10% FBS as basal medium). The closure of scratch was monitored by time-lapse videomicroscopy with a frame rate of 10/min for 18 h in Etaluma Lumascope 720. The Etaluma software was used to obtain the movies and to analyze the speed of wound closure quantitatively.

Proliferation analysis was performed at different concentrations of the active compound (2, 10, 20, 50, 100, 500, and 1000 µM diluted in EBM2 medium + 10% FBS). HUVECs were seeded on 24-well plates at a low density of 10,000 cells/cm². The cells were cultured using EBM2 medium containing 10% FBS without any growth factors for basal medium +/- active compound, while the positive control medium was the complete medium EGM-2MV. For the proliferation assay on day 1 and 7, the neutral red assay was performed as described for the cytotoxicity study.

2.7. *In vivo* experiments

Subcutaneous injection of hydrogels into mice. All animal studies were carried out in accredited animal facilities at the University of Bordeaux (accreditation number: A33-063-917) and approved by the animal ethical committee of Bordeaux. The four different hydrogels were prepared as described above and collected in 1 ml syringes when the solution was in viscous form. Ten-week-old OF-1 female mice (Charles Rivers, France) were then anaesthetized using 4.5% isoflurane gas and maintained throughout surgery at 2.5% isoflurane with a face mask and depilated before surgery. The hydrogels were injected subcutaneously using 21-gauge needle bilaterally on the dorsal side of the animals (1 hydrogel/side).

In vivo toxicity assays. Hepatocellular injury that might result from toxicity of implanted hydrogels was quantified by serum biochemical evaluation for alanine aminotransferase (ALT, Activity Assay Kit, Sigma-Aldrich, ref MAK052), aspartate aminotransaminase (AST, Activity Assay Kit, Sigma-Aldrich, ref MAK055), and lactate dehydrogenase (LDH, Assay Kit, Abcam, ab102526). Just before surgery and 3, 7, and 21 days after hydrogel implantation, blood was collected from retro-orbital sinus, allowed to clot, and spun down to collect serum. Serum was used for analysis, as recommended by the kit manufacturers.

Histology, staining and immunohistochemistry. Animals were sacrificed by cervical dislocation 1 and 3 weeks after hydrogel implantation. The hydrogels were harvested with the subcutaneous tissue and fixed in 4% paraformaldehyde (Antigenfix, Diapath, France) overnight at 4°C, followed by dehydration, embedding in paraffin, and sectioning by a microtome (5 µm

thickness). The sections were either stained with Masson's trichome or used for immunolabelling after antigen retrieval was performed by sodium citrate buffer 95°C for 30 min. Blood vessels in and around the hydrogels 21 days after implantation were identified by immunolabelling with rabbit anti-CD31 antibody (Abcam, ref ab28364 dilution:1/100) followed by incubation with HRP-conjugated anti-rabbit secondary antibody (Vector MP-7401, dilution:1/2). The inflammatory response to the biomaterials 21 days post-implantation was studied with the following primary antibodies: rabbit anti-CD68 (Abcam, ref ab1252012, 1/200), rabbit anti-CD206 (Abcam, ref ab64693, 1/500), and rabbit anti-CCR7 (Abcam, ref ab32527, dilution:1/100) followed by detection with Alexa568-conjugated goat anti-rabbit antibody. The fibrosis reaction around the hydrogels was detected by staining mesenchymal cells for vimentin (Cell Signal, ref 5741, 1/100), activated fibroblasts for the myofibroblasts marker α -smooth muscle actin (α -SMA) (α -SM-1, mouse IgG2a, a kind gift from Giulio Gabbiani, University of Geneva, Switzerland, dilution 1/50), and fibronectin (Santa Cruz, sc59826, 1/300). As secondary antibodies, we used goat anti-rabbit conjugated to TRITC (tetramethylrhodamin, Sigma Aldrich, T5268, dilution 1/100), goat antimouse IgG2a 647(Invitrogen, ref A21241, dilution 1/100), goat antimouse IgG1 FITC (Sigma Aldrich, dilution 1/200). All the images were acquired using a nanozoomer (Hamamatsu, Nanozoomer 2.0 HT).

Chick Chorioallantoic membrane (CAM) assay. To quantify angiogenesis, we used the CAM of chick embryos (*Gallus gallus*) (E.A.R.L. Morizeau, Dangers, France) that were incubated at 37°C and 70 % humidity to initiate fertilization. On day 3 of development, 3-5 ml of egg white was withdrawn by punctuating the air chamber with the syringe, and a window was made by cutting the eggshell and sealed with Durapore® tape. On day 13, prepared plastic rings (made from

Nunc Thermanox® coverslips, diameter 13 mm and thickness 0.2 mm) were placed on the intact CAM. 20 µl of the molecule (concentration 500 µg/ml in DMEM medium) or an equivalent volume of DMEM alone as control were deposited in the centre of the plastic rings. The treatment was repeated the following day, followed by photo documentation (day 14). On day 17, the eggs were fixed by the addition of 2 ml of 4 % paraformaldehyde (Antigenfix) for 30 min at room temperature. Imaging was performed with a stereomicroscope (Nikon SMZ800) using a digital camera (Nikon Coolpix 950). The images (1 per egg that showed almost all the surface inside the plastic ring) were scored for morphological changes of blood capillaries such as sprouting and tortuosity (0=normal, 1=overrepresented) by 5 observers using a blinded screening test.

2.8. Statistical analyses

Data are presented as mean \pm s.d. Differences between groups were evaluated using Kruskal–Wallis (for at least three compared groups) and Mann–Whitney tests (for two compared groups) for non-parametric measures. To analyze hydrogel degradation over time, the Friedman test was used; the comparison of paired values was then done with the use of the Wilcoxon matched-pair test. The Fisher exact test was used for the analysis of angiogenesis on CAM. Two-tailed *p* values less than 0.05 were considered significant.

3. RESULTS

3.1. Structure of molecules

To produce four different hydrogels, LMWHs were stabilized by synthetic bioconjugates, which possess a sugar, nucleoside and lipid moiety linked covalently with the triazole bridges. Among the four hydrogels tested in this study, GNF was produced to contain a highly fluorinated and a carbohydrate moiety linked to the central thymidine, whereas the remaining three GNBA were produced as bolaamphiphilic structures with different functional groups. GNBA-1 and GNBA-2 were functionalized with one ureido group but differed in one carbon atom whereas GNBA-3 contains one amide group (**Fig. 1**).

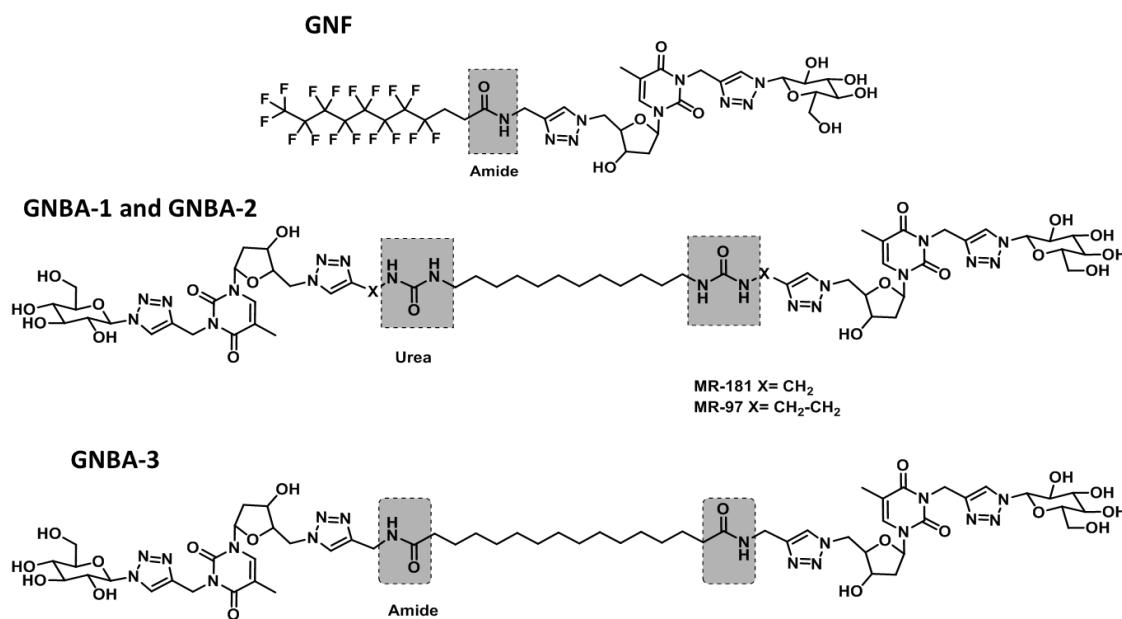


Figure 1. Chemical structures of GNF and GNBA. GNF (a) and GNBA-3 (c) contain an amide group, whereas GNBA-1 and GNBA-2 (b) contain a urea group (highlighted in gray).

3.2. *In vitro* degradation/disassembly of LMWHs

Hydrogel stability is a critical feature for clinical applications. To quantify degradation/disassembly, the weight loss of our four LMWHs was first tested *in vitro* after different periods of incubation in PBS. After 3 weeks at 37°C, the remaining weights were $65 \pm 4 \%$, $63 \pm 1 \%$, $51 \pm 11 \%$, and $55 \pm 2 \%$, for GNF, GNBA-1, GNBA-2, and GNBA-3, respectively. Friedman analysis of variance was performed ($F_r=17.76$, df 10,4, $p<0.01$), followed by Wilcoxon analysis to show that GNF degraded with slower kinetics compared with GNBA-2 ($p = 0.007$) and GNBA-3 ($p = 0.007$) (**Fig. 2a**). Thus, the LMWHs were divided into two categories: GNBA-2 and GNBA-3 with slightly faster degradation kinetics, compared to GNF and GNBA-1.

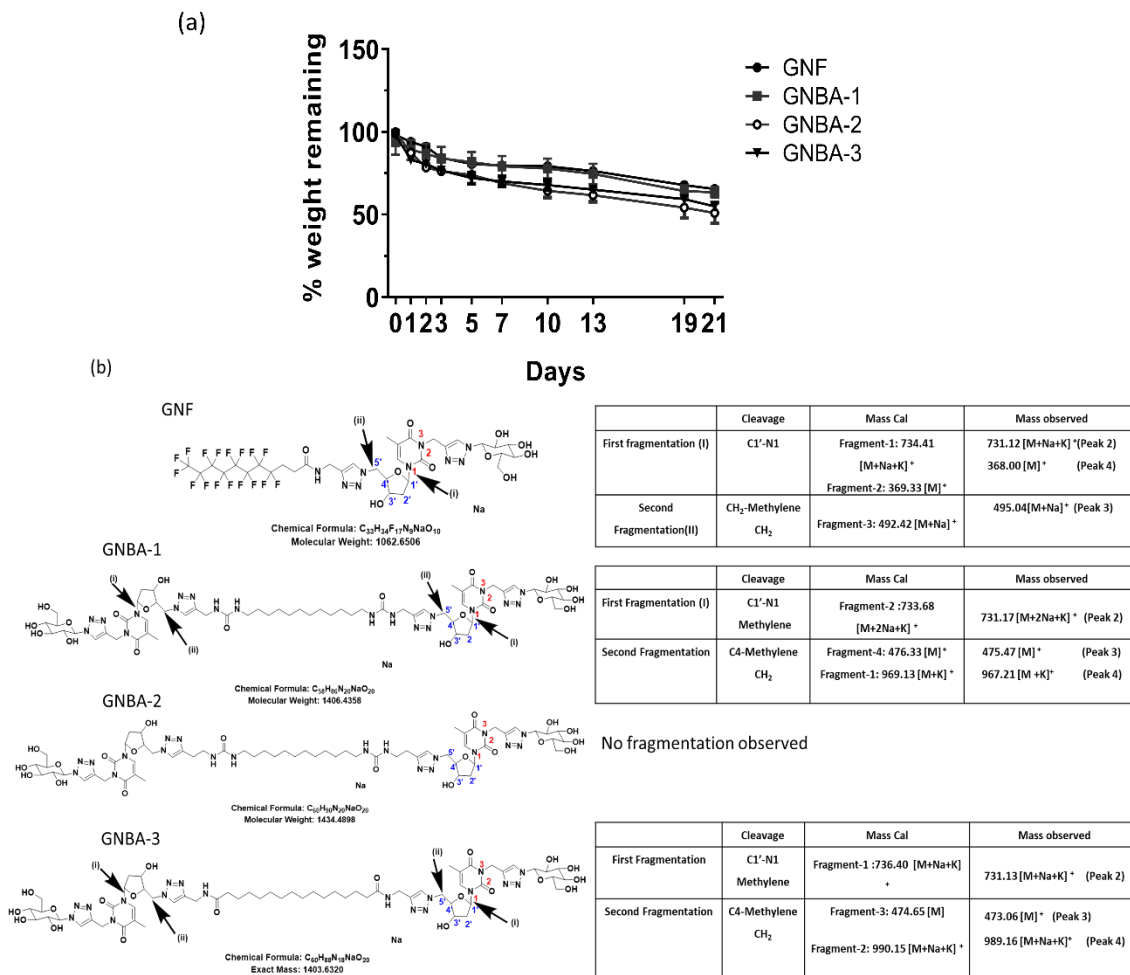


Figure 2. Analysis of *in vitro* degradation. **a)** Hydrogels (100 μ L) were incubated at 37°C in PBS. **a)** The percentage of weight loss was calculated at different time points. All the data are presented as mean \pm s.d. (n=4). **b)** The degradation products released in PBS after a 21-day incubation at 37°C were analysed by MALDI-TOF mass spectrometry. The positions of hypothetical hydrolysis are shown by arrows. The calculated and observed mass of the products is shown on the right. The mass spectra are available in supplementary material **S1**.

To assess the fragmentation of the molecules during incubation, the by-products of degradation present in the buffer were analysed by MALDI-TOF mass spectrometry at the end of the experiment (21 days) (**Fig. 2b and S1**). The analysis of the products released in PBS by GNF, GNBA-1, -2, and -3 after the 21-day incubation showed the molecular peaks (**P-1**) corresponding to intact molecules: their mass was in close agreement with the calculated mass. Other peaks **P-2**, **P-3**, and **P-4** were observed in the mass spectra of the products released from hydrogels GNF, GNBA-1 and -3 which were due to fragmentations of the hydrogel molecules as a result of degradation (**Suppl Fig S1**). The first possible fragmentation is due to the cleavage of the bond between the C1'-carbon of pentose ring and the N1'- nitrogen of the nucleobase (Fig. 2b, thick arrow (i), **Peak 2** in mass spectrum); the second possible fragmentation is due to the bond cleavage between bridged 5'-CH₂ and pentose ring (Fig. 2b, thick arrow (ii), **Peak 3** in mass spectrum). Calculated mass and observed mass for the fragments due to possible cleavages are summarized in Figure 2b. With GNBA-2, one single base peak (pure sample) was observed with minimal fragmentation peaks suggesting that weight loss hydrogel after 21 days primarily resulted from the dissociation of building block molecules,

due to weak hydrogen bonding between ureido groups and secondly, to less stable interactions between the triazole rings.

The fragmentation of three out of four molecules showed a similar pattern. Profound degradation was observed in GNF and GNBA-3, whereas GNBA-1 and 2 were less degraded or they disassembled. The urea linkage (GNBA-1 and -2) underwent more stabilised self-assembly due to two hydrogen bonds compared to one hydrogen bond in the amide linkage (GNF and GNBA-3). This self-association of urea is much stronger than that of amides or urethanes, usually one hydrogen bond donors. However, for GNBA-2, ethylene bridges weaken hydrogen bonding between the ureido groups and might be responsible for the less stable aromatic interactions with the tetrazolium ring. The ethylene group flanking the tetrazolium ring and the ureido group is responsible for the disassociation of the GNBA-2 before the fragmentation during the degradation studies.

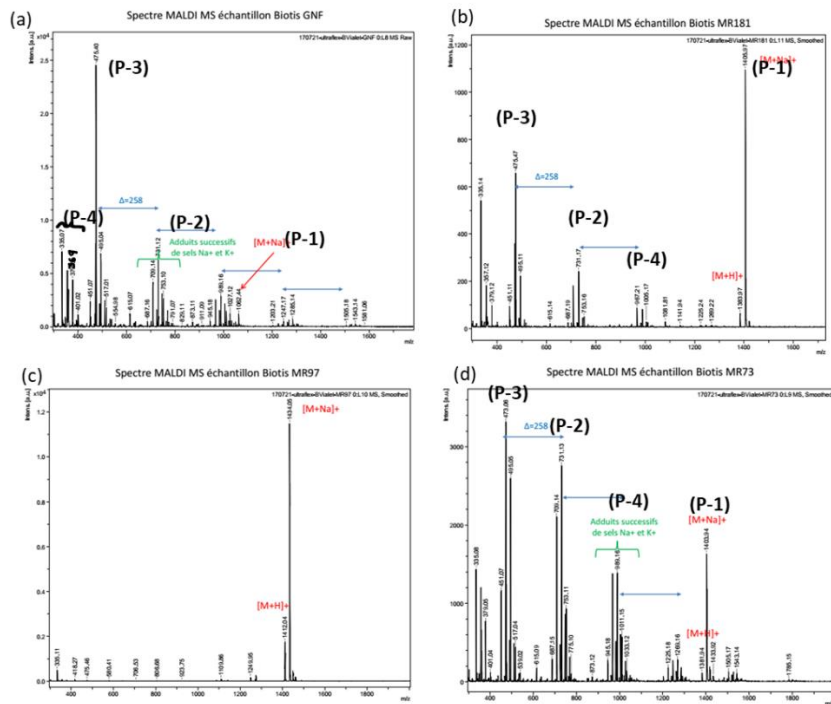


Figure S1. MALDI-TOF Mass spectra. Spectra of molecules at day 21 after incubation in PBS at 37°C for degradation. **a)** GNF; **b)** GNBA-1; **c)** GNBA-2; **d)** GNBA-3.

3.3. Evaluation of LMWH cytotoxicity

To verify that our LMWHs are not cytotoxic and thus suitable for clinical applications, MTT and neutral red assays were carried out using L929 cells (recommended by the international standard for such controls) and adipose mesenchymal stromal cells (MSCs, primary cells), to assess the viability and metabolic activity of cells in presence of GNF, GNBA-1, -2, and -3 (**Fig. 3**). The viability of L929 cells and MSCs, and the metabolism of L929, cultured with molecules released in contact of hydrogels showed that no cytotoxicity and no significant difference was observed in comparison to control medium (viability and metabolism above 70% as defined in the international standard) (**Fig. 3a, b, c**). In contrast, a low decrease of MSC metabolism was

observed with the four hydrogels during the first 24 hours: metabolism was between 60 and 70% as shown by the MTT assays (**Fig. 3b**).

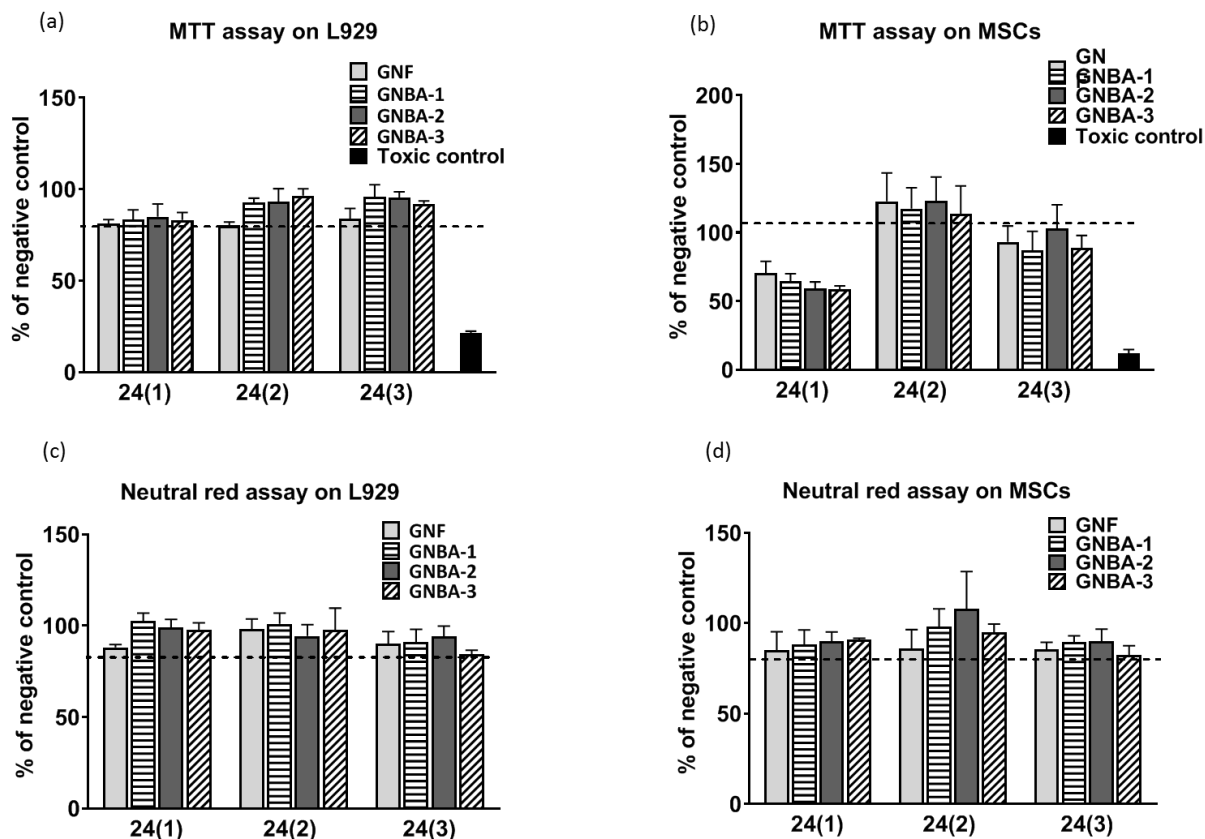


Figure 3. Evaluation of Cytotoxicity for four hydrogels on L929 and adipose MSCs. MTT assays were performed to determine the metabolic activity of L929 cells (a) and MSCs (b) cultured during 24h in the presence of the media containing compounds released from the four hydrogels during the first 24 hours (“24(1)”), and during the two following 24 hours “24(2)” and “24(3)”, respectively. As a positive control of toxicity, cells were also grown with the medium containing 0.1 % (w/v) Triton-X100 (toxic control). The viability of L929 cells (c) and MSCs (d) was tested using neutral red assays with the same media. Results are expressed in percentage of the cells grown in the control medium. All the data are presented as mean \pm s.d. (n=5 for L929 and n = 4 for MSCs).

To confirm that the degradation by-products are also biocompatible *in vivo*, we injected LMWHs subcutaneously in mice and investigated potential toxicity. Systemic toxicity was assessed by measuring biochemical serum parameters at day 3, day 7 and day 21 following hydrogel injection. The time points were selected based on the *in vitro* degradation behaviour of the hydrogels showing that, by day 3, 70-80 % of the hydrogels remained whereas after 21 days, between 35 % and 50 % of the hydrogels were degraded. Hydrogels and their degradation products did not produce significant variation in serum hepatic function markers alanine aminotransferase (ALT) and aspartate aminotransaminase (AST) or the cardiac toxicity marker lactate dehydrogenase (LDH) compared with serum levels in non-injected control mice (**Fig. S2**). This confirms that the degradation by-products of the hydrogels did not show any toxicity.

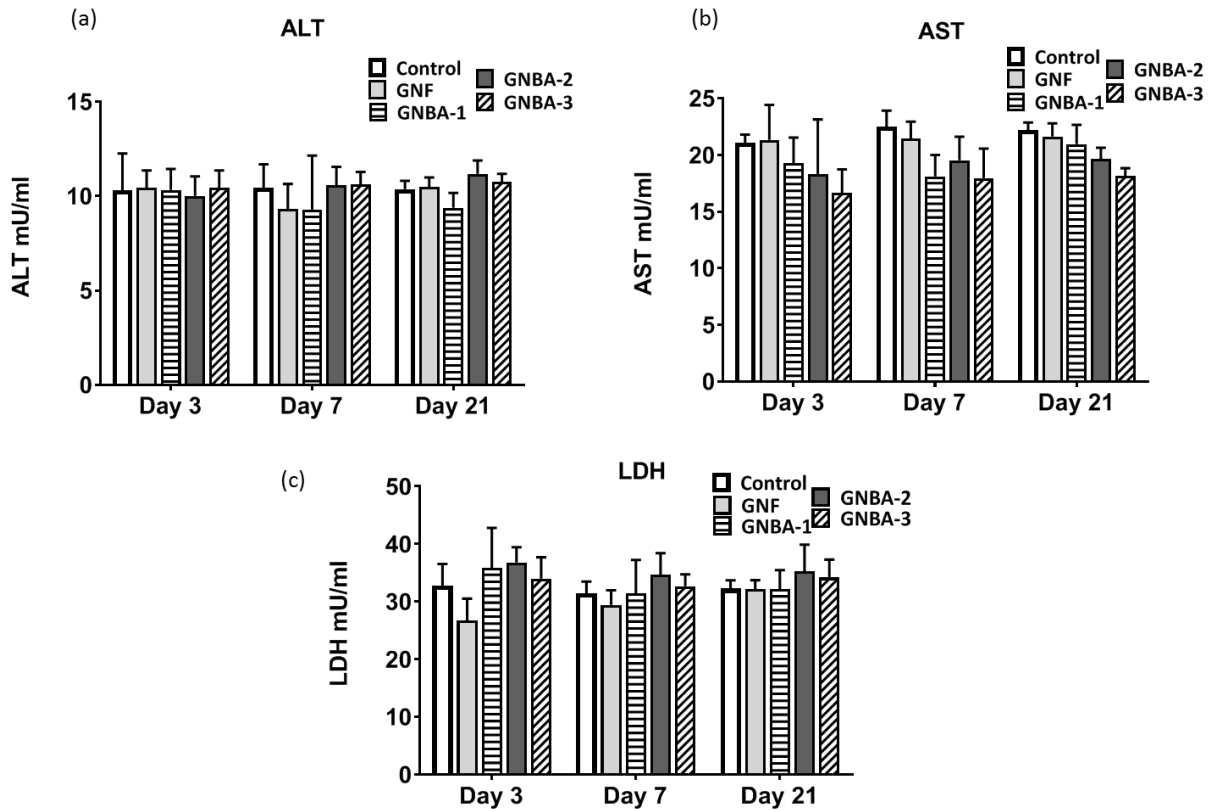


Figure S2. Analysis of *In vivo* toxicity by determination of biochemical serum markers. Alanine transaminase ALT (a), aspartate transaminase AST (b), and lactate dehydrogenase LDH (c) were determined and compared to the control animals, at three different time points after subcutaneous injection (3, 7, and 21 days). Data are presented as mean \pm s.d (n = 3/group). No statistical difference with the control mice was observed (Kruskal-Wallis test).

3.4. LMWHs evade a strong FBR

Adsorption of proteins at the surface of biomaterials is the initial step in triggering an FBR. To assess their protein binding capacity, LMWHs were first incubated *in vitro* for 2 h at 37°C in BSA solution, and the amount of adsorbed protein was subsequently measured (**Fig. 4**). GNBA-3 showed significantly higher protein adsorption ($118 \pm 21 \mu\text{g}/\text{cm}^2$) compared to GNBA-1 ($78 \pm 6 \mu\text{g}/\text{cm}^2$) and GNBA-2 ($88 \pm 17 \mu\text{g}/\text{cm}^2$), $p = 0.05$, 2-tailed). GNBA-1 ($78 \pm 6 \mu\text{g}/\text{cm}^2$) and GNBA-2 ($88 \pm 17 \mu\text{g}/\text{cm}^2$) had intermediate BSA adsorption levels; hydrogels incubated without BSA produced no substantial signal.

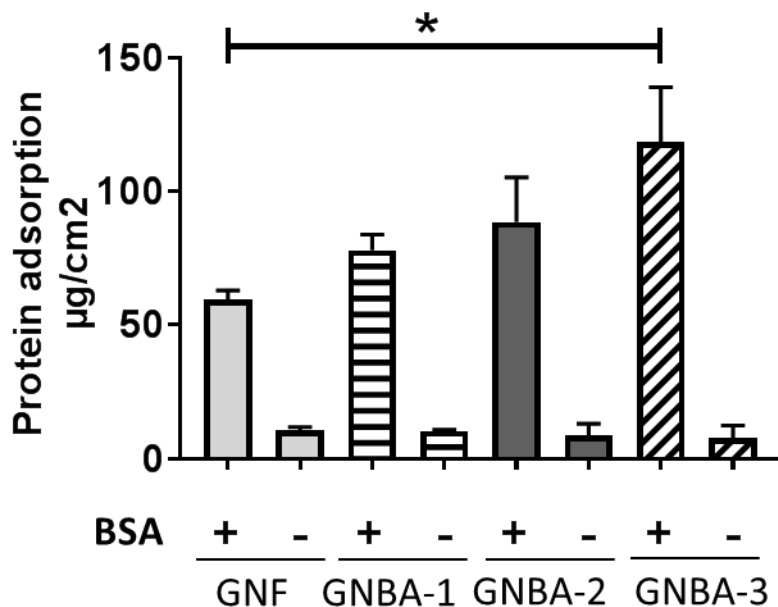
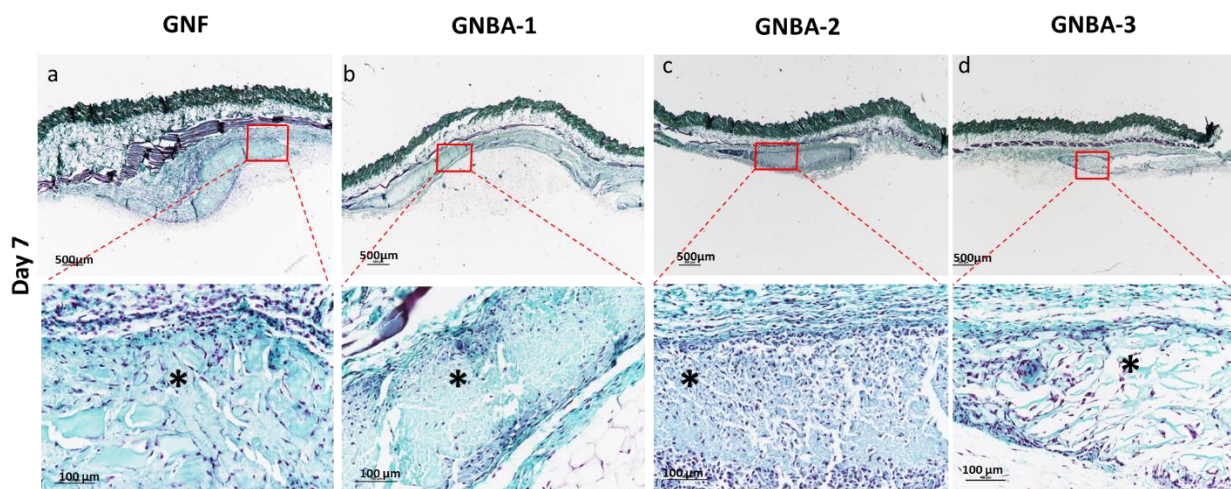


Figure 4. Analysis of BSA adsorption on the four hydrogels. Hydrogels (100 μL with a surface area of 1.3 cm^2) were incubated for 2 hours at 37°C in 400 μL PBS is containing either 2 mg/mL of bovine serum albumin (BSA) or not. After sodium dodecyl sulfate extraction, the proteins adsorbed to the hydrogels were quantified by BCA test. Statistical analysis with Kruskal-Wallis followed by Mann-Whitney tests (2-tailed) was performed to compare the adsorption of BSA to the four hydrogels (mean \pm s.d, n = 3, * $p \leq 0.05$).

To characterize tissue morphology and FBR around LMWHs after subcutaneous injection and *in situ* gelification, the biomaterials and the surrounding skin were harvested after 7 days and 21 days to assess collagen accumulation, degradation pattern, cell infiltration, and angiogenesis in histological sections (**Fig. 5**). Masson trichrome-blue stained but sparse collagen fibrils were observed throughout the area of the implants, which disappeared after the degradation of hydrogel without forming scar tissue (**Fig. 5**). Based on the amount of gel remaining on day 21, we confirmed that GNBA-2 was degrading faster than GNF and GNBA-1, whereas GNBA-3 showed intermediate degradation kinetics (**Fig. 5**).



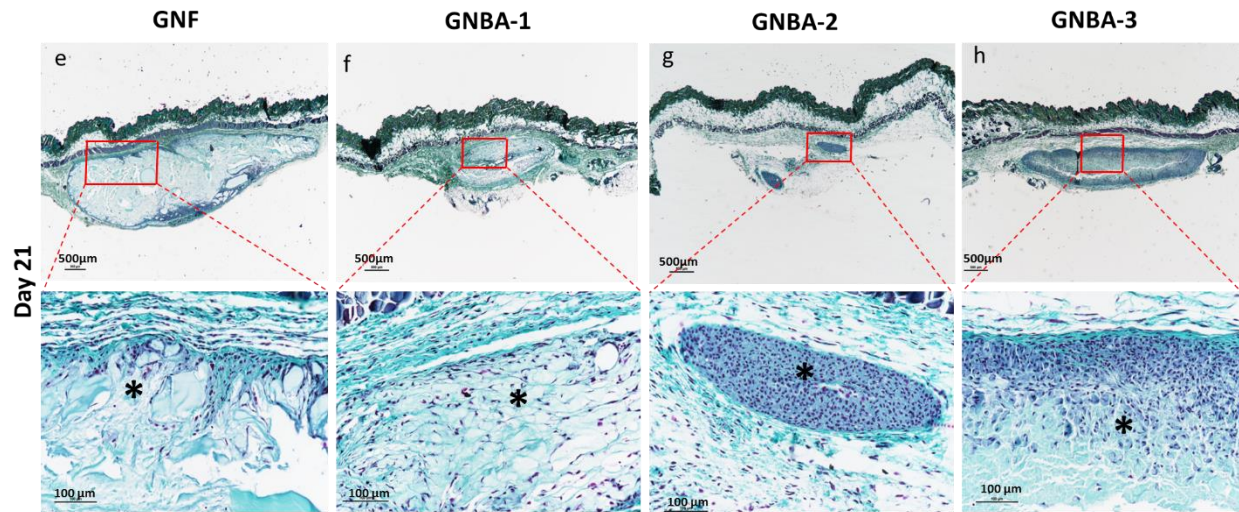


Figure 5. Masson's trichrome staining of hydrogels, and surrounding tissues dissected after 7 d (a–d), and 21 d (e–h). Representative images are showing the degradation and cell infiltration (n = 6/group). * in the image denotes the position of the hydrogel. The images of Masson's trichrome staining after 7 days and 21 days after hydrogel injection are shown with magnified images at the lower panel. Blue staining indicates collagen and purple represents nuclei. The hydrogels are also stained in blue. Scale bars of 500µm for the upper panels and the magnified images are represented in lower panels with a scale bar 100µm.

Next, fluorescent DAPI staining of nuclei was performed to quantify cell infiltration (**Fig. S3**, supplementary materials). In the portions of remaining hydrogels, we observed a significantly higher cell infiltration in GNBA-3 (348 ± 58 cells/ 0.5 mm^2 , $p = 0.006$) and GNBA-2 (399 ± 28 cells/ 0.5 mm^2 , $p = 0.006$) compared to GNF (145 ± 32 cells/ 0.5 mm^2); GNBA-1 exhibited an intermediate quantity of infiltrated cells (245 ± 18 cells/ 0.5 mm^2).

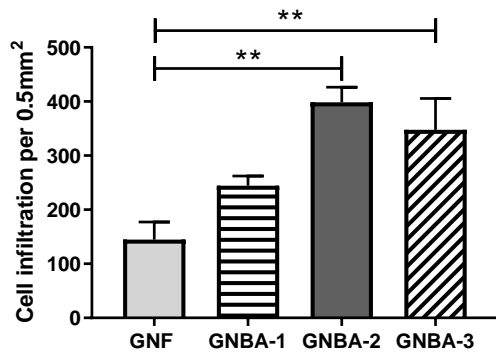
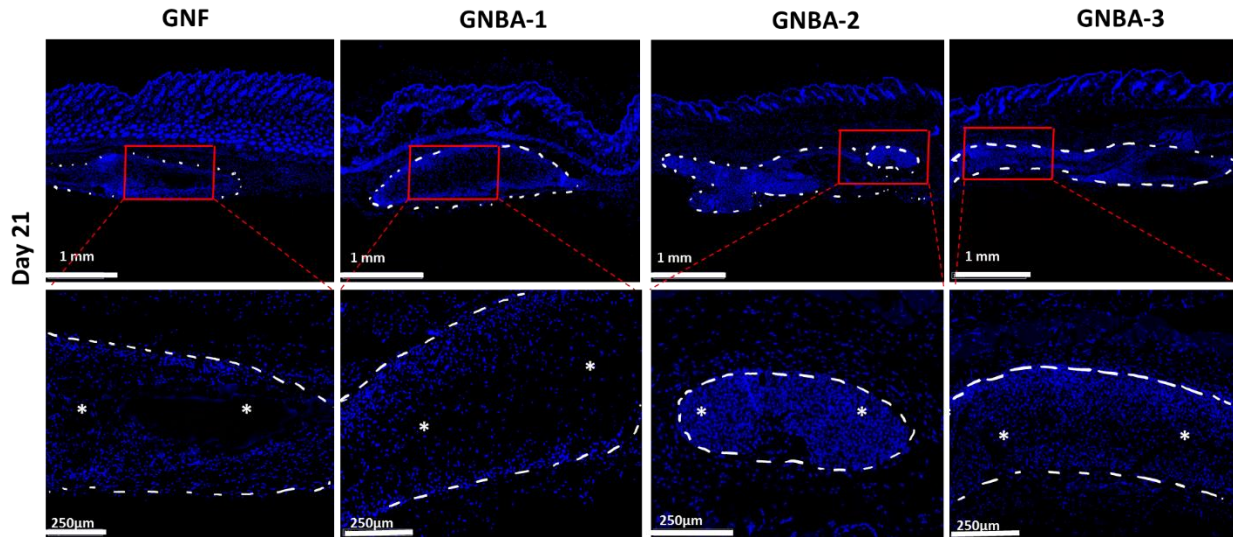


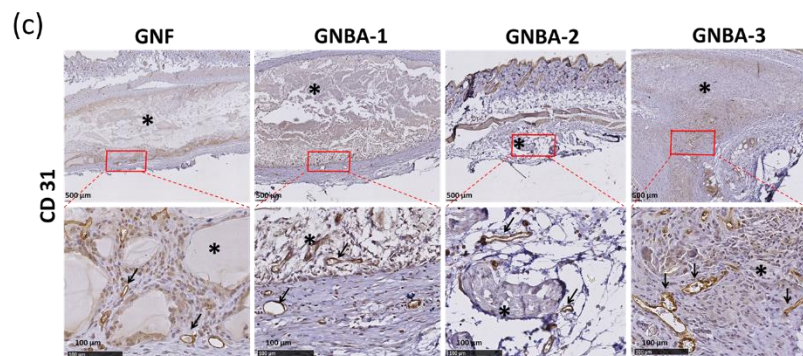
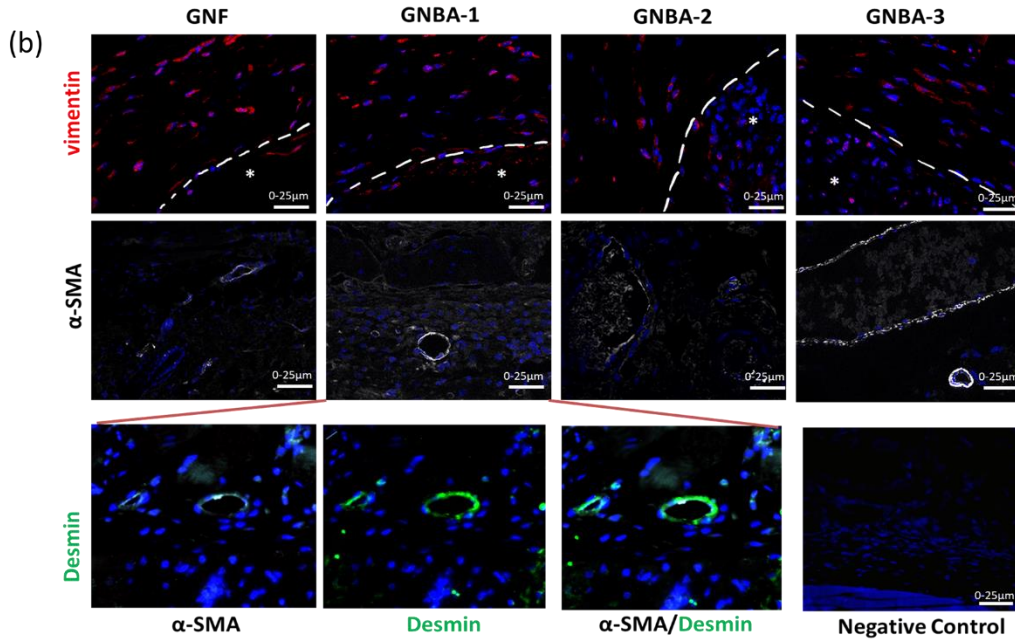
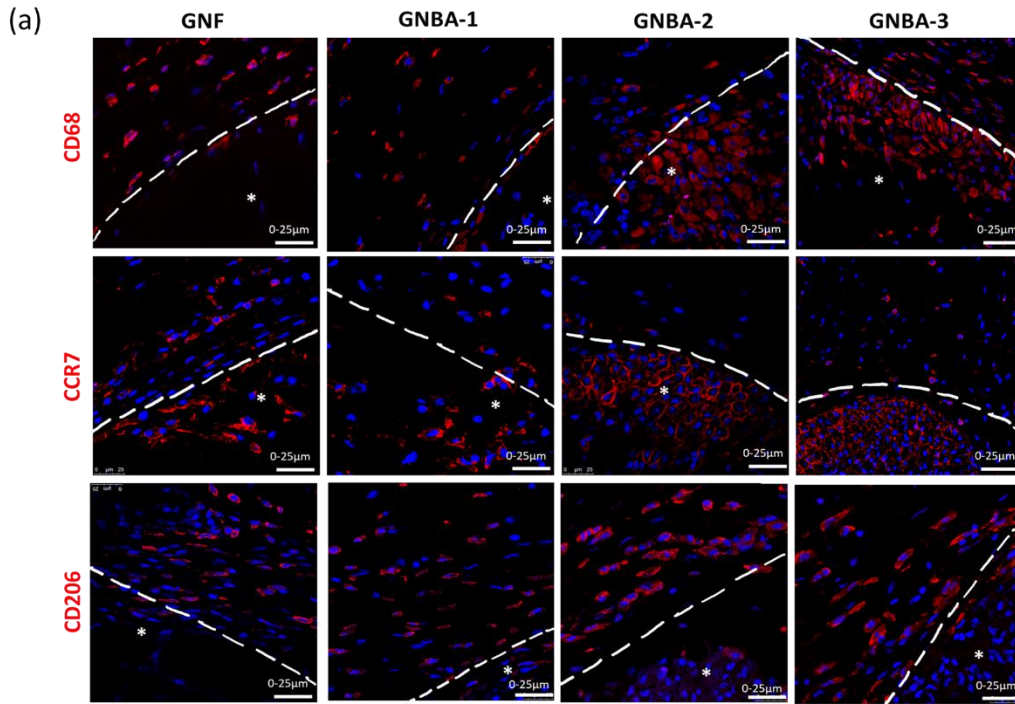
Figure S3. Analysis of cell infiltration by nucleus staining. a) The cell infiltration of cells in the remaining hydrogels 21 d after implantation was evidenced by DAPI staining (blue staining of nuclei). The hydrogels are denoted by * in the image, the boundary of hydrogels is marked with white dotted lines. Scale bar of 1 mm for upper panel and 250 μm for magnified images at the lower panel. b) Quantitative analysis of cell infiltration in the four hydrogels. The quantification of cell infiltration intensity was performed in at least five different fields with an area of 0.5 mm^2 using automated MIPAR software analysis. Statistical significance was determined by Kruskal-Wallis and Mann-Whitney tests (2-tailed). All the data are presented as mean \pm s.d. (n=5/group), $**p \leq 0.01$.

Next, macrophage recruitment and phenotype were investigated, using CD68 as a pan-macrophage marker, CCR7 as a pro-inflammatory marker (M1) and CD206 as a marker of immunomodulation (M2) [9] (**Fig. 6**). CCR7 positive cells were densely populating all LMWHs, especially GNBA-3 and GNBA-2, in comparison to GNF and GNBA-1 (**Fig. 6a**, second lane). CD206 positive cells were confined to the periphery of the hydrogels suggesting the remodelling of the tissue (**Fig. 6a**, third lane). To further investigate the formation of granulation tissue around hydrogels and to analyze the degree of fibrosis, tissue sections were stained against vimentin and α -SMA as markers of fibroblasts and myofibroblast, respectively. Only a few cells showed vimentin-positive staining in the periphery of the hydrogels (**Fig. 6b**, the hydrogels are shown by an asterisk and their limit by a dashed line). However, α -SMA staining was negative in the cells surrounding the hydrogels, whereas it efficiently stained the smooth muscle cells around the blood vessels (Desmin is indeed a specific marker of specific marker of smooth muscle cells). Thus, LMWHs did not induce an FBR or formation of a fibrous capsule.

3.5. Analysis of proangiogenic properties of LMWHs

During tissue regeneration, development of neo-vessels is of major importance. To assess angiogenesis when hydrogels were mostly degraded/disassembled, we immunostained endothelial cells against CD31 21d post-injection of LMWHs. CD31 positive cells with luminal structure (**Fig. 6c**, arrows) were observed in close proximity of the hydrogels, and in the tissue that replaced the degrading hydrogels. CD31-positive endothelial cells were not found inside the hydrogels, showing that non-degraded hydrogels are not susceptible to blood vessel ingress. **Fig. 6d** depicts the quantification of blood vessels counted manually per 0.2 mm^2 at four different random regions

in the tissue surrounding each hydrogel. With the fast degrading hydrogel GNBA-2, we observed 2.7-fold and 2.1-fold reduced numbers of blood vessels (bv) in the vicinity of this hydrogel (2.95 ± 0.27 bv/0.2 mm²) than in the vicinity of fast degrading GNBA-3 (7.95 ± 0.74 bv/0.2 mm², $p=0.009$), and slow degrading GNF (6.10 ± 1.07 bv/0.2 mm², $p=0.009$), respectively (**Fig. 6d**). The slow degrading hydrogel GNBA-1 induced intermediate angiogenesis (4.30 ± 0.41 bv/0.2 mm², $p>0.05$) (**Fig. 6d**).



(d) Angiogenesis at hydrogel and tissue interface

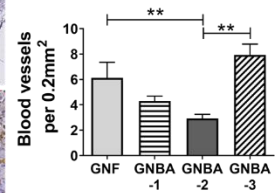
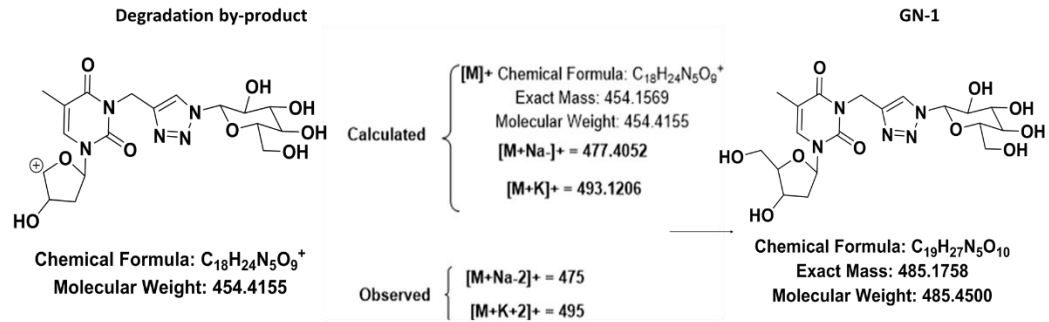


Figure 6. Foreign body response and angiogenesis. 21 days after implantation, the tissue was paraffin embedded, and sections were stained with different antibodies; *(asterisk) in the images denotes the position of hydrogels. **a)** Macrophage staining: CD68 (pan-macrophage marker, upper lane), the pro-inflammatory marker CCR7 (medium lane) and the immuno-modulatory marker CD206 (lower lane). M1 macrophages were found more inside the hydrogel, very few around the hydrogel and M2 were observed in the periphery of the hydrogels. **b)** Analysis of fibrosis: vimentin and α -SMA were detected as markers of fibroblasts and myofibroblasts, respectively. Vimentin-positive cells were visible in the tissue, but not at the interface with hydrogels. α -SMA was observed only to the smooth muscle cells of vessels around endothelial cells and Desmin was co-labelled with α -SMA to confirm staining of endothelial cells. Scale bar is 25 μ m (n=4 in each group). **c)** Angiogenesis at hydrogel/tissue interface: CD31 staining showed blood vessels in the tissue surrounding the hydrogels; arrows indicate some CD31 positive cells. Scale bar of 500 μ m for upper panel and 100 μ m for magnified images at the lower panel. **d)** Quantitative analysis of blood vessels counted in the vicinity of the four hydrogels (at least five different fields were randomly examined in each section). Statistical significance was determined by Kruskal-Wallis and Mann Whitney (2-tailed analysis). All the data are presented as mean \pm s.d. (n=5/group), ** $p \leq 0.01$.

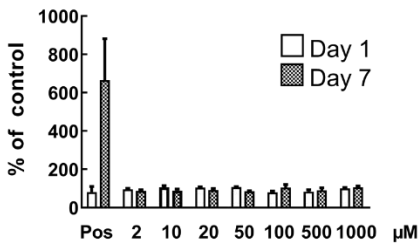
Because GNF, GNBA-1, and GNBA-3 that released a common product during their degradation were associated with higher angiogenesis, rather than disassembly of GNBA-2 that induced less angiogenesis *in vivo*, we hypothesized that glyconucleoside (GN)-1, the main hydrolytic degradation product of GNF, GNBA-1, and GNBA-3 detected in mass spectroscopy (peak 3, **Fig. 2b**), has yet undiscovered angiogenic properties. To test this hypothesis, GN-1 was chemically synthesized (**Fig. 7a** and **suppl S4**). It was first tested *in vitro* with the common model of human umbilical vein endothelial cells (HUVECs). Both the proliferation and cell migration were analyzed. A basal medium (EGM2 containing 10% fetal calf serum) was chosen, as cells were able to survive in this medium but without proliferation. GN-1, added to HUVEC

basal medium cultures in different concentrations did not induce cell proliferation after 1 d or 7 d (**Fig. 7b**). In contrast, a significant proliferation was measured by culturing HUVECs in endothelial cell growth medium used as a positive control (6.x more proliferation) (**Fig. 7b**). Addition of GN-1 (1 mM) to scratched HUVEC monolayers in basal medium moderately increased the scratch wound healing efficiency without reaching significance (film in **Fig. S4** in supplementary materials), in contrast to significantly enhanced HUVEC migration in EGM2-MV positive control medium (**Fig. 7c, d and S4**). Next, we used the CAM model to measure the angiogenic potential of GN-1 (0.5 mg/ml) with a first dose on an embryonic day 13 after the beginning of egg incubation and a second dose at day 14; DMEM was used as control. The angiogenic response was evaluated on day 17 based on vessel sprouting, and tortuosity (**Fig. 7e**). CAMs could show either a normal vasculature (**Fig. 7e**, 1st column), a pattern with massive sprouting (**Fig. 7e**, 2nd column) and/or a pattern with many tortuous capillaries (**Fig. 7e**, 3rd column). The quantification of eggs with or without sprouting, and/or tortuous vessels showed that more CAMs that were treated with the active compound GN-1 exhibited sprouting and tortuous vessels compared to the control CAMs (**Fig. 7f**, “sprouting yes” and “tortuous vessels yes”, respectively). In line with these results, CAMs without sprouting or without tortuous vessels were more frequent in the control group (**Fig. 7f**, “sprouting no” and “tortuous vessels no”, respectively). The differences between treated and non-treated CAMs were statistically significant: $p = 0.0046$ and $p = 0.0195$, for the sprouting and tortuous vessel effects, respectively (**Fig. 7f**, Fisher’s exact test).

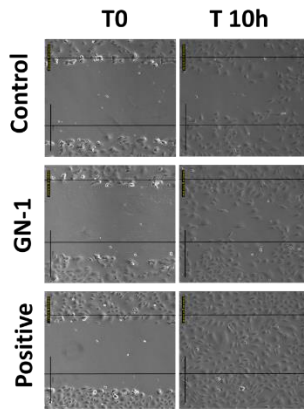
(a) Chemical structure of degradation by-product and of GN-1



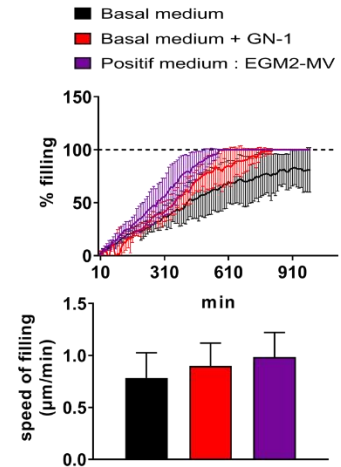
(b) Cytotoxicity of GN-1 on HUVEC Cells



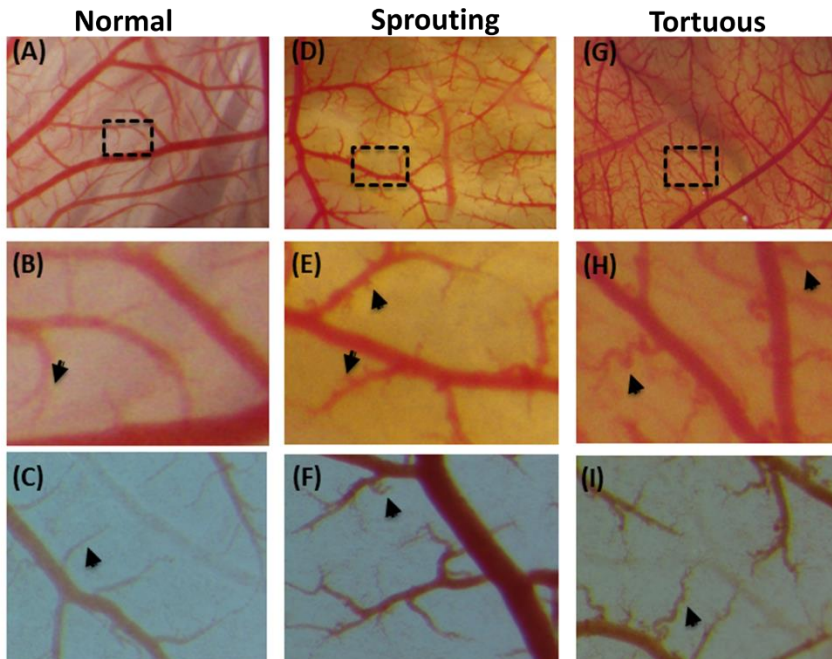
(c) Migration study by scratch test



(d) Quantification of migration study



(e) Angiogenesis analysed by CAM assay.



(f) Quantification of the presence or absence of sprouting and tortuous vessels

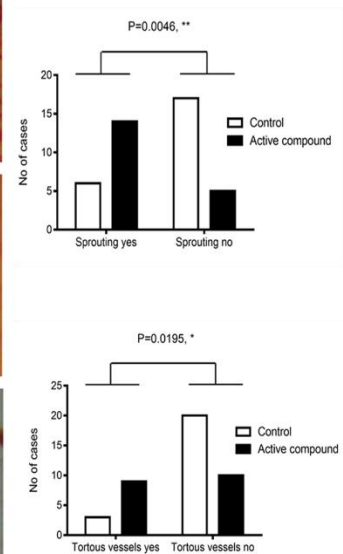


Figure 7. Angiogenesis analysed in HUVECs and CAM assay. **a)** Chemical structure of the degradation by-product: the common peak observed in the mass spectra after hydrolysis of GNF, GNBA-1, and GNBA-3 was in the close agreement with the possible degradation by-product. Mimic of the possible by-product was synthesised chemically (called GN-1). **b)** Cytotoxicity of the compound on HUVECs: different concentrations 2, 10, 20, 50, 100, 500, and 1000 μ M did not show any toxicity compared to the control (basal medium) (n = 5). **c)** Migration study by scratch test on HUVECs: representative pictures of scratch assays at a time lapse of 17h in basal medium EGM2 (Upper), basal medium + active compound: 1000 μ M (middle) and positive medium EGM2-MV. **d)** Percentage of filling during all the time lapse and speed of filling for each condition. **e)** Angiogenesis analysed with CAM assay: representative photographs of the CAM on day 17, treated with vehicle (DMEM media alone, n = 23), or 10 μ g of GN-1 (n = 19). Photos of large fields of view (A, D, G) and magnified images before (B, E, H), and after (C, F, I) fixation with 4% PFA were done; the first column (A, B, C) shows a CAM with a normal (non-stimulated) angiogenesis; examples of CAMs exhibiting efficient sprouting (D, E, F), and tortuous capillaries (G, H, I) are shown. **f)** Quantification of the presence or absence of sprouting and tortuous vessels in control and treated groups by blind screening (made independently by 5 observers), and the statistics performed by Fisher's exact test.

Suppl. S4. Synthesis and characterization of the compound GN-1.

a) The compound 1 and 2 were synthesized by literature procedures [18]. Reagents and conditions: (a) 1-azido-2, 3, 4, 6-tetra-O-acetyl- β -D-glucopyranoside, CuSO₄·5H₂O, sodium ascorbate, tBuOH/water (1:1), 75°C; 83% (b) NaOMe 1M, MeOH (96%). Synthesis and characterization of compounds 3-4.

N-3-[1-((β -D-Glucopyranosidetetraacetate)-1H-1, 2, 3-triazol-4-yl) methyl] thymidine (3).

Copper sulfate (0.547 g, 2.19 mmol) and sodium ascorbate (0.87 g, 4.38 mmol) were successively added to the suspension of compound **1** (6.14 g, 21.91 mmol) and 1-deoxy-1-azido-2, 3, 4, 6-tetra-

O-acetyl glucopyranose **2**¹ (8.18 g, 21.91 mmol) in 130 mL of ¹BuOH/H₂O (1:1). The mixture was stirred at 75 °C overnight. Next day, after cooling to room temperature, the solvents were removed under reduced pressure and extracted with DCM and washed with water. Dried over Na₂SO₄ and concentrated and purified by eluting ethyl acetate and methanol (100 to 5:95) to obtain the desired compound **3** as white foam 12 g (83%). ¹H NMR (CDCl₃, 300 MHz) δ 7.92 (s, 1H, H triazole), 7.65 (s, 1H, H-6 thymine), 6.28-6.24 (t, *J* = 6 Hz, 1H, H-1'), 5.88-5.85 (d, *J* = 9 Hz, 1H, H-1), 5.50-5.44 (t, *J* = 9 Hz, 1H, H-2), 5.43-5.37 (t, *J* = 9 Hz, 1H, H-3), 5.29-5.12 (m, 3H, H-4, NCH₂triazole), 4.57-4.52 (m, 1H, H-3'), 4.29-4.10 (m, 2H, H-5' or H-6), 4.06-3.97 (m, 2H, H-4', H-5), 3.84-3.81 (m, 2H, H-5' or H-6), 3.78 (bs, 2H, H-5'), 2.38-2.21 (m, 2H, H-2'), 1.87 (s, 3H, CH₃ thymine), 2.05, 2.04, 2.00, 1.81 (s, 12H, 4 CH₃(C=O)), ¹³C NMR (CDCl₃, 75 MHz) δ 170.69, 170.02, 169.42, 168.95 (C=O acetate), 163.2, 150.67, (C=O thymine), 143.63 (Cq triazole), 135.26 (C-6 thymine), 122.85 (CH triazole), 109.95 (C-5 thymine), 87.22, 86.36 (C-4', C-1'), 85.51 (C-1), 74.93 (C-5), 72.67, 70.76, 70.19 (C-3', C-3, C-2), 67.61 (C-4), 61.91, 61.56 (C-6, C-5'), 40.24 (C-2'), 35.81 (triazole CH₂N thymine), 20.71-20.16 (CH₃(C=O)), 13.18 (CH₃ thymine).

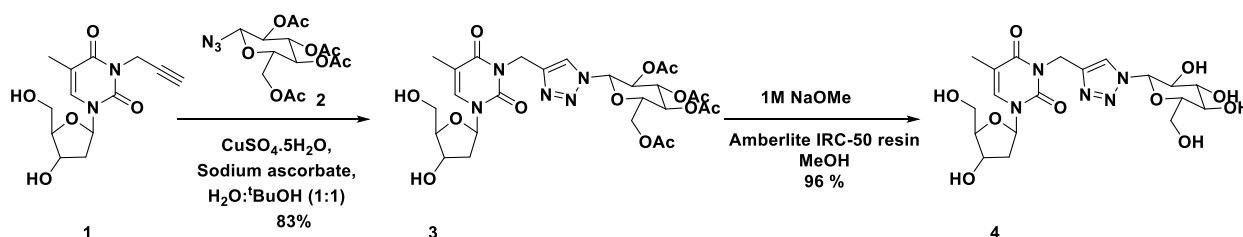
N-3-[1-((β-D-Glucopyranoside)-1H-1, 2, 3-triazol-4-yl) methyl] thymidine (**4**).

To the stirred solution of compound **3** (0.7 g, 1.07 mmol) in anhydrous methanol (10 mL) was treated with freshly prepared 1N sodium methoxide solution at room temperature. After 1h stirring, Amberlite IRC-50 ion exchange resin was added to the reaction mixture and stirred for 30 min and filtered. After filtration, the solvent was removed under reduced pressure. The solid residue was applied to a column of silica gel, and the product eluted with DCM:MeOH (100 to 8:2) to afford the title compound **4** as a white amorphous solid 0.5 g (96%). ¹H NMR (CDCl₃, 300 MHz) δ 8.12 (s, 1H, H triazole), 7.89 (s, 1H, H-6 thymine), 6.36-6.31 (t, *J* = 9 Hz, 1H, H-1'), 5.60-5.57 (d, *J* = 9

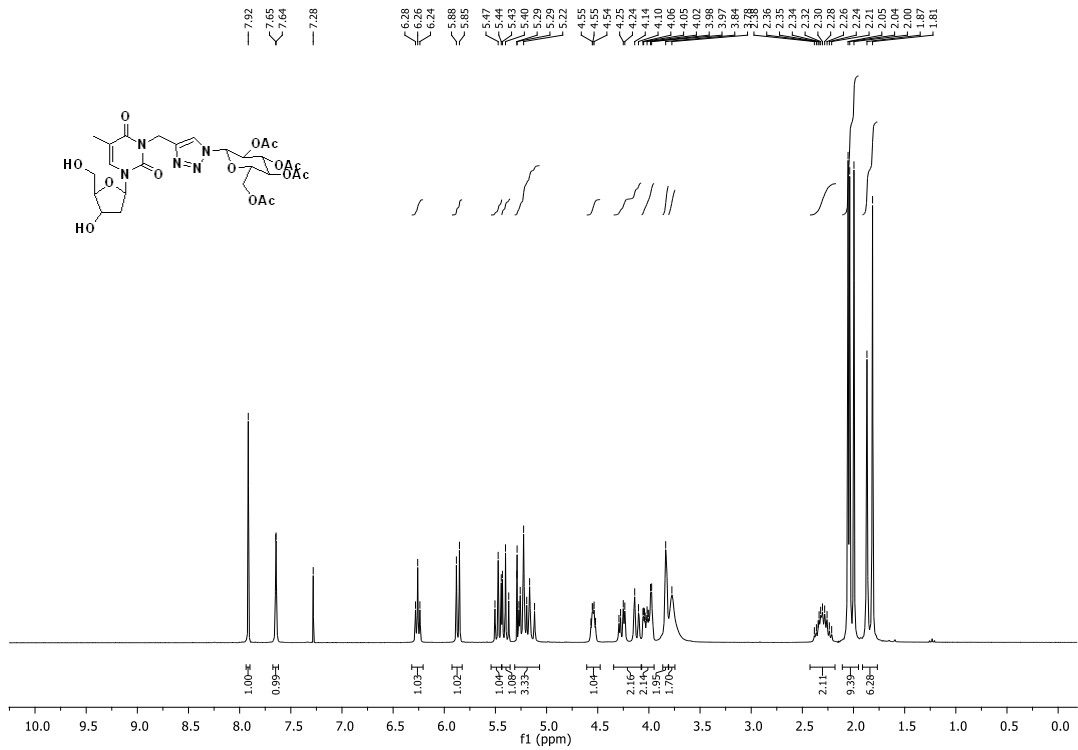
Hz, 1H, H-1), 5.29-5.19 (m, 2H, NCH₂triazole), 4.43-4.39 (m, 1H, H-4'), 3.94-3.68 (m, 6H, H3', H2, H3, H4, H5, H6'), 3.46-3.60 (m, 3H, H6', H6), 2.34-2.15 (m, 2H, H-2'), 1.93 (s, 3H, CH₃ thymine), ¹³C NMR (CDCl₃, 75 MHz) δ 163.54, 150.74 (C=O thymine), 143.26 (C_q triazole), 135.36 (C-6 thymine), 122.85 (CH triazole), 109.36 (C-5 thymine), 88.19, 87.45 (C-4', C-1'), 85.76 (C-1), 79.69 (C-5), 76.98, 72.53, 70.67 (C-3', C-3, C-2), 69.44 (C-4), 61.33, 60.96 (C-6, C-5'), 39.90 (C-2'), 35.66 (triazole CH₂N thymine), 11.79 (CH₃ thymine); HRMS (m/z): Calculated [M+Na]⁺ (C₁₉H₂₇N₅O₁₀Na) 508.1656, found 508.1650.

b-e) NMR characterization of the products. F) High resolution mass spectrometry of compound 4 (GN-1).

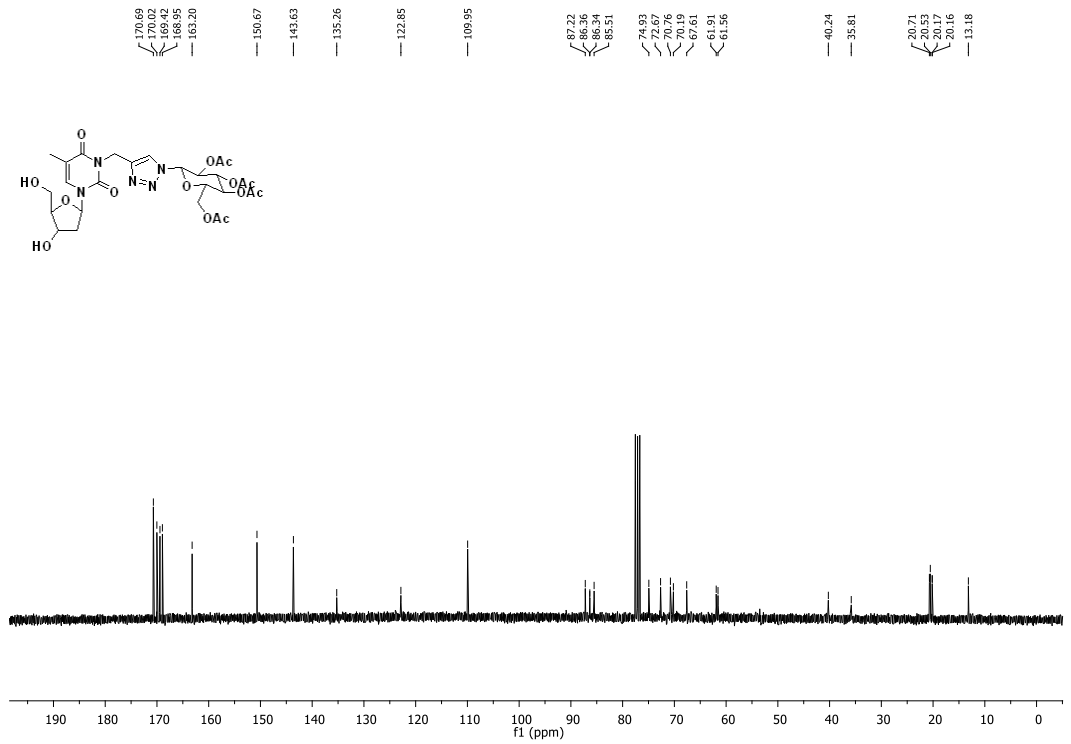
a)

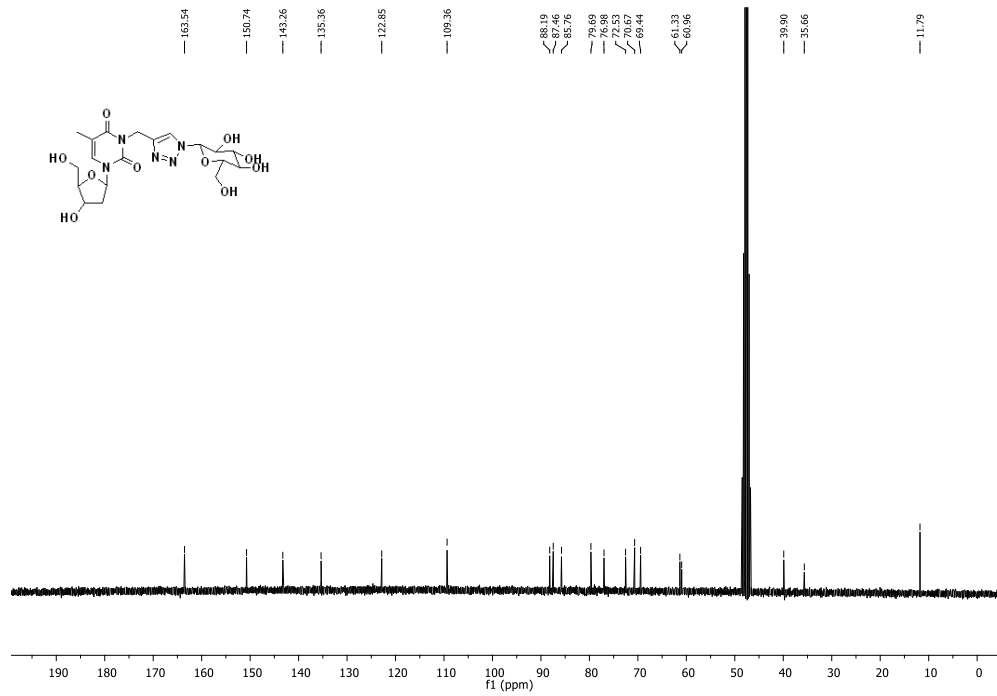


b) ¹H-NMR compound 3

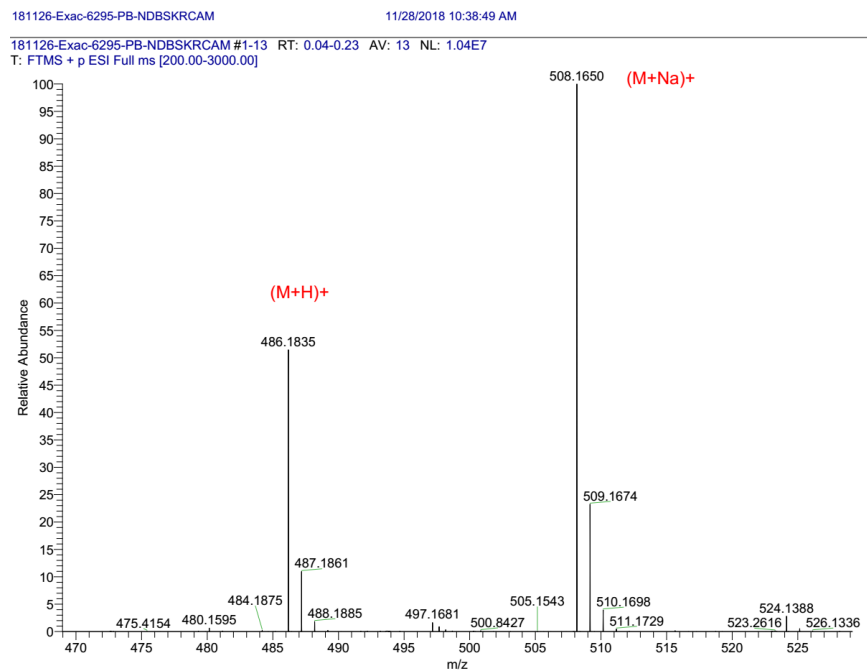


c) ¹³C-NMR compound 3





f) HRMS of the compound 4 (GN-1)



4. DISCUSSION

Hydrogels are receiving more and more attention in the field of tissue engineering, drug delivery, and more generally for biomedical applications, as their tunable properties offer a large range of potential developments. Although extensive research has been made, yet only a few hydrogels are brought into the clinic, in the context of drug delivery, wound dressings, and contact lenses [25]. Medical applications largely depend on their degradation rate, on their tolerance by the host tissue and on the intimate interactions they will have with the cells at the site of implantation or injection. The possibility to form hydrogels from the self-assembly of small molecules provide additional properties compared to gels formed with polymeric materials, the LMWGs: as pointed by Draper and Adams [26], the final properties of LMWGs (viscosity, fibre organisation) are process-dependent, giving access to properties with the same molecules. In this study, we have analyzed some of the key properties of four hydrogels obtained by the self-assembly of GNF and GNBA, to predict their potential medical applications. All four compounds share a glyco-nucleo-lipid moiety consisting of a thymidine block linked to a glucose molecule by a triazole heterocycle. They differ in two ways: GNF is single chain amphiphile, whereas the GNBA feature bola-amphiphilic structures, consisting of two GNs symmetrically separated by a hydrocarbon chain. The GNBA show different hydrocarbon chains or chemical functions (amide, urea). Interestingly, all four molecules stabilize hydrogels at low concentrations (<2% v/w) within less than one hour in aqueous media, and within less than 2 minutes when injected subcutaneously. This property can be explained by the strain induced during circulation through the needle. This allows for an easy subcutaneous injection and formation of gels that are visible one week later (Fig. 5).

Noteworthy, all hydrogels are fully injectable, a property which is very useful for several applications, and which is not fulfilled by many types of hydrogels. Previous studies have shown that the self-assembly of GNBA creates unique hydrogel supramolecular assemblies featuring fast gelation kinetics, high elastic moduli, thixotropic, and thermal reversibility properties. Such viscoelastic properties establish all four gels in the category of intermediate hard gels, much above the weak collagen gels, but below the commonly used PEG-based hydrogels.

None of the gels exhibited any toxicity in cell culture tests, and none of the gels showed any systemic toxicity when injected subcutaneously in mice. As three of these gels have shown to be degraded by cleavage of specific chemical bonds in aqueous solution, it is likely that these products are released in the tissues, and presumably in the blood of injected mice. Nevertheless, our data suggest that these degradation products are not toxic. Collectively, these data point these gels as safe products for *in vivo* applications.

Many currently used hydrogels elicit strong foreign body reaction resulting in the isolation of the gel from the tissues, which may alter tissue regeneration processes or prevent efficient drug release into the bloodstream. Evaluation of the tissue response elicited by implantation or injection of the gel is a prerequisite before any application. The foreign body reaction is first initiated by adsorption of proteins on the implanted material. It is well known that the lowest the non-specific protein adsorption is, the lowest the subsequent neutrophil and macrophage recruitment will occur, hence promoting low inflammatory reaction [7,27]. It was shown that the denaturation of fibrinogen due to adsorption to a material surface exposes hidden epitopes that recruit macrophages [28]. Minimizing non-specific protein adsorption is, therefore, an important challenge that can be overcome by hydrophilic materials. Indeed, the decrease of wettability of a

surface increases the adsorption of BSA, fibrinogen and FXII [29]. As hydrophilic materials, hydrogels are receiving a growing interest; polyethylene glycol (PEG) is recognized as the gold standard due to hydrogen bonds with water molecules that allow for hydration layer formation [30], but PEG was shown to induce a strong FBR that generates formation of a thick fibrous capsula [31,32]. In comparison with PEG that shows protein adsorption levels approximately 500 $\mu\text{g}/\text{cm}^2$ when incubated in fetal bovine serum [33], the four hydrogels that we analysed showed non-specific BSA adsorptions, that were in the range of 60-120 $\mu\text{g}/\text{cm}^2$. The highest adsorption was observed with GNBA-3 that retained non-specifically BSA twice as GNF (**Fig. 4**); the two other hydrogels had intermediate adsorption efficacy. From this result, we could expect a better biocompatibility of GNF compared to GNBA-3.

It is thus of major interest to propose new compositions of hydrogels that could induce minimal fibrosis. Our study shows that the injected gels can be classified into two categories. GNF and GNBA-1, which exhibit relatively limited cell infiltration and GNBA-2 and GNBA-3, which show a high infiltration by pro-inflammatory macrophages. These different biological responses are well-correlated with the *in vitro* protein adsorption capacity of these gels since GNF and GNBA-1 exhibit the lowest protein adsorption. Careful analysis of gel-tissue interactions also revealed that there is a good correlation between cell infiltration and degradation rate, as GNBA-2 and GNBA-3, which show a high cell infiltration, are those with the quickest degradation. These analyses suggest that gel degradation is essentially cell-mediated and that the spontaneous degradation observed *in vitro* probably accounts for a minimal part. Together, our analyses suggest that GNF and GNBA-1, which show slow degradation and mild inflammatory reaction, are well suited to tissue engineering applications, whereas GNBA-2 and GNBA-3, which degrade rapidly,

are more adapted to drug delivery applications, in which drug released could be coupled to gel degradation/disassembly.

One interesting point is the macrophage phenotype in and around the remaining hydrogels. During the last years, many studies with implanted biomaterials have been concentrating on the macrophage phenotype, as it was realised that macrophages are cells that participate in tissue regeneration [10]. The M1/M2 paradigm (which is a very simplified view of the macrophage polarization heterogeneity) is well accepted: M1 to M2 phenotype switch is considered as a prominent factor of material outcome success, including the development of a blood vessel network. Indeed, *in vitro* procedures of macrophage activation have shown that differentiated pro-inflammatory M1 macrophages express high levels of VEGF what favours endothelial cell sprouting, whereas immunomodulatory macrophages M2a express high levels of PDGF-BB (*in vitro* activation with IL4 + IL13) that recruits pericytes to stabilize the neovessels and M2c macrophages (activated with IL10) express increased levels of MMP9 that allows for the vessel remodelling [34]. Compared to other biomaterials like poly(lactic acid) [35] or chitosan [36] that are invaded by macrophages displaying both M1 and M2 markers, the phenotypes that were observed in our hydrogels were highly contrasted: macrophages that had invaded the materials almost exclusively expressed CCR7, a cell receptor considered as a marker essentially expressed by M1 macrophages. At the same time (three weeks after implantation), macrophages present in the surrounding tissue mostly expressed CD206, a receptor associated with an alternative activation phenotype. In agreement with the concept that the presence of M2 macrophages is associated with a better *in vivo* biointegration [37], we observed here that biointegration was optimal, as no sign of any fibrous capsule formation was evidenced (**Fig. 6b**). During material

biodegradation and tissue remodelling, the development of a vascular network is of major importance. In this context, we found that three out of four hydrogels gave the same degradation by-product *in vitro* (a glyconucleoside, *i.e.* glucose covalently bound to thymidine, **Fig. 7a**) and that these three hydrogels induced a better vascularization three weeks after sub-cutaneous implantation (**Fig. 6c, d**). We hypothesized that this glyconucleoside might have angiogenic properties. Its chemical synthesis confirmed *in vitro* that this compound was able to improve endothelial cell migration in a scratch assay (**Fig. 7d**). In a culture experiment with HUVECs grown in a basal medium, we confirmed that no cytotoxicity was observed but that this compound did not favor cell proliferation.

The problem of the relative contributions of proliferation and migration is very important for the understanding of angiogenesis regulation and some studies identified agents that can specifically target migration. Along this line, serpin-derived peptides have shown anti-angiogenic effects by sustaining the phosphorylation of the focal adhesion kinase, thus diminishing specifically cell migration [38]. Moreover, in a recent paper by Norton and Popel, they used a 3D model of angiogenesis well characterized into which tip cell migration, endothelial cell proliferation and sprouting were simulated [39]. They were able to predict that the proliferation rate has a greater effect on the spread and extent of the vascular growth in comparison to the migration rate. Based on our *in vitro* assays, we can take advantage of the fact that our molecule is more active for migration to combine it with a scaffold designed for tissue engineering. Thus, it can promote colonization by surrounding tissue to help bio integration without excessive proliferation, or it can be incorporated advantageously into bioprinting methods to help the structuration of a vascular network [40,41]. The tortuosity of neovessels that was evidenced with

the *in vivo* CAM model treated with the active compound (**Fig. 7e**) is evocative of an active angiogenic process. Indeed, such tortuosity has been observed for a long time in the presence of VEGF and is shown to be also associated with local hypoxia [42,43] . In our experiments, among 23 CAM control assays (only the vehicle was added), only 3 CAM vascular networks showed some tortuosity that may be associated with local hypoxia induced by the plastic ring used to limit the area receiving the medium. In contrast, the addition of the active compound induced the formation of these tortuous vessels in half of the group (9/19) (**Fig. 7f**). Chong *et al.* [44] demonstrated in a mouse model of ear wound healing, that tortuous microvessels were detected already 3 days after wound and peaked at 17 days post-wound, and that the alteration of blood flow promoted sprouting in these regions, thus generating efficient angiogenesis in the area surrounding the wound.

The structure similarity of the degradation product with nucleoside may suggest that the compound exerts its action as an agonist of P2Y receptors. Several studies have shown that AMP, Adenosine and ATP stimulate angiogenesis via receptors on endothelial cells and that this effect mainly involves the stimulation of cell migration. Although further studies are required to investigate the mechanisms responsible for favored vascularization, our data demonstrate the angiogenic properties of three of our four hydrogels.

In conclusion, the present article presents four hydrogels formed with self-assembling of low molecular weight molecules, that degrade with different kinetics when sub-cutaneous implanted, and that does not induce the formation of any fibrous capsule; three among these four hydrogels promote angiogenesis by the release of a degradation by-product with angiogenic

properties. We suggest that GNF and GNBA-1 are promising candidates for applications in tissue engineering, whereas GNBA-3 could be efficiently used for drug release applications.

BIBLIOGRAPHIC REFERENCES

- [1] B. Lei, B. Guo, K.J. Rambhia, P.X. Ma, Hybrid polymer biomaterials for bone tissue regeneration, *Frontiers of Medicine*. (2018). doi:10.1007/s11684-018-0664-6.
- [2] J. Saliba, A. Daou, S. Damiati, J. Saliba, M. El-Sabban, R. Mhanna, Development of Microplatforms to Mimic the In Vivo Architecture of CNS and PNS Physiology and Their Diseases, *Genes*. 9 (2018) 285. doi:10.3390/genes9060285.
- [3] E. Anitua, P. Nurden, R. Prado, A.T. Nurden, S. Padilla, Autologous fibrin scaffolds: When platelet- and plasma-derived biomolecules meet fibrin, *Biomaterials*. 192 (2019) 440–460. doi:10.1016/j.biomaterials.2018.11.029.
- [4] M. Jorfi, J.L. Skousen, C. Weder, J.R. Capadona, Progress towards biocompatible intracortical microelectrodes for neural interfacing applications, *J Neural Eng*. 12 (2015) 011001. doi:10.1088/1741-2560/12/1/011001.
- [5] Z.J. Du, C.L. Kolarcik, T.D.Y. Kozai, S.D. Luebben, S.A. Sapp, X.S. Zheng, J.A. Nabity, X.T. Cui, Ultrasoft microwire neural electrodes improve chronic tissue integration, *Acta Biomater*. 53 (2017) 46–58. doi:10.1016/j.actbio.2017.02.010.
- [6] S. El Ichi-Ribault, J.-P. Alcaraz, F. Boucher, B. Boutaud, R. Dalmolin, J. Boutonnat, P. Cinquin, A. Zebda, D.K. Martin, Remote wireless control of an enzymatic biofuel cell implanted in a rabbit for 2 months, *Electrochimica Acta*. 269 (2018) 360–366. doi:10.1016/j.electacta.2018.02.156.
- [7] J.M. Anderson, A. Rodriguez, D.T. Chang, Foreign body reaction to biomaterials, *Semin. Immunol*. 20 (2008) 86–100. doi:10.1016/j.smim.2007.11.004.
- [8] B.J. Kwee, D.J. Mooney, Manipulating the intersection of angiogenesis and inflammation, *Ann Biomed Eng*. 43 (2015) 628–640. doi:10.1007/s10439-014-1145-y.

- [9] A. Mantovani, A. Sica, S. Sozzani, P. Allavena, A. Vecchi, M. Locati, The chemokine system in diverse forms of macrophage activation and polarization, *Trends in Immunology*. 25 (2004) 677–686. doi:10.1016/j.it.2004.09.015.
- [10] B.N. Brown, B.M. Sicari, S.F. Badylak, Rethinking regenerative medicine: a macrophage-centered approach, *Front Immunol*. 5 (2014) 510. doi:10.3389/fimmu.2014.00510.
- [11] S. Gordon, P.R. Taylor, Monocyte and macrophage heterogeneity, *Nat. Rev. Immunol*. 5 (2005) 953–964. doi:10.1038/nri1733.
- [12] J. Baillet, V. Desvergnès, A. Hamoud, L. Latxague, P. Barthélémy, Lipid and Nucleic Acid Chemistries: Combining the Best of Both Worlds to Construct Advanced Biomaterials, *Advanced Materials*. 30 (2018) 1705078. doi:10.1002/adma.201705078.
- [13] G. Godeau, J. Bernard, C. Staedel, P. Barthélémy, Glycosyl–nucleoside–lipid based supramolecular assembly as a nanostructured material with nucleic acid delivery capabilities, *Chemical Communications*. (2009) 5127. doi:10.1039/b906212b.
- [14] M.A. Ramin, K.R. Sindhu, A. Appavoo, K. Oumzil, M.W. Grinstaff, O. Chassande, P. Barthélémy, Cation Tuning of Supramolecular Gel Properties: A New Paradigm for Sustained Drug Delivery, *Advanced Materials*. 29 (2017) 1605227. doi:10.1002/adma.201605227.
- [15] L. Latxague, M.A. Ramin, A. Appavoo, P. Berto, M. Maisani, C. Ehret, O. Chassande, P. Barthélémy, Control of Stem-Cell Behavior by Fine Tuning the Supramolecular Assemblies of Low-Molecular-Weight Gelators, *Angewandte Chemie International Edition*. 54 (2015) 4517–4521. doi:10.1002/anie.201409134.
- [16] L. Latxague, A. Patwa, E. Amigues, P. Barthélémy, Glycosyl-Nucleolipids as New Bioinspired Amphiphiles, *Molecules*. 18 (2013) 12241–12263. doi:10.3390/molecules181012241.
- [17] L. Latxague, A. Gaubert, D. Maleville, J. Baillet, M. Ramin, P. Barthélémy, Carbamate-Based Bolaamphiphile as Low-Molecular-Weight Hydrogelators, *Gels*. 2 (2016) 25. doi:10.3390/gels2040025.

- [18] M.A. Ramin, L. Latxague, K.R. Sindhu, O. Chassande, P. Barthélémy, Low molecular weight hydrogels derived from urea based-bolaamphiphiles as new injectable biomaterials, *Biomaterials*. 145 (2017) 72–80. doi:10.1016/j.biomaterials.2017.08.034.
- [19] G. Godeau, C. Brun, H. Arnion, C. Staedel, P. Barthélémy, Glycosyl-nucleoside fluorinated amphiphiles as components of nanostructured hydrogels, *Tetrahedron Letters*. 51 (2010) 1012–1015. doi:10.1016/j.tetlet.2009.12.042.
- [20] S. Ziane, S. Schlaubitz, S. Miraux, A. Patwa, C. Lalande, I. Bilem, S. Lepreux, B. Rousseau, J.-F. Le Meins, L. Latxague, P. Barthélémy, O. Chassande, A thermosensitive low molecular weight hydrogel as scaffold for tissue engineering, *Eur Cell Mater*. 23 (2012) 147–160; discussion 160.
- [21] D. Jain, A. Karajic, M. Murawska, B. Goudeau, S. Bichon, S. Gounel, N. Mano, A. Kuhn, P. Barthélémy, Low-Molecular-Weight Hydrogels as New Supramolecular Materials for Bioelectrochemical Interfaces, *ACS Applied Materials & Interfaces*. 9 (2017) 1093–1098. doi:10.1021/acsami.6b12890.
- [22] M. Maisani, K.R. Sindhu, M. Fenelon, R. Siadous, S. Rey, D. Mantovani, O. Chassande, Prolonged delivery of BMP-2 by a non-polymer hydrogel for bone defect regeneration, *Drug Deliv Transl Res*. 8 (2018) 178–190. doi:10.1007/s13346-017-0451-y.
- [23] M. Maisani, S. Ziane, C. Ehret, L. Levesque, R. Siadous, J.-F. Le Meins, P. Chevallier, P. Barthélémy, H. De Oliveira, J. Amédée, D. Mantovani, O. Chassande, A new composite hydrogel combining the biological properties of collagen with the mechanical properties of a supramolecular scaffold for bone tissue engineering, *J Tissue Eng Regen Med*. 12 (2018) e1489–e1500. doi:10.1002/term.2569.
- [24] H. Li, R. Daculsi, M. Grellier, R. Bareille, C. Bourget, J. Amedee, Role of neural-cadherin in early osteoblastic differentiation of human bone marrow stromal cells cocultured with human umbilical vein endothelial cells, *American Journal of Physiology-Cell Physiology*. 299 (2010) C422–C430. doi:10.1152/ajpcell.00562.2009.

- [25] E. Caló, V.V. Khutoryanskiy, Biomedical applications of hydrogels: A review of patents and commercial products, *European Polymer Journal*. 65 (2015) 252–267. doi:10.1016/j.eurpolymj.2014.11.024.
- [26] E.R. Draper, T.O. McDonald, D.J. Adams, A low molecular weight hydrogel with unusual gel aging, *Chem. Commun. (Camb.)*. 51 (2015) 6595–6597. doi:10.1039/c5cc01334h.
- [27] R. Klopffleisch, F. Jung, The pathology of the foreign body reaction against biomaterials: Foreign Body Reaction to Biomaterials, *Journal of Biomedical Materials Research Part A*. 105 (2017) 927–940. doi:10.1002/jbm.a.35958.
- [28] W.J. Hu, J.W. Eaton, T.P. Ugarova, L. Tang, Molecular basis of biomaterial-mediated foreign body reactions, *Blood*. 98 (2001) 1231–1238.
- [29] L.-C. Xu, C.A. Siedlecki, Effects of surface wettability and contact time on protein adhesion to biomaterial surfaces, *Biomaterials*. 28 (2007) 3273–3283. doi:10.1016/j.biomaterials.2007.03.032.
- [30] A.W. Bridges, A.J. García, Anti-inflammatory polymeric coatings for implantable biomaterials and devices, *J Diabetes Sci Technol*. 2 (2008) 984–994. doi:10.1177/193229680800200628.
- [31] A.D. Lynn, A.K. Blakney, T.R. Kyriakides, S.J. Bryant, Temporal progression of the host response to implanted poly(ethylene glycol)-based hydrogels, *Journal of Biomedical Materials Research Part A*. 96A (2011) 621–631. doi:10.1002/jbm.a.33015.
- [32] L.E. Jansen, L.D. Amer, E.Y.-T. Chen, T.V. Nguyen, L.S. Saleh, T. Emrick, W.F. Liu, S.J. Bryant, S.R. Peyton, Zwitterionic PEG-PC Hydrogels Modulate the Foreign Body Response in a Modulus-Dependent Manner, *Biomacromolecules*. 19 (2018) 2880–2888. doi:10.1021/acs.biomac.8b00444.
- [33] M.D. Swartzlander, C.A. Barnes, A.K. Blakney, J.L. Kaar, T.R. Kyriakides, S.J. Bryant, Linking the foreign body response and protein adsorption to PEG-based hydrogels using proteomics, *Biomaterials*. 41 (2015) 26–36. doi:10.1016/j.biomaterials.2014.11.026.
- [34] K.L. Spiller, R.R. Anfang, K.J. Spiller, J. Ng, K.R. Nakazawa, J.W. Daulton, G. Vunjak-Novakovic, The role of macrophage phenotype in vascularization of tissue engineering scaffolds,

- Biomaterials. 35 (2014) 4477–4488. doi:10.1016/j.biomaterials.2014.02.012.
- [35] H. Oliveira, S. Catros, C. Boiziau, R. Siadous, J. Marti-Munoz, R. Bareille, S. Rey, O. Castano, J. Planell, J. Amédée, E. Engel, The proangiogenic potential of a novel calcium releasing biomaterial: Impact on cell recruitment, *Acta Biomaterialia*. 29 (2016) 435–445. doi:10.1016/j.actbio.2015.10.003.
- [36] D.P. Vasconcelos, A.C. Fonseca, M. Costa, I.F. Amaral, M.A. Barbosa, A.P. Águas, J.N. Barbosa, Macrophage polarization following chitosan implantation, *Biomaterials*. 34 (2013) 9952–9959. doi:10.1016/j.biomaterials.2013.09.012.
- [37] J. Barthes, C. Dollinger, C.B. Muller, U. Liivas, A. Dupret-Bories, H. Knopf-Marques, N.E. Vrana, Immune Assisted Tissue Engineering via Incorporation of Macrophages in Cell-Laden Hydrogels Under Cytokine Stimulation, *Front Bioeng Biotechnol*. 6 (2018) 108. doi:10.3389/fbioe.2018.00108.
- [38] J.E. Koskimaki, E.V. Rosca, C.G. Rivera, E. Lee, W. Chen, N.B. Pandey, A.S. Popel, Serpin-derived peptides are antiangiogenic and suppress breast tumor xenograft growth, *Transl Oncol*. 5 (2012) 92–97.
- [39] K.-A. Norton, A.S. Popel, Effects of endothelial cell proliferation and migration rates in a computational model of sprouting angiogenesis, *Sci Rep*. 6 (2016) 36992. doi:10.1038/srep36992.
- [40] J.-M. Bourget, O. Kérourédan, M. Medina, M. Rémy, N.B. Thébaud, R. Bareille, O. Chassande, J. Amédée, S. Catros, R. Devillard, Patterning of Endothelial Cells and Mesenchymal Stem Cells by Laser-Assisted Bioprinting to Study Cell Migration, *Biomed Res Int*. 2016 (2016) 3569843. doi:10.1155/2016/3569843.
- [41] O. Kérourédan, J.-M. Bourget, M. Rémy, S. Crauste-Manciet, J. Kalisky, S. Catros, N.B. Thébaud, R. Devillard, Micropatterning of endothelial cells to create a capillary-like network with defined architecture by laser-assisted bioprinting, *J Mater Sci Mater Med*. 30 (2019) 28. doi:10.1007/s10856-019-6230-1.

- [42] A. Saaristo, T. Veikkola, B. Enholm, M. Hytönen, J. Arola, K. Pajusola, P. Turunen, M. Jeltsch, M.J. Karkkainen, D. Kerjaschki, H. Bueler, S. Ylä-Herttuala, K. Alitalo, Adenoviral VEGF-C overexpression induces blood vessel enlargement, tortuosity, and leakiness but no sprouting angiogenesis in the skin or mucous membranes, *FASEB J.* 16 (2002) 1041–1049. doi:10.1096/fj.01-1042com.
- [43] S. Lee, S.M. Jilani, G.V. Nikolova, D. Carpizo, M.L. Iruela-Arispe, Processing of VEGF-A by matrix metalloproteinases regulates bioavailability and vascular patterning in tumors, *The Journal of Cell Biology.* 169 (2005) 681–691. doi:10.1083/jcb.200409115.
- [44] D.C. Chong, Z. Yu, H.E. Brighton, J.E. Bear, V.L. Bautch, Tortuous Microvessels Contribute to Wound Healing via Sprouting Angiogenesis, *Arteriosclerosis, Thrombosis, and Vascular Biology.* 37 (2017) 1903–1912. doi:10.1161/ATVBAHA.117.309993.

Results

3.Optimisation of hydrogel coating of the cathode electrode

My contribution: Performed enzyme immobilisation techniques on to the electrode. Optimisation of hydrogel coatings with different thickness to monitor their oxygen diffusion ability. Also, the measurement of enzyme functionality and stability by subcutaneous implantation in mice.

Thanks to Nicolas Mano and his group for the isolation, purification and characterisation of enzymes and polymers used for the immobilisation techniques and to Alexander Kuhn and his group for providing the gold electrodes.

3 Optimisation of hydrogel coating of the cathode electrode

Introduction

Glucose-based EBFC is generally limited by the current density generated at the cathode. The cathode is the electrode where the oxygen is reduced to water. The primary goal of EBFC is to produce enough current from the available analytes and oxygen when implanted in the body. The oxygen-reducing cathode is often limited by the concentration of oxygen in the body (partial pressure: 3-5 kPa). Besides this, the local hypoxic environment formed upon implantation of EBFC in the body limits the mass transfer of oxygen to the cathode surface. Therefore the first objective was focused on optimising the cathode function. The experiments were focused on improving the functional efficiency of the cathode by maximising the stability of enzymes. The hydrogel coating was optimised onto the electrode to protect enzymes from leaching and the external environment. The different hydrogel thickness was optimised with its uniform coating and oxygen diffusion ability.

3.1 Materials

All chemicals and biochemicals were purchased from Sigma-Aldrich unless otherwise stated: sulfuric acid 98% analytical grade, hydrogen peroxide, sodium chloride, sodium phosphate. Bilirubin oxidase was isolated and purified from two different sources, *Magnaporthe oryzae* and *Bacillus pumilus* at CRPP lab (25,27,140). All the buffers were prepared in ultrapure water unless otherwise stated.

A potentiostat and the dip coating instrument were used in the experiments (CH-Instruments, model CHI 842B, Austin, TX, USA). The electrochemical measurements were performed using the CH Instrument multichannel potentiostat in a three-electrode cell and a dip coating instrument (Homemade) that allowed for a reproducible hydrogel coating of the electrodes by controlling the speed of dipping.

3.2 Methods.

3.2.1 Preparation of electrodes

The bare gold electrodes (diameter 250 μ m) were cleaned in piranha solution (75% v/v H₂SO₄ (98% wt.)/25% v/v H₂O₂ (30% wt.)) for 10 min. The cleaned electrode was thoroughly rinsed with ultrapure water (to remove the sulfuric acid and hydrogen peroxide) and air-dried.

3.2.2 Cathode enzyme preparation method

The cleaned electrodes were placed on precleaned glass slides. The co-immobilization method, containing the enzyme and redox polymer, was prepared. 20 μ l of a mixture containing redox polymer (62.57 Wt.%), BOD enzyme (30 Wt.%) and crosslinker (7.43 Wt.%) was immobilised by drop cast method on each electrode. The electrodes were dried overnight at 4°C in the vacuum chamber.

3.2.3 Preparation of GNF hydrogel (Glycosyl-nucleosyl-fluorinated compound) and MR181

As described in the published and submitted articles, GNF hydrogel was prepared by weighing 15mg of GNF powder in a microtube, and 200 μ l of rhodamine 6G (20 μ M in PBS from stock solution 100 μ M) and 800 μ l of PBS (PH of 7.2) was added to the preparation (141,142). The solution was heated at 65°C until the powder dissolved completely (about 20 min) (142). The

solution was sonicated to remove the air bubbles and let at room temperature. It was used before complete gelation.

The MR181 hydrogel (1.5%) was prepared as per the published article (143). 15 mg of the powder was weighed in a microtube, and 800ml of PBS (PH of 7.2) and 200 μ l of rhodamine 6G (20 μ M in PBS from stock solution 100 μ M) were added to the preparation. The solution was heated at 80°C until the powder dissolved completely (about 20 min) (143). The solution was kept at room temperature and used before complete gelation.

3.2.4 Coating of the electrode with GNF or MR181

The prepared GNF or MR181 were coated to the electrode by dip coating instrument. The cleaned bare electrodes were dipped for 2min in the viscous solution (before forming hydrogel) of 1.5% GNF or MR181 in PBS at 38 °C. The dipping speed was 2.5 cm/min while the removing speed was 1.7cm/min. The coated electrode was dried for 5min at room temperature.

The similar procedure of dipping was repeated to have different thicknesses of hydrogel around the electrode. 3 and 10 dip coatings were done in 1.5% GNF in PBS, while only 2 dip coatings were carried out for MR181 hydrogel. Once the coating was dried, the electrodes were stored (within a day) in the PBS until the confocal and electrochemical studies.

3.2.5 Electrochemical measurements

The electrochemical measurements were performed using a potentiostat in a three-electrode cell. Phosphate buffer saline (PBS, 50mM phosphate and 150mM sodium chloride) of pH 7.4 at 37 °C was used as an electrolyte and gold as a working electrode, platinum as a counter electrode, and Ag/AgCl (silver/silver chloride) as a reference electrode. The enzyme catalytic activity was

performed by cyclic voltammetry, with continuous oxygen bubbling. The Os concentration deposited on the surface of the electrode was measured in the absence of oxygen (bubbling with argon), where the Os undergo oxidation and reduction. Chronoamperometry was performed by keeping the potential constant (current vs time) to measure the stability of the enzyme. The electrochemical measurement was performed at a cyclic rate of 5mV/s.

3.2.6 Measurement of Oxygen diffusion and enzyme activity by simple cyclic voltammogram

The thermowell containing PBS was saturated with oxygen (continuous bubbling), and the temperature was maintained at 37°C. Oxygen reduction on the electrode surface without the enzymes takes place by a 2-step mechanism, reduction of O₂ to H₂O₂ and then to H₂O, whereas in the case of BOD enzyme, the oxygen is directly reduced to water. The capacity of oxygen reduction on the surface of the electrode surface coated with hydrogel and without coating was tested.

3.2.7 Subcutaneous implantation of electrodes

The animal studies were carried out in accredited animal facilities at the University of Bordeaux (accreditation number: A33-063-917) and were approved by the animal ethical committee of Bordeaux. 10-week-old OF-1 female mice (Charles Rivers, France) were used for this study. Mice were anaesthetized using 4.5% isoflurane gas via an induction chamber and maintained throughout surgery at 2.5% isoflurane with a face-mask. The animals were depilated using depilation cream and disinfected with Chlorhexidine 0.05% w/v in methylated spirit 70%. The initial electroenzymatic O₂ reduction was measured for the BOD modified cathode by *in vitro* electrochemical measurement before implantation. Further, electrodes were implanted on the dorsal side of the mice (one electrode on each side, inserted length 3.5 cm). After 24hrs of

implantation, animals were sacrificed, and the electrodes were harvested to measure the enzyme activity by electrochemical measurements.

3.3 Results and discussion.

3.3.1 Optimisation of coating of electrodes by GNF

The BOD modified electrodes were coated by dip coating with 1.5% GNF containing rhodamine 6G. The electrodes were dipped during the viscous form of the gel at 38°C. Confocal microscopy was performed to check the uniformity and thickness of the gel on the surface of the electrode. As depicted in **Figure 3.1** with the 2-dip coating strategy, the GNF was not covering all over the electrode surface, while in the three-dip coating, a uniform layer was obtained and was evidenced by the fluorescence of rhodamine (**Figure 3.1**). The thickness of the layer was measured by focusing at the edges of the electrodes and was found to be 3- 4µm thickness for 3 dip coating. Hence the process of three dip coating was optimised to coat the electrodes for in vitro and in vivo enzyme activity. The coating thickness can be increased to 10 dips up to a thickness of around 10 µm. In the case of MR181 hydrogel, the coating around the electrode was not uniform in 2 dips (not shown). The fast gelation property of hydrogel (formation of the hydrogel in 40secs) limited the coating of electrodes.

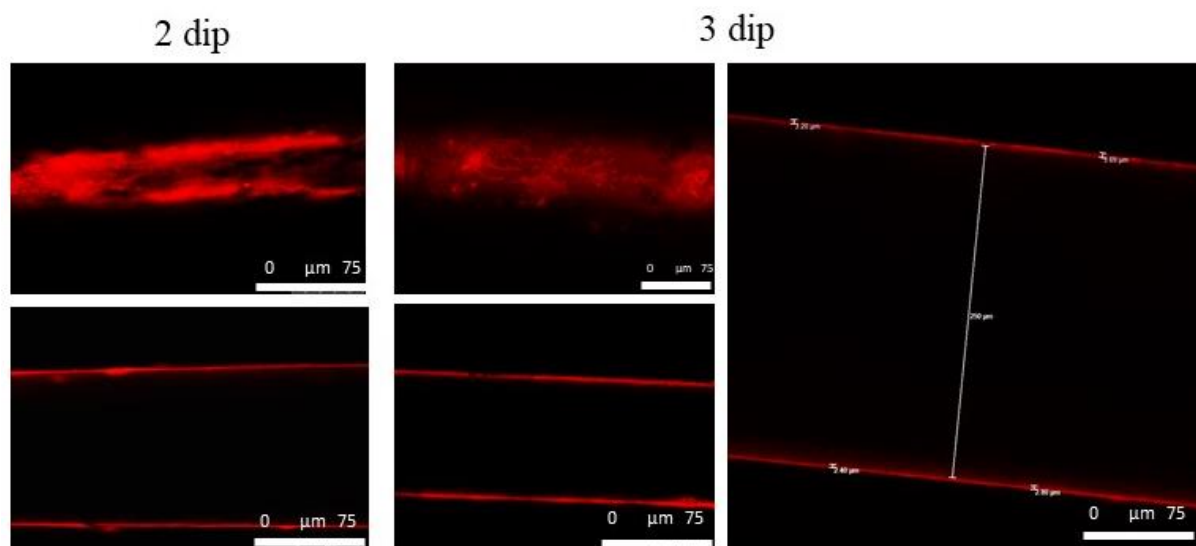


Figure 3.1: Confocal images of two and three dip coating of electrodes with GNF at 38°C with an interval of 15 min drying between each coating. The speed of 2.5cm/min for dipping and 1.75cm/min for removing the electrodes. Scale bar 0-75 μm

3.3.2 Measurement of Oxygen diffusion on the electrode surface by cyclic voltammetry

The ability of oxygen diffusion was measured to investigate the effect of GNF and MR181 coating onto the electrode by electrochemical measurements. The non-enzymatically modified electrodes coated with GNF (1 and 1.5%) and MR181(1%) hydrogel were compared to the bare gold electrode without coating. The catalytic reduction of oxygen on the surface of the electrode without the enzyme was performed to check the O₂ mass transport efficiency on the bare, GNF, and MR181 coated electrode surface. As seen in **Figure 3.2**, the catalytic reduction of oxygen on the electrode surface occurs at a potential of ~0.1 V vs Ag/AgCl. The current density was around 200 μA for the bare electrode, while on GNF coated electrode, it was around 150μA, suggesting that GNF coating slightly impeded the O₂ mass transport to the surface of the electrode. However, the difference between the bare and GNF coated for the O₂ catalysis was not significant. In contrast,

the electrode coated with MR181 blocked the O₂ diffusion. Hence GNF was selected to coat the electrodes for further experiments to protect the enzyme and to improve the biological activity.

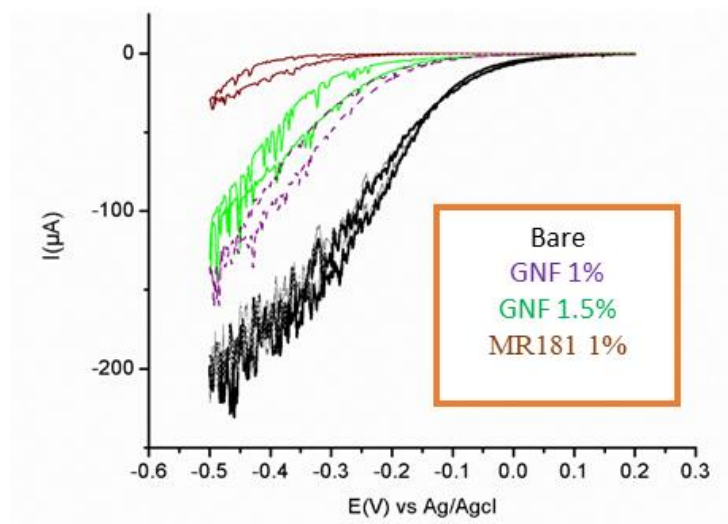


Figure 3.2: CV curves obtained for the reduction of oxygen on the gold surface in O₂ saturated PBS Buffer. (20mM phosphate, 140mM NaCl), pH=7.2. The O₂ reduction current was compared for Bare alone (black), GNF coated (1%) and GNF coated (1.5%) in green and purple, MR181 coated (1%) in brown by catalytic reduction of O₂ alone on the gold surface.

3.3.3 Quantification of the Os redox polymer coated on the electrode surface

The concentration of Os polymer in the modified electrodes (Os polymer (62.57 Wt%), BOD enzyme (30 Wt%) and crosslinker (7.43 Wt%)) was quantified in the absence of oxygen.

As seen in **Figure 3.3** a pair of symmetric peaks (corresponding to oxidation and reduction to Os-redox sites) was observed for both bare and GNF coated electrode at +0.34V vs Ag/AgCl which are characteristic of Osmium based redox polymer. The symmetric peak is an indication of the good reversibility of the system. GNF coated by 3 dips showed slightly reduced osmium

concentration compared to the electrodes without GNF, indicating the slight detachment of Os polymer during dip coating. The intensity of the peak recorded in argon is essential as it is directly proportional to the current density.

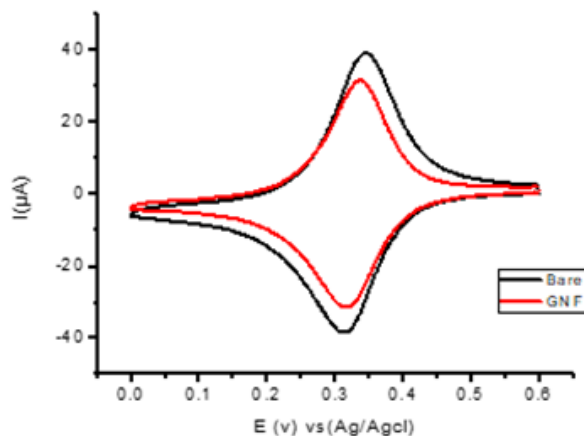


Figure 3.3: CV curves in argon (20mM phosphate,140mM NaCl) phosphate buffer saline , pH=7,2 Scan rate 50mv/s for the osmium oxidation and reduction. Bare is the gold electrode with an enzyme and GNF is the gold electrode coated with the enzyme and GNF. % Os % Enzyme

3.3.4 Functionality measurement of BOD (*Magnaporthe oryzae*) modified electrode in mice by cyclic voltammetry

Electrochemical experiments were performed to investigate the functionality of the co-immobilised enzyme (*Magnaporthe oryzae*)(28,144)/Os-polymer modified electrode with and without GNF coating. The measurements were performed in a saturated PBS solution by bubbling with O₂ before and after 24h subcutaneous implantation in mice. Usually, the onset of enzyme catalysis was at ~+0.5 V/ AgAgCl. As seen in **Figure 3.4** (a and b), the initial current of electroenzymatic O₂ reduction for the bare and GNF coated electrodes was around 120μA and 100

μA before implantation. The GNF coated electrode showed a slightly lower current compared to the bare electrode. The small difference might be due to a problem of O_2 diffusion or slight detachment of osmium polymer during dip coating. After 24hrs of implantation in mice (**Figure 3.4 b**), the current density was declined to 90% of the initial current in both bare and GNF coated electrodes. Apart from reduced current, the onset potential for enzyme catalysis was shifted from 0.5V to 0.35V, which might be due to the *in vivo* protein adsorption and provisional matrix formation.

To further investigate the current loss observed both on bare and GNF coated electrode, we performed *in vitro* stability test for BOD (*Magnaporthe oryzae*) modified electrodes with and without GNF coating (3 dips) (not shown in the results). The modified electrodes were incubated at 37°C in PBS solution. At predetermined time points, electroenzymatic O_2 reduction was measured. The enzyme catalytic activity measured after 24h of incubation in PBS was lost up to 90 % of initial current density. These results were in concurrent with *in vivo* results. The stability results indicated that BOD (*Magnaporthe oryzae*) enzyme was sensitive to chloride ions and temperature, which resulted in the deactivation of enzyme during incubation in PBS at 37°C.

To overcome the limitation of enzyme (*Magnaporthe oryzae*) instability, we decided to change the enzyme to BOD isolated from *Bacillus pumilus* for further experiments. Indeed, BOD from *B. pumilus* (27,145) is considered as a more stable enzyme and is less sensitive to chloride ions and temperature.

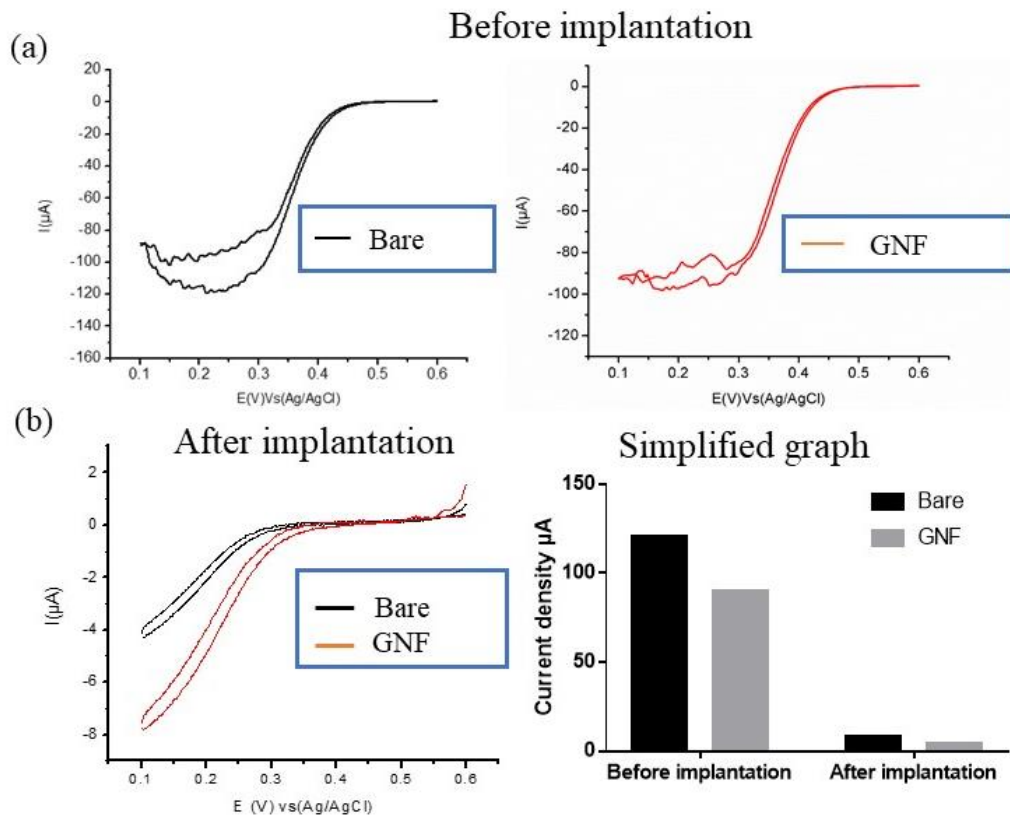


Figure 3.4: CV curves for electroenzymatic reduction of oxygen obtained in O_2 saturated (20mM phosphate, 140mM NaCl) phosphate buffer saline, pH=7.2, scan rate 5mv/s. (a) catalytic activity before implantation, (b) *In vitro* catalytic current showing more than 90% of the current loss after 24hrs of implantation, (c) comparison graph of before and after implantation.

3.3.5 *In vitro* stability of BOD enzyme from *B. pumilus* in PBS at 37°C

The initial stability of the enzyme was performed by *in vitro* studies by incubating the enzyme-modified bare and GNF (3 dips) coated electrodes in PBS at 37°C. At different time intervals, on day 0, 1, 2, 5, 7, 8, and 10, electroenzymatic O_2 reduction was recorded electrochemically. As can be seen in **Figure 3.5**, the current density was declined rapidly for the bare electrode after 24 hrs, while for GNF coated electrode, the reduction in current density was slower. On day 8 no more

enzyme catalytic current was observed for the bare electrode, while the GNF coated electrode showed a small current of $8\mu\text{A}$ till on day 10. These results indicated that the enzyme was stable and the presence of GNF protected the enzyme from the rapid decline in the catalytic current.

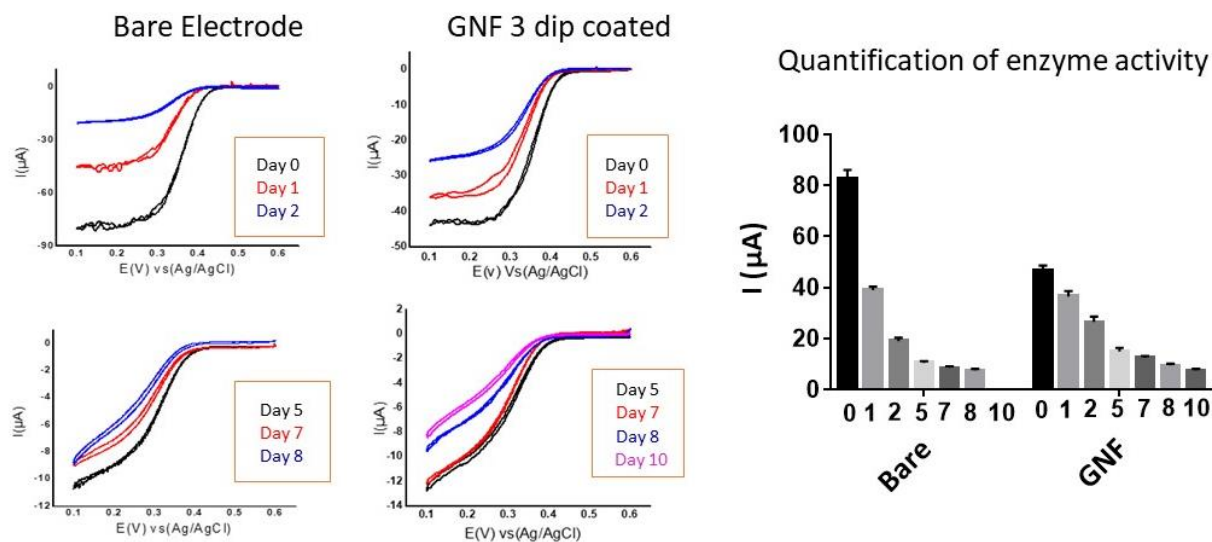
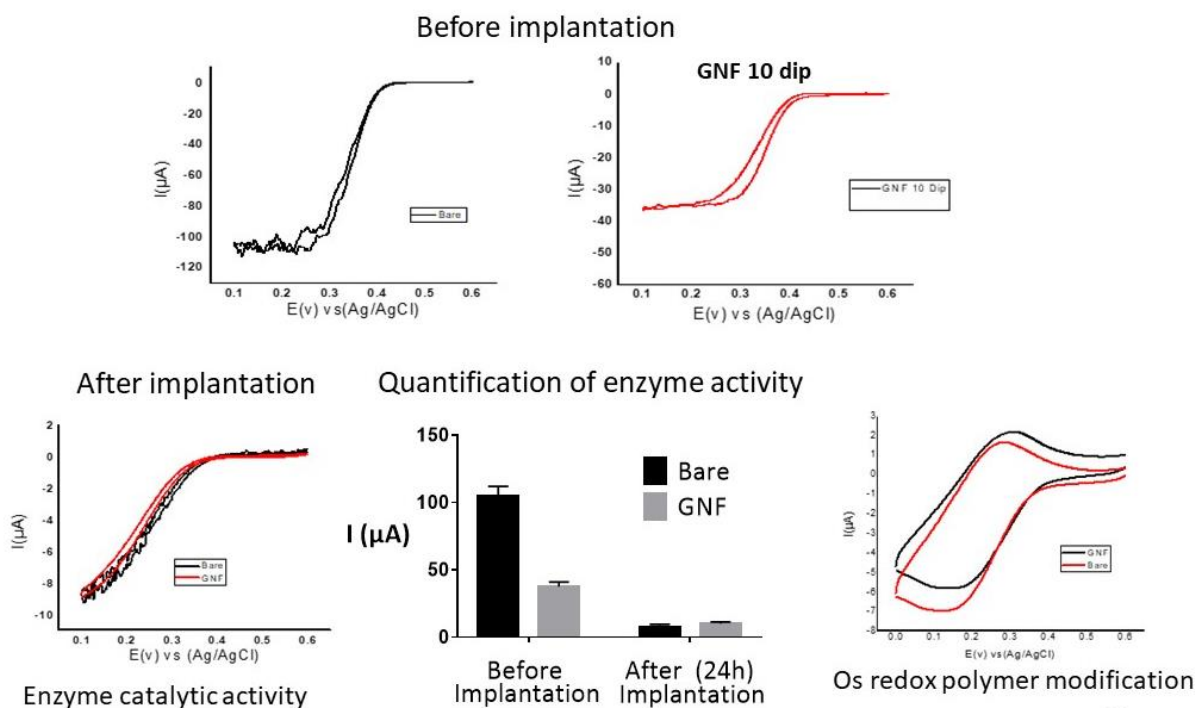


Figure 3.5: CV curves for electroenzymatic reduction of oxygen obtained in O_2 saturated (20mM phosphate, 140mM NaCl) phosphate buffer saline, $\text{pH}=7.2$, scan rate 5mv/s. (a) enzyme-modified electrode without GNF (b) GNF coated (3 dips) enzyme-modified electrode. The stability of enzyme catalytic activity measured at a different interval of time day 0, 1, 2, 5, 7, and 8 by incubating in PBS at 37°C .

3.3.6 Functionality measurement of BOD (*B.pumilus*) modified electrode in mice by cyclic voltammetry

Furthermore, the thickness of the GNF coating was increased to 10-dip coating to observe better protection during subcutaneous implantation in vivo. The functionality of BOD (*B. pumilus*), a modified electrode with and without GNF coating, was evaluated by electrochemical

measurements before and after 24h of subcutaneous implantation. As seen in **Figure 3.6**, the initial current for GNF coating (10 dips) was reduced to 50% to the bare electrode without GNF. The decrease in the current might be due to the loss of Os during the coating process, or GNF coating impeded the O₂ transport with increased thickness. The current density after 24h of subcutaneous implantation was declined to more than 90% of the initial current. By further investigation, it was revealed that Os polymer was modified upon implantation. The Os polymer which is responsible for efficient electron shuttle was modified, resulting in the loss of current. The modification of Os polymer can be due to the protein adsorption or inflammatory cells.



35

Figure 3.6: CV curves for reduction of oxygen obtained in O₂ saturated (20mM phosphate, 140mM NaCl) phosphate buffer saline, pH=7.2, scan rate 5mv/s. (a) before implantation, (b) after 24h subcutaneous implantation in mice, the First graph shows the modification of osmium and the second graph enzyme

catalytic activity,(c) comparison graph of before and after implantation.

3.4 Conclusion

In summary, the self-assembled GNF hydrogel coating onto the electrodes was optimised by a simple protocol. The GNF (3 dips) layer maintained the O₂ diffusion and enzyme catalytic activity as revealed by electrochemical measurements, while the increase in the number of coatings (10 dip) slightly declined the catalytic activity. However, the presence of GNF coating slowed down the rapid decline in the current, which was confirmed by the *in vitro* stability measurement of the enzymatic electrodes. Also, reduced stability and functionality of enzyme and mediator were observed upon subcutaneous implantation in mice. Despite the change in enzyme from *Magnaporthe oryzae* to *B. pumilus*, upon implantation, 90% of the current was lost after 24hrs of implantation. Although the enzyme was stable at *in vitro* measurements, the declined current density upon implantation was due to the modification of Os redox polymer, thereby reducing the electron shuttle to the enzyme.

Further modification in the experiments was made by considering the limitations mentioned above to improve the enzyme stability and power output. One typical strategy to avoid cathode current limitation is to increase the surface area. Hence macroporous gold electrode was selected to enhance the power output, considering its larger surface area against the bare electrode (146). The *in vitro* stable *B. pumilus* was modified with the cysteine (disulphide) residues for the covalent attachment of enzyme onto the electrode. The use of macroporous electrodes (developed in the laboratory of Pr Alexander Kuhn, University of Bordeaux) will be detailed in the next chapter.

Results

4. Optimisation of EBFC implantation and functionality (ongoing studies)

My contribution: Optimization of subcutaneous implantation of EBFC in the rat and the measurement of enzyme functionality non-invasively by the wireless antenna and finally the effect of implantation procedure on the foreign body reaction.

Thanks to Nicolas Mano and his group for the isolation, purification and characterisation of enzymes and polymers used for the immobilisation techniques, to Alexander Kuhn and his group for providing the functionalised macroporous gold electrodes and to Simon Hemour, Christine Dejous and their lab (IMS Bordeaux) for the development of an antenna to monitor wirelessly the enzyme activity.

4 Optimisation of EBFC implantation and functionality

Introduction.

The primary mechanism for the failure of the implantable device is foreign body response. Implantation of any device can lead to tissue damage, tissue strain, shearing, and tearing of extracellular matrix damages. This can trigger acute inflammation, which can lead to chronic implantation around electrodes. The initial injury formed during implantation can affect the enzyme function, which is labile to the hostile environment. As mentioned by Diane J. Burgess (147), the insertion of probe or needle and then of the implanted electrode results in a mechanical trauma. The initial injury can trigger the development of acute inflammation. Hence, the study was focused on the impact of an insertion probe and electrode on the tissue for the initial level of the inflammatory response, which was analysed by histology.

To determine the functionality of EBFC, macroporous electrodes were subcutaneously implanted in the rat (modified with enzymes glucose oxidase GoX (anode) and bilirubin oxidase BOD (cathode)). The *in vitro* enzyme functionality was measured using a wireless antenna and *in vivo* by wireless antenna and multimeter. The wireless antenna measures the potential difference of the implanted electrodes (Open circuit voltage: OCV). Information obtained here will help to develop adequate strategies for implantation/modification of electrode and understanding the *in vivo* performance of EBFC.

With the collaboration from Simon Hemour's and Christine Dejous' lab (IMS Bordeaux), we used an antenna to monitor wirelessly the enzyme activity. The goal is to monitor the enzyme activity continuously to understand the long-term performance and interaction of EBFC with living tissue.

4.1 Materials

Macroporous gold Electrodes (4cm inside the rat +3 cm outside for connection), surgical box (scissors, forceps, cannulas, steel rods and scotch), depilation cream and chlorhexidine (antiseptic) jacket from Harvard apparatus and Potentiostat. GoX and BOD produced in the laboratory of Pr Nicolas Mano (University of Bordeaux).

4.2. Methods

4.2.1 Electrode modification

BOD electrode preparation: The electrodes were dipped in glass capillary containing BOD enzyme overnight at 4°C to allow penetration. (BOD mutant stock: 52.84 mg/mL (final enzyme concentration 6 mg/mL with buffer NaPi 50 mM pH=6 for 1 electrode).

GoX electrode preparation: Immobilization was performed on a glass slide by a drop cast method. The mixture of enzymes/polymer/hydrogel was prepared with the 4 µL GOx of the enzyme (stock: 38.92 mg/mL) 7.35 µL of polymer and 4.77 µL of the crosslinker. The prepared mixture was drop cast onto the electrode placed on the glass slide and kept overnight at 4°C to allow complete drying and penetration.

4.2.3 In vitro measurement of enzyme functionality wirelessly

The functionality of the biofuel cell was measured by dipping the electrodes in Phosphate buffer saline (PBS, 50mM phosphate and 150mM sodium chloride) of pH 7.4 at 37 °C and 40mM glucose. The potential difference between the electrodes was measured continuously using a wireless antenna.

4.2.4 Effect of insertion probe for foreign body response

The animal studies were carried out in accredited animal facilities at the University of Bordeaux (accreditation number: A33-063-917) and were approved by the French animal ethical committee (APAFIS#16443-2018072016398155 v4). Lewis female rats (6 weeks) were used. The rat was anaesthetized with 4% isoflurane and maintenance of anaesthesia by the mask with 2 to 1.5 % isoflurane. Small incisions were made on the points marked. The groove probe was inserted subcutaneously through the incision, 0.9% NaCl was used as a lubricant while implanting the electrode. At day 3, animals were sacrificed. The subcutaneous tissue was harvested and fixed by using 4% paraformaldehyde (Antigenfix, ref 2017X11385) for 7days at 4°C. The fixed samples were dehydrated, embedded in paraffin and sectioned by a microtome (5µm thickness).



Figure 4.1: Subcutaneous implantation of the probe

4.2.5 Functionality measurement of EBFC by subcutaneous implantation

One day before the implantation of the biofuel cell, the commercial jacket (Harvard apparatus, ref 62-0057) was wrapped to the rat for habituation. The day of implantation, the rat was anaesthetized, and the electrode was inserted, guided through the groove. The electrodes modified with GoX and BOD were implanted on either side of the vertebral column. The Potential difference was measured between the electrodes using a multimeter, before connecting to the antenna. The commercial jacket was used to place the antenna on the back of the rat. The electrodes were connected to the antenna and then protected by the piece of scotch. The enzyme functionality was measured continuously by the wireless antenna for the first 5 hrs after implantation, and a multimeter was used to measure the enzyme activity at each day for 3 days.

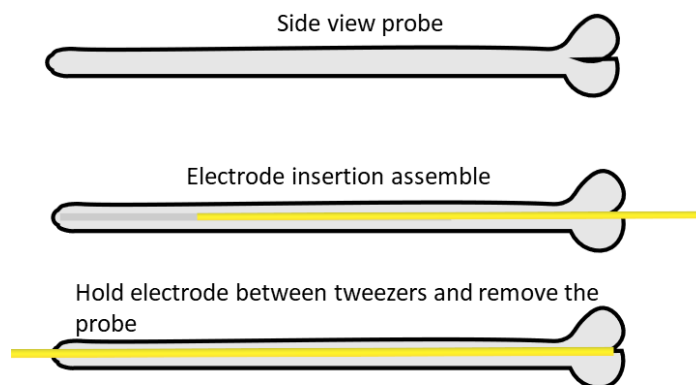


Figure 4.2: Illustration of implant assembly, insertion and wire electrode release.

4.3 Results

4.3.1 In vitro measurement of enzyme functionality by the wireless antenna

The performance of EBFC operating *in vitro* in Phosphate buffer saline at 37 °C containing 40mM glucose is shown in Figure 4.3. We observed that the voltage was decreased from the open circuit voltage (OCV) 550 mV to 400 mV during 2hrs of continuous operation. The wireless measurement offered an advantage to monitor the voltage continuously *in vitro* and to compare these results with *in vivo* operation.

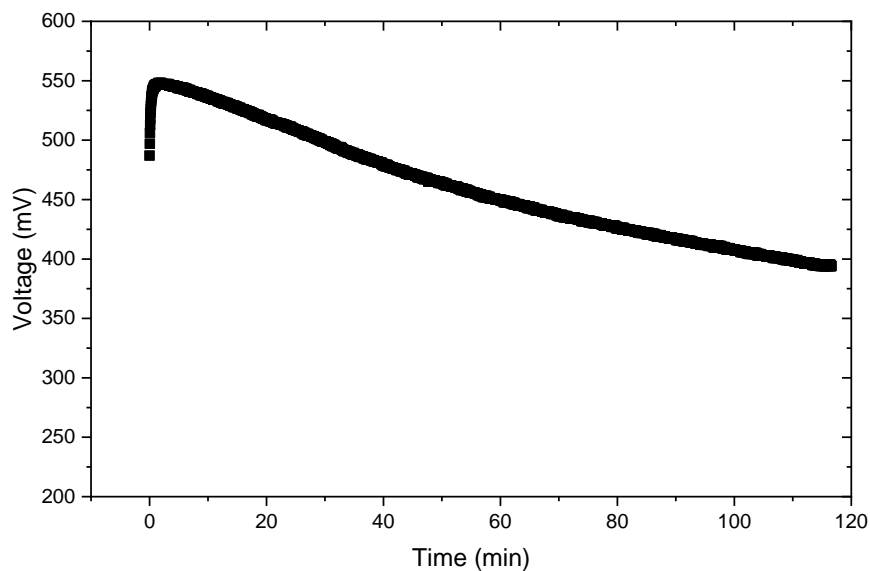


Figure 4.3: *In vitro* continuous measurement of enzyme functionality using a wireless antenna

4.3.2 Impact of insertion probe for the first steps of foreign body response

The probe was inserted subcutaneously in the rat and removed. Three days later, the tissue was collected at the vicinity of the inserted probe and compared with healthy normal tissue. As shown in **Figure 4.4**, tissue stained with Masson's trichrome did not show any signs of initial inflammation. These results indicate that the probe used to guide the electrode implantation does not provoke initial injury.

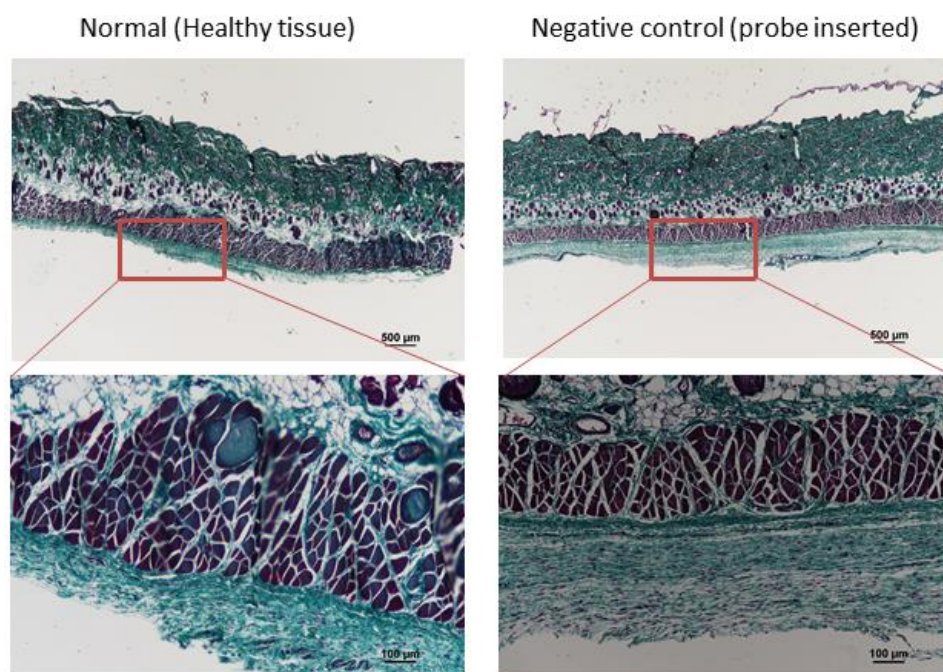


Figure 4.4: Masson's trichrome staining of tissue. The upper panels show lower magnification, scale bar 500 µm, and the lower panel with the magnified image of the highlighted place, scale bar 100 µm. n = 6.

4.3.3 Optimisation of jacket

Different types of jackets were optimised to immobilise the antenna on rat back. The main problem was the lack of jacket retainment, due to which the measurement with the antenna was hindered. In the initial assays, the jackets which were immobilised were dislodging within minutes, from the rat during its recovery from anaesthesia. After various designs, two models were able to retain for one day. The silicone jacket (developed in the laboratory of Dr Simon Hémour, University of Bordeaux) was taking more time to wrap than the commercial jacket (Harvard Apparatus). Hence, we decided to use the commercial jacket, which was not showing any signs of skin abrasion and moreover was easy to immobilise. The jackets were wrapped one day before the surgery for habituation.

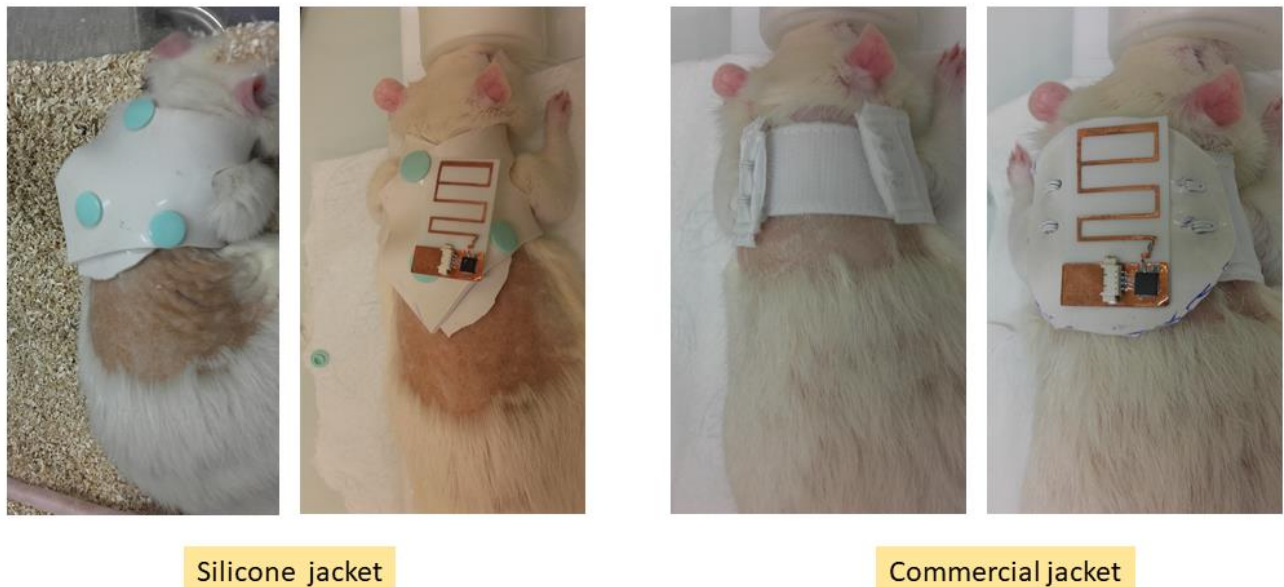


Figure 4.5: Two different jackets wrapped to the rat. On the right panels, the antenna is fixed to the jacket. The connection chip is in the distal position.

4.3.4 Functionality measurement of EBFC by subcutaneous implantation

The performance of EBFC *in vivo* during subcutaneous implantation in the rat is shown in **Figure 4.6**. For the first 5h, the operation of implanted EBFC was monitored by a wireless antenna placed on the back of the rat. Then, each day, OCV was measured using a multimeter for 3 days. During the first 5h of implantation, the OCV decreased from 600 mV to 500 mV, and the measurement made with a multimeter showed the decline from 600 mV to 200 mV on day 3. The decrease in OCV can be due to the initial inflammatory response, which might affect the enzyme catalysis and stability or due to the enzyme deactivation. Moreover, in these preliminary assays (n = 2 rats), EBFC was not protected with any type of hydrogel or membrane. The direct exposure of EBFC to the complex medium inside the body might result in the decline of OCV. Also, due to the flexibility of electrodes, implanted electrodes had undergone total deformation (twisted) and formed haemorrhage (not shown here) at day 3, which might also be the reason for reduced OCV.

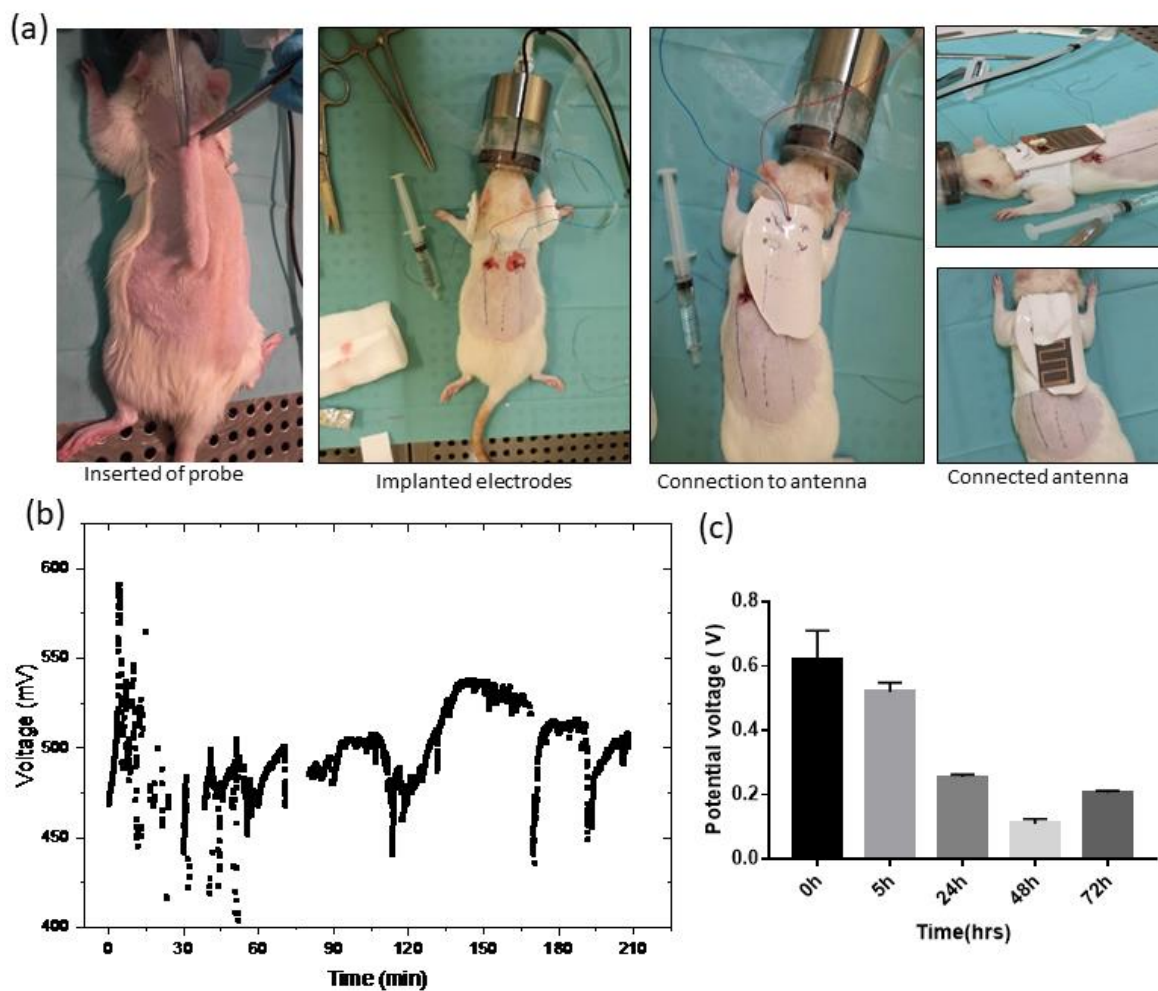


Figure 4.6: (a) subcutaneous implantation of enzyme modified macroporous electrodes in the rat, (b) *In vivo* continuous measurement of EBFC functionality using the wireless antenna (c) enzyme activity measured at different time points using a multimeter. n = 2 rats.

4.4 Conclusion

As mentioned earlier, the short lifetime of implanted EBFC is often due to the *in vivo* physiological conditions. Much efforts have been made to improve the lifetime of EBFC. The essential step is to monitor the *in vivo* performance of EBFC continuously to provide a system that allows deeper understanding of the long-term performance and the interaction of EBFC with living tissue. In this context, we have attempted to monitor the EBFC *in vivo* functionality wirelessly for a short duration, where the OCV was declined from 600 mV to 500 mV in 5h.

Only a few studies addressed the impact of insertion needle size on biocompatibility and their effect of biofouling on the stability of EBFC. The size of the insertion needle, which is employed to guide the EBFC implantation can contribute to the acute inflammation and the enzyme instability. Our histological analysis on initial trauma on the impact of probe insertion alone did not show any signs of inflammation, indicating that the method of implantation employed to implant the electrode will not contribute to a strong initial inflammation. Analysis of tissue at the vicinity of implanted electrodes showed intense haemorrhage, which might be due to the mechanical stress of the electrode. We also observed the deformation the electrodes due to their flexibility. Our ongoing studies aim to investigate further in detail these aspects. However, in the present results, the decline in the OCV might be due to the enzyme instability. The lack of protection around the EBFC might have affected the enzyme stability. This latter possibility would suggest using the hydrogel for protecting the enzyme from a hostile environment. Despite that, we also observed the haemorrhage and deformation of the electrode after 72h of implantation. From the results, it indicates that it is very much essential to improve the design of electrode and enzyme stability to enhance the EBFC functionality.

Discussion and Conclusion

4. Discussion

The development of implantable EBFCs that can provide reliable, real-time, clinically relevant results remains elusive. The major advances have been made in the development of miniaturized electrochemical sensors that have adequate sensitivity, selectivity and stability operated *in vitro*. However, implantation of such devices in the *in vivo* environment creates a physiological response that greatly influences the long-term stability of the devices, associated with biocompatibility problems. As mentioned in the introduction, progress in this area mandates the development of appropriate biocompatible coating material that can mitigate the activation of protein adsorption and inhibition of the inflammatory response upon subcutaneous implantation. In these aspects, a wide range of active and passive biomaterial coatings have been investigated in recent years to enhance *in vivo* biocompatibility and stability of the implantable devices. However, until now, no known materials or coatings can completely prevent capsule formation (88). Among the most commonly employed hydrogels as a coating material, PEG (148) and zwitterionic hydrogels are considered as low fouling materials (88). However, even these materials are ultimately encapsulated when used on implants (149). Besides this, the formation of the hydrogel is tedious, and it involves crosslinker that might cause toxicity.

As an alternative to these classically used polymers, we have demonstrated the LMWHs, which are self-assembled, with fast gelation kinetics and thixotropy, enable to coat the EFBC in a facile manner. LMWGs are receiving a lot of attention due to their self-assembling property, driven by non-covalent interactions through Π - Π and hydrogen bonding. Their functional group impacts on their mechanical, and supramolecular formation. Urea-based hydrogels MR181 and MR97 feature faster gelation kinetics and high elastic modulus (11-12 kPa) compared to the amide group

GNF (142) and MR73 (1 and 5 kPa) indicating that hydrogen bonding (urea contains two hydrogen bonds, amide contains one single bond) plays a significant role in supramolecular assembly (143).

As we know, the function of implantable devices is impeded by foreign body reaction (FBR) initiated by non-specific protein adsorption, the first event that occurs instantaneously upon implantation (1,150). Inflammatory cells recognise these materials as a foreign body through protein adsorption, initiating a cascade of events that leads to FBR. Thus, the initial event affects the fate of implantable devices, i.e., the formation of fibrosis or constructive remodelling, depending on surface topography, mechanical properties, and chemical composition of the material (85). FBR, which might result in fibrosis, isolates the material from surrounding tissue, thereby blocking mass transport and communication between the body and the implant (81).

The *in vitro* and *in vivo* biocompatibility evaluation of LMWH elicited low protein adsorption, reduced fibrosis and inflammation for 21 days of implantation. However, the hydrogels were abundantly infiltrated with macrophages, especially M1 phenotype, which may interfere with the device functionality. From these results, the hydrogels (GNF and MR181) showing less protein adsorption, slow degradation, and less macrophage infiltration were selected to coat the EBFC.

Protection of enzyme from denaturation and preventing leaching from the electrode surface are essential to make EBFC for practical use (8). The selection of hydrogel to protect the enzyme from a hostile environment is crucial, as extreme low permeability barrier membrane imposes a dominant diffusion resistance to analytes which can lead to the decline in enzyme functionality (64). In our case, the selected hydrogels GNF and MR181 were analysed for their oxygen diffusion capacity to the bare electrode surface. GNF coating slightly interfered with the O₂ diffusion, while an increase in the coating thickness is significantly reducing the oxygen permeability. In contrast,

MR181 hydrogel coating blocked the O₂ diffusion to the electrode surface. The *in vivo* and *in vitro* evaluation of the GNF coated electrodes failed to exhibit optimal enzyme protection except reducing the rapid decline in the initial current density against the non coated bare electrode.

In order to improve the power out, macroporus gold electrodes were adopted over the bare gold electrodes. This increase in the surface area helps in wiring the sufficient number of enzymes to the electrode. By assembling the anode and the O₂ diffusion BOD cathode, the fuel cell performance was evaluated by subcutaneous implantation in the rat. The open circuit potential (OCV) obtained *in vivo* are similar to the values demonstrated *in vitro* for similar electrodes measured by using wireless antenna (600mv). As mentioned by Ichi-Ribault *et al.* 2018 (64), the EBFC which was covered with chitosan and Dacron mesh required 18 days to reach OCV steady state after implantation in the rabbit. At the 18th day of implantation, the OCV was increased to 500mv. After 34 days, the OCV reduced considerably and reached 180 mv on the 60th day of implantation. In our preliminary assays, the EBFCs were not covered with any hydrogel or membrane, and direct exposure of the device to the hostile environment declined the OCV from 600 mV to 200 mV for 3 days of subcutaneous implantation. Despite that, the histological analysis of tissue at the vicinity of implanted electrodes showed intense haemorrhage, which can be due to the mechanical stress of the electrode. We also observed the deformation and break of the electrodes due to their flexibility. All these issues together explain the reasons for the decline in the OCV of EBFC.

5. Conclusion and Future perspective

This project aimed to produce a biocompatible EBFC that can monitor the glucose and generate power from glucose found naturally in interstitial fluids in the human body with a view to potential implantation. State of the art implantable EBFCs do not work reliably and have a short life after implantation. It is believed that the performance of the implantable EBFC can greatly influence the use of biocompatible hydrogel outermost coatings. Therefore, to improve the overall function of EBFC, four different hydrogel molecules were synthesized and characterized for the use of implantable EBFC.

Based on the results, further studies are focused on improving the design of electrodes and the selection of the desired hydrogel to improve the EBFC efficiency. To improve the efficiency of implantable EBFC, it is essential to use the hydrogels in combination with other well-established hydrogels such as PEG and zwitterionic hydrogels to improve their mechanical properties and biological properties. Based on the limitation observed in the present work, there is, however, much more work to do to develop a prototype device that can generate sufficient power and is safe for implantation.

Hydrogel selection.

Although the hydrogels selected to coat the EBFC showed potential biological properties, their mechanical properties remain too low to protect the device upon implantation. Also, the abundant macrophage infiltration (M1 phenotype) and oxygen diffusion limitation will probably be problematic to the EBFC function. Hence, as a long-term goal, the hydrogels can be compared alone and in combination with the hydrogels which are well established in other clinical

applications such as PEG and zwitterionic hydrogels; other hydrogels could also be analysed in collaboration with the chemists. To further suppress the initial biofouling process, anti-inflammatory drugs such as dexamethasone can be incorporated into the hydrogels to do the targeted drug delivery.

EBFC Design and wireless measurement

The present results collected so far from the EBFC point to some limitation in the architecture of electrodes. Hence, in the very near future, we are focusing on the modification of electrode design. And the wireless antenna will be used to monitor the enzyme functionality continuously.

Research questions

➤ **Are the four newly synthesised hydrogels biocompatible?**

- All the hydrogels are biocompatible without inducing fibrosis and detrimental inflammation in the surrounding tissues.
- We found that three out of four hydrogels gave the same degradation by-product *in vitro* (a glyconucleoside, *i.e.* glucose covalently bound to thymidine,) and that these three hydrogels induced a better vascularization three weeks after sub-cutaneous implantation. It will be interesting to analyse in more details the mechanisms of angiogenic properties, to allow chemists to propose new molecules forming LMWHs with proangiogenic properties; the aspect of macrophage recruitment is also an important parameter to consider.

➤ **Do the selected hydrogels meet the desired properties for coating the EBFC?**

Although the four hydrogels show desired biological properties such as low protein adsorption, reduced fibrosis and inflammation, their abundant infiltration by macrophages (M1 phenotype) may limit the enzyme functionality upon coating the EBFC.

➤ **Was the hydrogel coating improving the EBFC functionality and stability?**

To improve the long-term biocompatibility of EBFC *in vivo*, the hydrogel coating must be thick enough to be durable. On the other hand, if the coating is too thick, the enzymatic function will be hindered due to the limitation of oxygen diffusion. Preliminary *in vitro* and *in vivo* evaluation of GNF coating slightly protected the initial rapid decline of the current. In fact, in the end, it fails to show the optimal stable enzyme protection upon coating against non coated electrode. However, the studies are yet to be done on *in vivo* hostile environment protection and their coating stability on macroporous electrodes.

➤ **How was the subcutaneous implantation of EBFC optimised?**

Rats were chosen for the implantation of EBFC. Groove probe was adopted to guide the electrode implantation with minimal initial injury. The insertion of the probe and then the implanted electrode result in a mechanical trauma, which can then contribute to the acute inflammation and the enzyme instability. Our histological analysis on the impact of probe insertion alone did not show any signs of inflammation, indicating that the method of implantation employed to implant the electrode should not enhance the inflammatory reaction.

➤ **How was the enzyme functionality measured?**

The capability to wirelessly monitor and control an implanted EBFC provides deeper understanding of the long-term performance. We attempted to monitor the EBFC *in vivo* functionality wirelessly for a short duration, where the OCV was declined from 600 mV to 500 mV in 5h. Studies are in progress for long term measurements.

➤ **Communications and publications**

Oral Communications

Low molecular weight hydrogel injectable scaffolds help tuning the foreign body reaction

2018: 2nd Symposium of the Occitanie Network on Monocytes-Macrophages – Toulouse, France.

Low molecular weight hydrogels as injectable scaffolds for tuning the foreign body reaction

2018: BxCRm 3rd workshop on regenerative medicine. Bordeaux, France.

Poster Communications

Low molecular weight hydrogels as injectable scaffolds for tuning the foreign body reaction

2018: 5th European Congress of Immunology (Eci 2018) Amsterdam, Netherlands.

In-vitro and *in-vivo* assessment of the biocompatibility of drug delivery device components

2017: 1st international conference on tissue repair, regeneration and Fibrosis. Rhodes, Greece.

Biocompatible and bio functional porous electrodes for miniaturized enzymatic biofuel cells.

2017: Trans biomed young scientist day. Bordeaux, France.

Publications

Low molecular weight hydrogels derived from urea based-bola amphiphiles as new injectable biomaterials.

Ramin MA, Latxague L, Sindhu KR, Chassande O, Barthelemy P.

Biomaterials. November 2017; 145: 72-80. doi: 10.1016 / j. biomaterials.2017.08.034.

Epub 2017 Aug 19.

Tuning cation of Supramolecular Properties Gel: A New Paradigm for Sustained Drug Delivery.

Ramin MA, Sindhu KR, Appavoo A, Oumzil K, Grinstaff MW Chassande O, Barthelemy

P. Adv Mater. 2017 Apr; 29 (13). doi: 10.1002 / adma.201605227. Epub 2017 Feb 2.

Two articles in preparation:

Proangiogenic Supramolecular Gels through Biodegradation

Sindhu, K.R.¹, Bansode, N.², Rémy, M.¹, Morel, C.¹, Bareille, R.¹, Hagedorn, M.³, Hinz, B.⁴, Barthélémy, P.², Chassande, O.¹ & Boiziau, C.^{1,*}

(journal: Biomaterials)

Design and Synthesis of Redox Responsive Disulfide Containing Low Molecular Weight Hydrogelators (LMWGs) for Controlled Drug Release

Nitin D Bansode * KR * Sindhu, Chassande O, Boiziau C, Barthelemy P.

(journal: Angewandte chemistry)

Patent under review.

PRO-ANGIOGENIC COMPOUNDS; **Patent** application; (**In Progress**)

➤ References

1. Bernard Mélisande JE, Pungente MD, Yagoubi Najet. Biocompatibility of polymer-based biomaterials and medical.pdf. *Biomater Sci.* 2018;6(8):1–56.
2. Khan W, Muntimadugu E, Jaffe M, Domb AJ. Implantable Medical Devices. In: *Advances in Delivery Science and Technology.* 2014:1–59.
3. Zebda A, Alcaraz JP, Vadgama P, Shleev S, Minter SD, Boucher F, et al. Challenges for successful implantation of biofuel cells. *Bioelectrochemistry.* 2018;124:57–72.
4. Heller A. Miniature biofuel cells. *Phys Chem Chem Phys.* 2004;6(2):209–16.
5. Bandodkar AJ. Review—Wearable Biofuel Cells: Past, Present and Future. *J Electrochem Soc.* 2017;164(3):H3007–14.
6. Slaughter G, Kulkarni T. Enzymatic Glucose Biofuel Cell and its Application. *J Biochips Tissue Chips.* 2015;05(01):1–10.
7. Atanassov P, Apblett C, Banta S, Brozik S, Barton SC, Cooney M, et al. Enzymatic biofuel cells. *Interface-Electrochemical Soc.* 2007;16(2):28–31.
8. Falk M, Narváez Villarrubia CW, Babanova S, Atanassov P, Shleev S. Biofuel cells for biomedical applications: Colonizing the animal kingdom. *ChemPhysChem.* 2013;14(10):2045–58.
9. Reitz W. Fundamentals, Technology, and Applications. Vol. 22, *Materials and Manufacturing Processes.* 2007:789–789.
10. Shukla AK, Suresh P. Biological fuel cell and their application. *Curr Sci.* 2004;87(4):455–67.
11. Kerzenmacher S. Biofuel cells as sustainable power sources for implantable systems. In: *Implantable Sensor Systems for Medical Applications.* Woodhead Publishing Limited; 2013:183–212.
12. Andrade SAN and AR De. New Energy Sources: The Enzymatic Biofuel Cell Sidney. *J Braz Chem Soc.* 2013;24(2):1891–912.
13. Gamella M, Koushanpour A, Katz E. Biofuel cells – Activation of micro- and macro-electronic devices. *Bioelectrochemistry.* 2018;119:33–42.
14. Yahiro AT, Lee SM, Kimble DO. *Bioelectrochemistry. I. Enzyme utilizing bio-fuel cell studies.* *BBA - Spec Sect Biophys Subj.* 1964;88(2):375–83.
15. Yin Song VP and CW. Recent Development of Miniatured Enzymatic Biofuel Cells. In: *Bernardes DMADS, ISBN, editors. Biofuel's Engineering Process Technology.* 2011: 742.
16. Mano N, Mao F, Heller A. A Miniature Membraneless Biofuel Cell Operating at 0.36 V under Physiological Conditions. *J ofThe Electrochem Soc.* 2003;150(8):A1136–8.

17. Leech D, Kavanagh P, Schuhmann W. Enzymatic fuel cells: Recent progress. *Electrochim Acta*. 2012;84:223–34.
18. Cooney MJ, Svoboda V, Lau C, Martin G, Minteer SD. Enzyme catalysed biofuel cells. *Energy Environ Sci*. 2008;1(3):320–37.
19. Yuhashi N, Tomiyama M, Okuda J, Igarashi S, Ikebukuro K, Sode K. Development of a novel glucose enzyme fuel cell system employing protein engineered PQQ glucose dehydrogenase. *Biosens Bioelectron*. 2005;20(10 SPEC. ISS.):2145–50.
20. Ogawa Y, Kato K, Miyake T, Nagamine K, Ofuji T, Yoshino S, et al. Organic Transdermal Iontophoresis Patch with Built-in Biofuel Cell. *Adv Healthc Mater*. 2015;4(4):506–10.
21. Ruff A. Redox polymers in bioelectrochemistry: Common playgrounds and novel concepts. *Curr Opin Electrochem*. 2017;5(1):66–73.
22. Leskovac V, Trivić S, Wohlfahrt G, Kandrač J, Peričin D. Glucose oxidase from *Aspergillus niger*: The mechanism of action with molecular oxygen, quinones, and one-electron acceptors. *Int J Biochem Cell Biol*. 2005;37(4):731–50.
23. Wong CM, Wong KH, Chen XD. Glucose oxidase: Natural occurrence, function, properties and industrial applications. *Appl Microbiol Biotechnol*. 2008;78(6):927–38.
24. Milton RD, Giroud F, Thumser AE, Minteer SD, Slade RCT. Bilirubin oxidase bioelectrocatalytic cathodes: The impact of hydrogen peroxide. *Chem Commun*. 2014;50(1):94–6.
25. Mano N, De Poulpiquet A. O₂ Reduction in Enzymatic Biofuel Cells. *Chem Rev*. 2018;118(5):2392–468.
26. Cracknell JA, McNamara TP, Lowe ED, Blanford CF. Bilirubin oxidase from *Myrothecium verrucaria*: X-ray determination of the complete crystal structure and a rational surface modification for enhanced electrocatalytic O₂reduction. *Dalt Trans*. 2011;40(25):6668–75.
27. Durand F, Kjaergaard CH, Suraniti E, Gounel S, Hadt RG, Solomon EI, et al. Bilirubin oxidase from *Bacillus pumilus*: A promising enzyme for the elaboration of efficient cathodes in biofuel cells. *Biosens Bioelectron*. 2012;35(1):140–6.
28. Solomon EI, Durand F, Gounel S, Mano N, Kjaergaard CH. Bilirubin oxidase from *Magnaporthe oryzae*: an attractive new enzyme for biotechnological applications. *Appl Microbiol Biotechnol*. 2012;96(6):1489–98.
29. Siepenkoetter T, Salaj-Kosla U, Xiao X, Conghaile P, Pita M, Ludwig R, et al. Immobilization of Redox Enzymes on Nanoporous Gold Electrodes: Applications in Biofuel Cells. *Chempluschem*. 2017;82(4):553–60.
30. Salaj-Kosla U, Pöller S, Beyl Y, Scanlon MD, Beloshapkin S, Shleev S, et al. Direct electron transfer of bilirubin oxidase (*Myrothecium verrucaria*) at an unmodified nanoporous gold biocathode. *Electrochem commun*. 2012;16(1):92–5.
31. Falk M, Blum Z, Shleev S. Direct electron transfer based enzymatic fuel cells. *Electrochim*

- Acta. 2012;82:191–202.
32. Yu EH, Scott K. Enzymatic biofuel cells-fabrication of enzyme electrodes. *Energies*. 2010;3(1):23–42.
 33. Heller A. Electrical Wiring of Redox Enzymes. *Acc Chem Res*. 1990;23(5):128–34.
 34. Heller A. Electrical connection of enzyme redox centers to electrodes. *J Phys Chem*. 1992;96(9):3579–87.
 35. Heller A. Electron-conducting redox hydrogels: design, characteristics and synthesis. *Curr Opin Chem Biol*. 2006;10(6):664–72.
 36. Gonzalez-solino C, Lorenzo M Di. Enzymatic Fuel Cells: Towards Self-Powered Implantable and Wearable Diagnostics. *Biosensors*. 2018;8(11):1–18.
 37. Hanefeld U, Gardossi L, Magner E. Understanding enzyme immobilisation. *Chem Soc Rev*. 2009;38(2):453–68.
 38. Mohamad NR, Marzuki NHC, Buang NA, Huyop F, Wahab RA. An overview of technologies for immobilization of enzymes and surface analysis techniques for immobilized enzymes. *Biotechnol Biotechnol Equip*. 2015;29(2):205–20.
 39. Chiang CJ, Hsiao LT, Lee WC. Immobilization of cell-associated enzymes by entrapment in polymethacrylamide beads. Vol. 11, *Biotechnology Techniques*. 1997:121–5.
 40. Tsai H chung, Doong R an. Preparation and characterization of urease-encapsulated biosensors in poly(vinyl alcohol)-modified silica sol-gel materials. *Biosens Bioelectron*. 2007;23(1):66–73.
 41. Tang J, Haddon R, Joshi K, Chen W, Wang J, Mulchandani A. A Disposable Biosensor for Organophosphorus Nerve Agents Based on Carbon Nanotubes Modified Thick Film Strip Electrode. *Electroanalysis*. 2004;17(1):54–8.
 42. Guisan JM. Immobilization of Enzymes as the 21st Century Begins. In: *Methods in Biotechnology*. 2007. p. 1–13.
 43. Li D, He Q, Cui Y, Duan L, Li J. Immobilization of glucose oxidase onto gold nanoparticles with enhanced thermostability. *Biochem Biophys Res Commun*. 2007;355(2):488–93.
 44. When A, The A. Chapter 3: Experimental. In: *Drugs*. 1997. p. 749–54.
 45. Vytřas K. Modern Electroanalytical Methods. Vol. 4, *Journal of Solid State Electrochemistry*. 2002:0305.
 46. Bard A F larry R. *Electrochemical methods & Fundamentals and Applications* Allen. Vol. 126, John wiley and sons inc. 1985. (225-5945).
 47. Nilsson S. *Electrodes and Electrokinetic Systems for Biotechnological Applications*. *Electrodes and Electrokinetic Systems for Biotechnological Applications*. 2015:1–44.
 48. Marusak RA, Doan K, Cummings SD. Appendix 6: A Brief Guide to Writing in Chemistry.

- Integr Approach to Coord Chem. 2007;252–9.
49. Wang J. Amperometric biosensors for clinical and therapeutic drug monitoring: A review. *J Pharm Biomed Anal.* 1999;19(1–2):47–53.
 50. Cosnier S, Gross AJ, Giroud F, Holzinger M. Beyond the hype surrounding biofuel cells: What's the future of enzymatic fuel cells? *Curr Opin Electrochem.* 2018;12:148–55.
 51. Gonzalez-Solino C, Lorenzo M, Gonzalez-Solino C, Lorenzo M Di. Enzymatic Fuel Cells: Towards Self-Powered Implantable and Wearable Diagnostics. *Biosensors.* 2018 Jan 29;8(1):11.
 52. Mano N, Mao F, Heller A. Characteristics of a Miniature Compartment-less Glucose-O₂ Biofuel Cell and Its Operation in a Living Plant. *JACS.* 2003;125(13):6588–94.
 53. Cinquin P, Gondran C, Giroud F, Mazabrard S, Pellissier A, Boucher F, et al. A Glucose BioFuel Cell Implanted in Rats. Haverkamp R, editor. *PLoS One.* 2010 May 4;5(5):e10476.
 54. Miyake T, Haneda K, Nagai N, Yatagawa Y, Onami H, Yoshino S, et al. Enzymatic biofuel cells designed for direct power generation from biofluids in living organisms. *Energy Environ Sci.* 2011 Nov 22;4(12):5008.
 55. Sales FCPF, Iost RM, Martins MVA, Almeida MC, Crespilho FN. An intravenous implantable glucose/dioxygen biofuel cell with modified flexible carbon fiber electrodes. *Lab Chip.* 2013;13(3):468–74.
 56. Rapoport BI, Kedziński JT, Sarpeshkar R. A Glucose Fuel Cell for Implantable Brain–Machine Interfaces. Egles C, editor. *PLoS One.* 2012 Jun 12;7(6):e38436.
 57. Castorena-Gonzalez JA, Foote C, MacVittie K, Haláček J, Halámková L, Martinez-Lemus LA, et al. Biofuel Cell Operating in Vivo in Rat. *Electroanalysis.* 2013 Jul 1;25(7):1579–84.
 58. Cosnier S, Le Goff A, Holzinger M. Towards glucose biofuel cells implanted in human body for powering artificial organs: Review. *Electrochem commun.* 2014;38:19–23.
 59. El Ichi S, Zebda A, Alcaraz JP, Boucher F, Boutonnat J, Cinquin P, et al. Biocompatible implantable biofuel cell. In: *IEEE Conference on Biomedical Engineering and Sciences: "* 2014:50–5.
 60. Cadet M, Gounel S, Stines-Chaumeil C, Brilland X, Rouhana J, Louerat F, et al. An enzymatic glucose/O₂biofuel cell operating in human blood. *Biosens Bioelectron.* 2016;83:60–7.
 61. Zebda A, Cosnier S, Alcaraz J-P, Holzinger M, Le Goff A, Gondran C, et al. Single Glucose Biofuel Cells Implanted in Rats Power Electronic Devices. *Sci Rep.* 2013; 22;3(1):1516.
 62. Szczupak A, Haláček J, Halámková L, Bocharova V, Alfonta L, Katz E. Living battery – biofuel cells operating in vivo in clams. *Energy Environ Sci.* 2012 Sep 20;5(10):8891.
 63. Halámková L, Haláček J, Bocharova V, Szczupak A, Alfonta L, Katz E. Implanted Biofuel

- Cell Operating in a Living Snail. *J Am Chem Soc.* 2012;21;134(11):5040–3.
64. El Ichi-Ribault S, Alcaraz JP, Boucher F, Boutaud B, Dalmolin R, Boutonnat J, et al. Remote wireless control of an enzymatic biofuel cell implanted in a rabbit for 2 months. *Electrochim Acta.* 2018;269:360–6.
 65. Morais JM, Papadimitrakopoulos F, Burgess DJ. Biomaterials/Tissue Interactions: Possible Solutions to Overcome Foreign Body Response. *AAPS J.* 2010;12(2):188–96.
 66. Corradetti B, Impact T. The Immune Response to Implanted Materials and Devices. In: Corradetti, Bruna Department of Life and Environmental Sciences Marche Polytechnic University Ancona I, editor. *The Immune Response to Implanted Materials and Devices.* Springer International Publishing Switzerland 2017; 1–237.
 67. Kwee BJ, Mooney DJ. Manipulating the Intersection of Angiogenesis and Inflammation. *Ann Biomed Eng.* 2015;43(3):628–40.
 68. Choi S., Chae J. Advancing Microfluidic-based Protein Biosensor Technology for Use in Clinical Diagnostics. 2011:1-127.
 69. Dee KC, Puleo DA, Bizios R. An Introduction to Tissue-Biomaterial Interactions Protein-Surface Interactions. *Blood Cells.* 2002;4:37–52.
 70. Santos TC, Marques AP, Reis RL. In vivo tissue response to natural-origin biomaterials. In: *Natural-Based Polymers for Biomedical Applications.* 2008:683–98.
 71. Gardner AB, Lee SKC, Woods EC, Acharya AP. Biomaterials-based modulation of the immune system. *Biomed Res Int.* 2013;1–8.
 72. Lin TH, Tamaki Y, Pajarinen J, Waters HA, Woo DK, Yao Z, et al. Chronic inflammation in biomaterial-induced periprosthetic osteolysis: NF- κ B as a therapeutic target. *Acta Biomater.* 2014;10(1):1–10.
 73. Jhunjhunwala S. Neutrophils at the Biological-Material Interface. *ACS Biomater Sci Eng.* 2018;4(4):1128–36.
 74. Christo SN, Diener KR, Bachhuka A, Vasilev K, Hayball JD. Innate Immunity and Biomaterials at the Nexus: Friends or Foes. *Biomed Res Int.* 2015;10:23.
 75. Yu T, Wang W, Nassiri S, Kwan T, Dang C, Liu W, et al. Temporal and spatial distribution of macrophage phenotype markers in the foreign body response to glutaraldehyde-crosslinked gelatin hydrogels. *J Biomater Sci Polym Ed.* 2017;27(8):721–42.
 76. Chung L, Maestas DR, Housseau F, Elisseff JH. Key players in the immune response to biomaterial scaffolds for regenerative medicine. *Adv Drug Deliv Rev.* 2017;114:184–92.
 77. Klopffleisch R. Macrophage reaction against biomaterials in the mouse model: phenotypes, functions and markers. *Acta Biomater.* 2016;16:30319–1.
 78. Weigel E, Smith C, Liu PG, Robison R, Neill KO. Journal of Clinical & Cellular Macrophage Polarization and Its Role in Cancer. *J Clin Cell Immunol.* 2015;6(4):338.

79. Sheikh Z, Brooks P, Barzilay O, Fine N, Glogauer M. Macrophages, Foreign Body Giant Cells and Their Response to Implantable Biomaterials. *Materials (Basel)*. 2015 Aug 28;8(9):5671–701.
80. Walraven M, Hinz B. Therapeutic approaches to control tissue repair and fibrosis: Extracellular matrix as a game changer. *Matrix Biol*. 2018;71–72(2017):205–24.
81. Pakshir P, Hinz B. The big five in fibrosis: Macrophages, myofibroblasts, matrix, mechanics, and miscommunication. *Matrix Biol*. 2018;68–69(2017):81–93.
82. Chandorkar Y, Krishnamurthy R, Basu B. The foreign body response demystified The Foreign body response demystified. *ACS Biomater Sci Eng*. 2018;(04 Jun 2018):1–77.
83. Berzina-Cimdina L, Prakasam M, Locs J, Largeteau A, Loca D, Salma-Ancane K. Biodegradable Materials and Metallic Implants—A Review. *J Funct Biomater*. 2017;8(4):44.
84. James M. Anderson, Analiz Rodriguez,* and DTC. Foreign body reaction to biometaterials. *Semin Immunol*. 2008;20(2):86–100.
85. Londono R, Badylak SF. Factors Which Affect the Host Response to Biomaterials. *Host Response to Biomaterials: The Impact of Host Response on Biomaterial Selection*. Elsevier Inc.; 2015. 1–12 p.
86. Zhang Z, Chao T, Liu L. Zwitterionic Hydrogels: an in Vivo Implantation Study. *J Biomater Sci*. 2008;20(13):1845–59.
87. Wisniewski N, Moussy F, Reichert WM. Characterization of implantable biosensor membrane biofouling. *Fresenius J Anal Chem*. 2000;366(6–7):611–21.
88. Zhang L, Cao Z, Bai T, Carr L, Irvin C, Ratner BD, et al. Zwitterionic hydrogels implanted in mice resist the foreign-body reaction. *Nat Biotechnol*. 2013;31(6):553–6.
89. Ulrike Klueh^{1, 2, 3}, Omar Antar^{1, 2}, Yi Qiao^{1, 2} and DLK. Continuous Glucose Monitoring in vivo. *J Biomed Mater Res A*. 2014;102(10):3512–22.
90. L.W. Norton, H.E. Koschwanez, N.A. Wisniewski, B. Klitzman and WMR. Vascular endothelial growth factor and dexamethasone release from nonfouling sensor coatings affect the foreign body response. *J Biomed Mater Res A*. 2007;81(4):858–69.
91. Upkar Bhardwaj MP, Radhakrishna Sura, DVM MS, Fotios Papadimitrakopoulos PD, Diane J. Burgess P. Controlling Acute Inflammation with Fast Releasing Dexamethasone-PLGA Microsphere/PVA Hydrogel Composites for Implantable Devices. *J Diabetes Sci Technol*. 2007;1(1):8–17.
92. Saroia J, Yanen W, Wei Q, Zhang K, Lu T, Zhang B. A review on biocompatibility nature of hydrogels with 3D printing techniques, tissue engineering application and its future prospective. *Bio-Design Manuf*. 2018;1(4):265–79.
93. Annabi N, Tamayol A, Uquillas JA, Akbari M, Bertassoni LE, Cha C, et al. 25th anniversary article: Rational design and applications of hydrogels in regenerative medicine. *Adv Mater*.

- 2014;26(1):85–124.
94. Ullah F, Othman MBH, Javed F, Ahmad Z, Akil HM. Classification, processing and application of hydrogels: A review. *Mater Sci Eng C*. 2015;57:414–33.
 95. Wichterle O L. Hydrophilic Gels for Biological Use. *Nature*. 1960;185(4706):117–8.
 96. Hennink W.E. VNCf. Novel crosslinking methods to design hydrogels. *Adv Drug Deliv Rev*. 2001;54(1):13–36.
 97. Sadtler K, Singh A, Wolf MT, Wang X, Pardoll DM, Elisseeff JH. Design, clinical translation and immunological response of biomaterials in regenerative medicine. *Nat Rev Mater*. 2016;1(7).
 98. Oh KS, Han SK, Choi YW, Lee JH, Lee JY, Yuk SH. Hydrogen-bonded polymer gel and its application as a temperature-sensitive drug delivery system. *Biomaterials*. 2004;25(12):2393–8.
 99. Raghavendra GM, Sadiku R, Yallapu MM, Jayaramudu T, Varaprasad K. A mini review on hydrogels classification and recent developments in miscellaneous applications. *Mater Sci Eng C*. 2017;79:958–71.
 100. Mahinroosta M, Jomeh Farsangi Z, Allahverdi A, Shakoori Z. Hydrogels as intelligent materials: A brief review of synthesis, properties and applications. *Mater Today Chem*. 2018;8:42–55.
 101. Peppas NA, Hilt JZ, Khademhosseini A, Langer R. Hydrogels in biology and medicine: From molecular principles to bionanotechnology. *Adv Mater*. 2006;18(11):1345–60.
 102. Liu SQ, Rachel Ee PL, Ke CY, Hedrick JL, Yang YY. Biodegradable poly(ethylene glycol)-peptide hydrogels with well-defined structure and properties for cell delivery. *Biomaterials*. 2009;30(8):1453–61.
 103. Priyadarshi Pandaa, Shamsher Alib, Edward Lob, Bong Geun Chungb, T. Alan Hattona, Ali Khademhosseinib and PSD, Priyadarshi. Stop-Flow Lithography to Generate Cell-Laden Microgel Particles. *Lab chip*. 2018;8(7):1056–1061.
 104. Stenekes RJH, Talsma H, Hennink WE. Formation of dextran hydrogels by crystallization. *Biomaterials*. 2001;22(13):1891–8.
 105. Constantin M, Cristea M, Ascenzi P, Fundueanu G. Lower critical solution temperature versus volume phase transition temperature in thermoresponsive drug delivery systems. *eXPRESS Polym Lett*. 2011;5(10):839–48.
 106. Taylor MJ, Tomlins P, Sahota TS. Thermoresponsive Gels. In: *gels*. 2017: 1–31.
 107. Ohseido Y. Low-Molecular-Weight Gelators as Base Materials for Ointments. *Gels*. 2016;2(2):13.
 108. Jain P, Hung HC, Lin X, Ma J, Zhang P, Sun F, et al. Poly(ectoine) Hydrogels Resist Nonspecific Protein Adsorption. *Langmuir*. 2017;33(42):11264–9.

109. Draper ER, Adams DJ. Low-Molecular-Weight Gels: The State of the Art. *Chem.* 2017;3(3):390–410.
110. Feng Q, Wei K, Lin S, Xu Z, Sun Y, Shi P, et al. Mechanically resilient, injectable, and bioadhesive supramolecular gelatin hydrogels crosslinked by weak host-guest interactions assist cell infiltration and in situ tissue regeneration. *Biomaterials.* 2016;101:217–28.
111. Yang G, Lin H, Rothrauff BB, Yu S, Tuan RS. Multilayered polycaprolactone/gelatin fiber-hydrogel composite for tendon tissue engineering. *Acta Biomater.* 2016;35:68–76.
112. Li X, Zhang J, Kawazoe N, Chen G, Li X, Zhang J, et al. Fabrication of Highly Crosslinked Gelatin Hydrogel and Its Influence on Chondrocyte Proliferation and Phenotype. *Polymers (Basel).* 2017;9(12):309.
113. Heo J, Koh RH, Shim W, Kim HD, Yim H-G, Hwang NS. Riboflavin-induced photocrosslinking of collagen hydrogel and its application in meniscus tissue engineering. *Drug Deliv Transl Res.* 2016;6(2):148–58.
114. Wei K, Zhu M, Sun Y, Xu J, Feng Q, Lin S, et al. Robust Biopolymeric Supramolecular “Host–Guest Macromer” Hydrogels Reinforced by in Situ Formed Multivalent Nanoclusters for Cartilage Regeneration. *Macromolecules.* 2016;49(3):866–75.
115. Shendi D, Dede A, Yin Y, Wang C, Valmikinathan C, Jain A. Tunable, bioactive protein conjugated hyaluronic acid hydrogel for neural engineering applications. *J Mater Chem B.* 2016;4(16):2803–18.
116. Kim DH, Martin JT, Elliott DM, Smith LJ, Mauck RL. Phenotypic stability, matrix elaboration and functional maturation of nucleus pulposus cells encapsulated in photocrosslinkable hyaluronic acid hydrogels. *Acta Biomater.* 2015;12:21–9.
117. Chaudhuri O, Gu L, Klumpers D, Darnell M, Bencherif SA, Weaver JC, et al. Hydrogels with tunable stress relaxation regulate stem cell fate and activity. *Nat Mater.* 2016;15(3):326–34.
118. Lee H, Gu L, Mooney DJ, Levenston ME, Chaudhuri O. Mechanical confinement regulates cartilage matrix formation by chondrocytes. *Nat Mater.* 2017;16(12):1243–51.
119. Liu Y, Chan-Park MB. Hydrogel based on interpenetrating polymer networks of dextran and gelatin for vascular tissue engineering. *Biomaterials.* 2009;30(2):196–207.
120. Baei P, Jalili-Firoozinezhad S, Rajabi-Zeleti S, Tafazzoli-Shadpour M, Baharvand H, Aghdami N. Electrically conductive gold nanoparticle-chitosan thermosensitive hydrogels for cardiac tissue engineering. *Mater Sci Eng C.* 2016;63:131–41.
121. Gao G, Schilling AF, Hubbell K, Yonezawa T, Truong D, Hong Y, et al. Improved properties of bone and cartilage tissue from 3D inkjet-bioprinted human mesenchymal stem cells by simultaneous deposition and photocrosslinking in PEG-GelMA. *Biotechnol Lett.* 2015 Nov 22;37(11):2349–55.
122. Zhang X, Xu B, Puperi DS, Yonezawa AL, Wu Y, Tseng H, et al. Integrating valve-inspired

- design features into poly(ethylene glycol) hydrogel scaffolds for heart valve tissue engineering. *Acta Biomater.* 2015;14:11–21.
123. Tseng T-C, Tao L, Hsieh F-Y, Wei Y, Chiu I-M, Hsu S. An Injectable, Self-Healing Hydrogel to Repair the Central Nervous System. *Adv Mater.* 2015;27(23):3518–24.
 124. Fan M, Zhang Z, Mao J, Tan H. Injectable Multi-Arm Poly(ethylene glycol)/Hyaluronic Acid Hydrogels for Adipose Tissue Engineering. *J Macromol Sci Part A.* 2015;52(5):345–52.
 125. Pacelli S, Rampetsreiter K, Modaresi S, Subham S, Chakravarti AR, Lohfeld S, et al. Fabrication of a Double-Cross-Linked Interpenetrating Polymeric Network (IPN) Hydrogel Surface Modified with Polydopamine to Modulate the Osteogenic Differentiation of Adipose-Derived Stem Cells. *ACS Appl Mater Interfaces.* 2018;10(30):24955–62.
 126. Takeno H, Kimura Y, Nakamura W. Mechanical, Swelling, and Structural Properties of Mechanically Tough Clay-Sodium Polyacrylate Blend Hydrogels. *gels.* 2017;3(1):10.
 127. Li X, Sun Q, Li Q, Kawazoe N, Chen G. Functional Hydrogels With Tunable Structures and Properties for Tissue Engineering Applications. *Front Chem.* 2018;6:499.
 128. Zhang T, Zhang X, Deng X. Annals of Biotechnology Applications of protein-resistant polymer and hydrogel coatings on biosensors and biomaterials. *Ann Biotechnol.* 2018;2:1006.
 129. Zuidema JM, Rivet CJ, Gilbert RJ, Morrison FA. A protocol for rheological characterization of hydrogels for tissue engineering strategies. *J Biomed Mater Res Part B.* 2014;102B:1063–73.
 130. Chen MH, Wang LL, Chung JJ, Kim Y, Atluri P, Burdick JA. Methods To Assess Shear-Thinning Hydrogels for Application As Injectable Biomaterials. *ACS Biomater Sci Eng.* 2017;3:3146–3160.
 131. Li X, Chen S, Li J, Wang X, Zhang J, Kawazoe N, et al. 3D Culture of Chondrocytes in Gelatin Hydrogels with Different Stiffness. *Polymers (Basel).* 2016;8(8):269.
 132. Wang L-S, Du C, Toh WS, Wan ACA, Gao SJ, Kurisawa M. Modulation of chondrocyte functions and stiffness-dependent cartilage repair using an injectable enzymatically crosslinked hydrogel with tunable mechanical properties. *Biomaterials.* 2014;35(7):2207–17.
 133. Yasuda K, Kitamura N, Gong JP, Arakaki K, Kwon HJ, Onodera S, et al. A Novel Double-Network Hydrogel Induces Spontaneous Articular Cartilage Regeneration in vivo in a Large Osteochondral Defect. *Macromol Biosci.* 2009;9(4):307–16.
 134. Thrivikraman G, Madras G, Basu B. In vitro/In vivo assessment and mechanisms of toxicity of bioceramic materials and its wear particulates. *RSC Adv.* 2014;4(25):12763–81.
 135. Bernard M, Jubeli E, Pungente MD, Yagoubi N. Biocompatibility of polymer-based biomaterials and medical devices-regulations,: In vitro screening and risk-management.

- Biomater Sci. 2018;6(8):2025–53.
136. Anderson JM. Future challenges in the in vitro and in vivo evaluation of biomaterial biocompatibility. *Regen Biomater*. 2016;3(2):73–7.
 137. Tseng J-C, Kung AL. In vivo Imaging Method to Distinguish Acute and Chronic Inflammation. *J Vis Exp*. 2013;(78):1–5.
 138. Bruen D, Delaney C, Florea L, Diamond D. Glucose Sensing for Diabetes Monitoring: Recent Developments. *Sensors (Basel)*. 2017;17(8).
 139. Matzeu G, Florea L, Diamond D. Advances in wearable chemical sensor design for monitoring biological fluids. *Sensors Actuators B Chem*. 2015;211:403–18.
 140. Durand F, Bordeaux U, Kjaergaard CH. Bilirubin oxidase from *Magnaporthe oryzae*: an attractive new enzyme for biotechnological applications. *Appl Microbiol Biotechnol*. 2013;96(6):1489–98.
 141. Mano N, Goudeau B, Karajic A, Jain D, Barthélémy P, Kuhn A, et al. Low-Molecular-Weight Hydrogels as New Supramolecular Materials for Bioelectrochemical Interfaces. *ACS Appl Mater Interfaces*. 2016;9(1):1093–8.
 142. Ziane S, Schlaubitz S, Miraux S, Patwa A, Lalande C, Bilem I, et al. A thermosensitive low molecular weight hydrogel as scaffold for tissue engineering. *Eur Cells Mater*. 2012;23:147–60.
 143. Michael A. Ramin, Laurent Latxague, Kotagudda Ranganath Sindhu, Olivier Chassande PB. Low molecular weight hydrogels derived from urea based-bolaamphiphiles as new injectable biomaterials. *Biomaterials*. 2017;145:72–80.
 144. Kjaergaard CH, Durand F, Tasca F, Qayyum MF, Kauffmann B, Gounel S, et al. Spectroscopic and crystallographic characterization of “alternative resting” and “resting oxidized” enzyme forms of bilirubin oxidase: Implications for activity and electrochemical behavior of multicopper oxidases. *J Am Chem Soc*. 2012;134(12):5548–51.
 145. Gounel S, Rouhana J, Stines-Chaumeil C, Cadet M, Mano N. Increasing the catalytic activity of Bilirubin oxidase from *Bacillus pumilus*: Importance of host strain and chaperones proteins. *J Biotechnol*. 2016;230:19–25.
 146. Reculosa S, Heim M, Gao F, Mano N, Ravaine S, Kuhn A. Design of catalytically active cylindrical and macroporous gold microelectrodes. *Adv Funct Mater*. 2011;21(4):691–8.
 147. Yan Wang P, Santhisagar Vaddiraju P, Bing Gu M, Fotios Papadimitrakopoulos P, and Diane J. Burgess P. Foreign Body Reaction to Implantable Biosensors: Effects of Tissue Trauma and Implant Size. *J Diabetes Sci Technol*. 2015;9(5):966–977.
 148. Chen EY-T, Liu WF, Peyton SR, Emrick T, Nguyen T V., Saleh LS, et al. Zwitterionic PEG-PC Hydrogels Modulate the Foreign Body Response in a Modulus-Dependent Manner. *Biomacromolecules*. 2018;19(7):2880–8.
 149. Swartzlander MD, Barnes CA, Blakney AK, Kaar JL, Kyriakides R, Bryant SJ, et al.

- Linking the foreign body response and protein adsorption to PEG-based hydrogels using proteomics. *Biomaterials*. 2015;(41):26–36.
150. Brooks P, Barzilay O, Sheikh Z, Glogauer M, Fine N. Macrophages, Foreign Body Giant Cells and Their Response to Implantable Biomaterials. *Materials (Basel)*. 2015;8(9):5671–701.

